Functional studies of β-arrestins and αB-crystallin as interaction partners of PAR-1 and PAR-2 and their involvement in protective and proliferative signaling pathways in astrocytes

Dissertation

zur Erlangung des akademischen Grades

doctor rerum naturalium
(Dr. rer. nat.)

genehmigt durch
die Fakultät für Naturwissenschaften
der Otto-von-Guericke-Universität Magdeburg

von **M. Sc. Zhihui Zhu**

geb. am 07.10.1982 in Inner Mongolia, China

Gutachter: Prof. Dr. Georg Reiser

Prof. Dr. med. Nikolaus Plesnila

eingereicht am: 28. April 2014

verteidigt am: 03. September 2014

Contents

Contents

Contents

Contents

1. Introduction

1.1 Protease activated receptor's expression and structures of protease activated receptors in brain

The protease-activated receptors (PAR) are seven transmembrane-domains G-protein-coupled receptors (GPCRs) with wide expression in the central nervous system (CNS). The four isoforms are named PAR-1, PAR-2, PAR-3, and PAR-4 which were detected in many kinds of neural cells, for example, neurons, astrocytes, oligodendrocytes and microglia. In rat primary neural cells, all of these four PAR are expressed abundantly [1].

1.1.1 Expression and structures of protease activated receptors

As shown in Fig. 1.1.1 modified based on the studies of Adams *et al* [2], the PAR contain seven transmembrane (TM) helices, an extracellular amino terminal domain (N-terminal) and three intracellular loops (ICL1-3), three extracellular loops (ECL1-3) and an intracellular carboxyl tail. An important disulfide bond connects ECL2 with TM3 to form most conserved structure amongst GPCRs and contributes to receptor structural stability [3]. Activation of PAR was demonstrated via proteolytic cleavage, which results in irreversible removal of an N-terminal peptide and unmasking of the new N-terminus. The newly generated N-terminus subsequently binds to ECL2, and therefore receptors are activated [4]. PAR-1 and PAR-3 contain a hirudin-like binding domain to facilitate thrombin binding and proteolysis. However, a cluster of anionic residues, D57, D59, E62 and D65 slows the dissociation of thrombin, which enables the activation of PAR-4 by thrombin [5, 6].

The protease agonists and synthesized peptides are found to activate PAR. For example, thrombin, trypsin, mesotrypsin, FVIIa, FXa, APC, and Arginine-specific gingiains-R are the protease agonists for PAR-1 and PAR-4. The peptide agonists of PAR-1 include SFLLR-NH2; TFLLR-NH2[a], Trag, and TFRIFD. The most common protease agonists for PAR-2 are trypsin and tryptase. Moreover, FVIIa and FXa are found to stimulate PAR-2 either. The peptide agonists of PAR-2 contain $SLIGKV-NH_2$, $SLIGRL-NH_2$, and $SFLLR-NH_2$. However there is no other protease or peptide agonist observed to activate PAR-3, except for thrombin. The agonists for each subtype of PAR are well summarized by Luo *et al* [7].
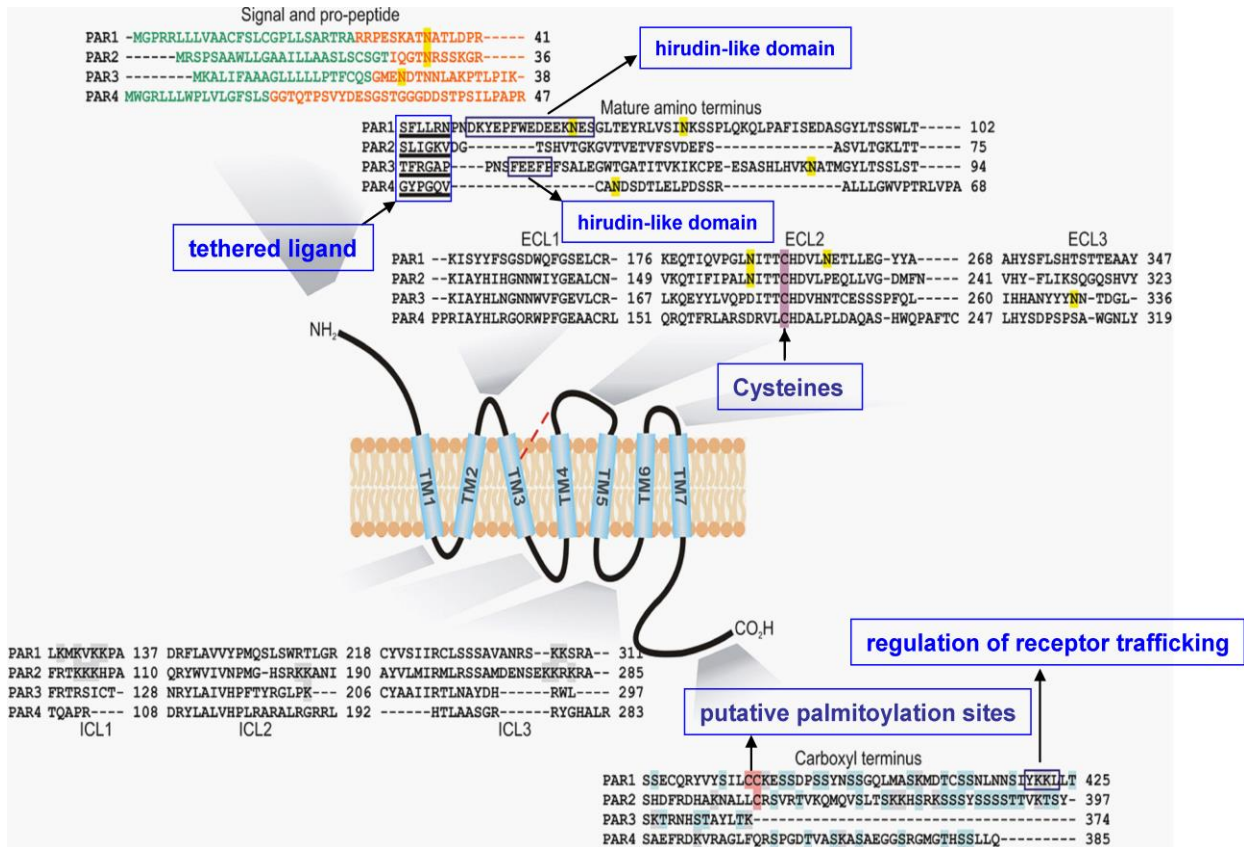
Fig. 1.1.1. PAR structural features. First, the N-terminal sequence alignments are shown of the signal (green lettering) and pro-peptide (orange lettering) regions. Consensus sites for N-glycosylation are highlighted yellow. The mature amino terminus, and the sequences of extracellular loop (ECL) regions 1, 2 and 3, sequences of intracellular loop (ICL) regions 1, 2 and 3, and the carboxyl terminal domain of the four human PAR are listed. Among them, the blue boxes specify the tethered ligand, hirudin-like domain, cysteines contained in ECL2. Besides, the putative palmitoylation sites are highlighted in red. Highlighted grey and blue residues indicate post-translational modification sites for ubiquitination and phosphorylation. The boxed residues in the PAR-1 carboxyl terminal display the tyrosine-based motif related to receptor trafficking [2].

1.1.2   Thrombin activates PAR-1, PAR-3 and PAR-4

Thrombin is generated by the cleavage of prothrombin in the presence of activated factors Xa and Va, calcium and membrane phospholipids [8]. Prothrombin is mainly produced in the liver, and secreted into the bloodstream [9], where it is converted into mature thrombin during the coagulation cascade in response to injury that requires the formation of a blood clot [10]. In this pathway, the main function of thrombin is working as coagulant to cleave fibrinogen into fibrin molecules to form the bulk of the clot or thrombus. In contrast, thrombin can also act as an anticoagulant through activation of protein C. Apart from the functions as coagulant and anticoagulant, thrombin has other activities, such as wound healing, inflammation, and atherosclerosis, emphasizing a broader physiologic role of thrombin as a cellular bioregulatory factor [11].

Two thrombin interaction sites have been proposed on the PAR-1 receptor: one is the cleavage site at Arg41/Ser42, while the second one, between residues 53 and 64, shows sequence similarity to a C-terminal region of hirudin and is involved in the thrombin anion-binding exosite [12]. PAR-3 is the second thrombin receptor with the cleavage site in the N-terminal sequence at Lys38/Thr39 of human PAR-3, and a hirudin-like binding domain positioned C-terminally to the cleavage site, were identified [13]. In addition, thrombin shows the ability to activate PAR-4 with cleavage at Arg47/Gly48 in the N-terminal sequence. However, PAR-4 requires relatively higher levels of thrombin for activation, possibly because of the lacking of hirudin-like thrombin binding sequence [14].

The cleavage of different sites of PAR-1 is connected to different functional results. For example, activated protein C (APC) preferentially cleave PAR-1 at R46, which enhanced the endothelial barrier function and decreased staurosporine toxicity in endothelial as well as in HEK 293T cells. These data suggest that cleavage at R46 but not R41 is required for cytoprotective APC signaling. Furthermore, in PAR-3, it was reported that the distinct cleavage site is K38 for thrombin and R41 for APC [15].

1.1.3 Collaboration of PAR for physiological functions of cells

Thrombin modulates a variety of cell functions through the activation of PAR-1, PAR-3 and PAR-4, including cell proliferation and differentiation, cytoprotection, cell migration, and controlling inflammatory mediator release from cells.

The crosstalks among the PAR were continued to be found. For instance, the effects of thrombin on experimental metastasis of tumour cells are commonly thought to be mediated by PAR-1. However, the further study pointed out that PAR-1 activation is not sufficient. In contrast, a combination of peptides agonist of PAR-1 and PAR-2 mimics the thrombin effect on migration, whereas the PAR-2 agonist alone has no effect. Moreover, agonist peptides for the thrombin receptors PAR-3 and PAR-4 used alone or plus PAR-1 agonist also have no effect. These results demonstrate that thrombin-mediated cancer cell migration needs the collaboration of PAR-1 and PAR-2 [16].

PAR-3 cooperates with PAR-1 to mediate the effect of thrombin on cytokine IL-6, IL-8 production and vascular cell adhesion protein 1 expression in endothelial cells and on cell proliferation in malignant B cells [17]. Furthermore, collaboration between PAR-1 and PAR-4 is important for the platelet secretion and aggregation. [18].

1.2   Thrombin: A Double-edged sword acting as the PAR-1 agonist in brain

Thrombin has been shown to play either protective or harmful roles in brain. Thrombin was found to be expressed in neural cells at both mRNA and protein levels which were associated with both extra- and intracellular neurofibrillary tangles in Alzheimer's disease (AD) and parkinsonism-dementia complex of Guam. This result suggested that thrombin failed to metabolize tau, which leads to tau aggregation in neurodegenerative diseases [19]. Thrombin was found in neuritic plaques in AD. The high level of thrombin is the hallmark of traumatic brain injury, and the traumatic brain injury is correlated with an increased incidence of AD. In addition, thrombin was suggested to enter brain tissue directly by increasing blood-brain barrier permeability during brain injuries.

Thrombin was demonstrated to induce neurotoxicity in rat hippocampus which is connected with cognitive deficits [20]. Especially, thrombin was shown to produce reactive oxygen species (ROS), such as superoxide (O_2^-) and O_2^--derived oxidants through activation of microglia, inducing or exacerbating neurotoxicity [21]. In cultured hippocampal neurons, thrombin-induced neurotoxicity is partially caused by neuronal NADPH oxidase-mediated oxidative stress. This strongly suggests that thrombin can act as an endogenous neurotoxin, to trigger ROS production which may contribute to the neurodegeneration occurring in AD [22]. Moreover, thrombin caused rapid tau hyperphosphorylation and aggregation in murine hippocampal neurons, which contributes to the pathogenesis of Alzheimer's disease [23]. This is believed to occur through stimulation of PAR-1 and PAR-4. In addition, thrombin might be responsible for neurodegenerative processes observed after various insults, like stroke, traumatic brain injury, and heart arrest or as a frequent consequence of bypass surgeries [24-27].

However, accumulating evidence suggests that stimulation of PAR-1 produces bimodal biological effects in CNS, which largely depends on the concentration of agonist used in clinical or experimental studies. For example, low level PAR-1 activation in astrocytes exerts a protective effect against deleterious stimuli [24], whereas high level of PAR-1 activation compromises neural cell viability [28, 29]. *In vitro* studies suggested that PAR-1 activation can have neuro-protective roles, which was consistent with neuro-protection through low doses of thrombin treatment in stroke models [30]. Stimulation of PAR-1 by thrombin induced release of cytokine-induced neutrophil chemo attractants (CINCs) from astrocytes and further prevented apoptosis of neurons and astrocytes due to chemical insults [31]. The neuroprotection through thrombin treatment was also examined *in vivo*. For example, PAR-1 mediated neuroprotection in a 6-hydroxydopamine model of Parkinson's disease [32, 33]. In

addition, thrombin was confirmed to increase the neuronal cell density in CNS. 1-7 days' injection of thrombin or PAR-1 agonist was reported to be effective in increasing the density of astrocytes and Flouro-Jade C positive cells in hippocampus[34]. Flouro-Jade C stains all of the degenerating neurons. These studies highlighted that either proliferative or degenerative effects can be produced by thrombin or agonist-activated PAR-1 in the mammalian brain.

The activation of PAR isoforms in CNS has protective effects through stimulation of various signaling cascades which has been studied in our laboratory over the last 10 years. For instance, thrombin or PAR-1-specific agonists stimulated proliferation of astrocytes through extracellular signal-regulated kinases 1/2 (ERK1/2) activation [35]. Moreover, the activation of PAR-1 by thrombin rescued astrocytes from C2-ceramide-induced cell death through stimulating c-Jun N-terminal kinases (JNK) and ERK1/2 to increase the levels of the chemokine growth-regulated oncogene/cytokine-induced neutrophil chemoattractant-1 (GRO/CINC-1) [36]; on the other side, PAR-2 activation in astrocytes remarkably protected the cells from C2-ceramide-induced cell death. PAR-2 activation elicited the upregulation of JNK, P38 (p38 mitogen-activated protein kinase) and ERK1/2. Low concentrations of thrombin (10 pM-10 nM) protected hippocampal neurons or astrocytes from cell death caused by oxygen-glucose deprivation, hypoglycemia, growth supplement deprivation, oxidative stress or C2-ceramide [30, 31, 37]. However, the detailed mechanisms of the protection by thrombin-activated PAR-1 are still largely unknown.

1.3   The good and the bad roles of thrombin–caused mitochondrial ROS production

Reactive Oxygen species (ROS) are well known as by-products of the normal metabolism. Mitochondria are believed to be the key target of oxidative damage and the major producer of ROS in cells. The largest part of mitochondrial ROS is generated at the electron transport chain [38]. Mitochondrial ROS can be produced under the different stimuli such as non-esterified polyunsaturated fatty acids [39]. Increased mitochondrial ROS production damages brain contributing to AD [40], PD [41], and stroke [42]. The potential mechanisms accounting for these pathologies are the decreased ATP production, abnormal mitochondrial membrane potential, permeability transition pore activation, and reduced mitochondrial Ca^{2+} capacity [43].

Accumulating studies show that ROS release inflicts cellular damage such as cell death. However, ROS can regulate the normal cellular growth and metabolism. The contradictory roles of ROS played in the cellular physiological effects highlight the two 'faces' of it. One face is that the excessive ROS plays a harmful role in cellular effects through oxidization of cellular protein, lipids and nucleic acids. Moreover, ROS targets mitochondrial DNA, which is probably a major factor of mitochondrial genomic instability leading to respiratory dysfunction [43]. The other face is that ROS works like a positive signaling molecule to mediate signal transduction of growth factors and cytokines [44].

Thrombin is reported to produce ROS in various cell types, such as human vascular smooth muscle cells (VSMC), endothelial cells, retinal pigment epithelial (RPE) cells, and hippocampal neurons [45] which is demonstrated to depend on the phosphorylation status of ERK1/2 in neurons from rat hippocampus [46]. The brain ROS production was confirmed to cause degeneration of hippocampal [47], cortical [48, 49], and mesencephalic neurons [50], *in vivo* and/or *in vitro* [22]. The mechanism of ROS production initiated by thrombin was found to be related with the activation of NADPH oxidase complex in VSMC, which, in turn, generates ROS and oxidative stress [51]. One of the potential mechanism is that the newly produced ROS targets to p38 MAPK and subsequently regulates thrombin-stimulated migration of VSMC [52].

Thrombin induced-ROS production was believed to induce cell death or apoptosis. For instance, in human platelets, thrombin induces ROS production and H_2O_2 generation, which was demonstrated to induce apoptosis [53]. Later, it was confirmed by the same group that thrombin induced activation and mitochondrial translocation of Bid, Bax and Bak, which was likely to be one of the mechanisms accounting for apoptotic events in human platelets [54].

In addition, ROS was demonstrated to play also a positive functional role in physiology. For example, thrombin-linked mitochondrial ROS production failed to alter mitochondrial function or trigger cell death, but rather contributed to activation of nuclear factor kappa B (NF-κB) and leukocyte cell adhesion [55]. Thrombin-induced ROS production is involved in thrombin-induced pulmonary vasoconstriction [45].

1.4 The mechanisms accounting for cell proliferation induced by thrombin

Thrombin, as a mitogen, was reported to stimulate the proliferation of many kinds of cells, such as RPE, astrocytes, endothelial cells, tumour cells and VSMC. Moreover, thrombin-induced ROS production contributed to cell proliferation, which was associated with a transcription factor, UPBEAT1. UPBEAT1 directly regulated the balance of ROS between cell proliferation and cell differentiation [56].

1.4.1 Thrombin-induced ROS/MAPK is responsible for the cell proliferation

MAPK signal transduction is an important mitogenic factor to induce cell proliferation. It is well known that thrombin effectively induces production of ROS and activation of MAPK signaling pathways. ROS as second messenger activates MAPK signal transduction, which in return regulates ROS generation and contributes to cell proliferation [57].

1.4.2 Thrombin stimulates the PI3K/cyclin D1 signal transduction pathway to regulate cell cycle

Thrombin triggered-phosphatidylinositol 3-kinase (PI3K), an important signaling pathway involved in cell survival, is implicated in regulating cell cycle protein-cyclin D1 [58]. Cyclin D1 is a key regulator of the G1-S transition. Several lines of evidence suggest that cyclin D and associated kinases (Cdks) 1 are among the targets of cell growth signals. Thrombin-caused increased expression of cyclin D1 promotes cell proliferation [58]. In contrast, inhibition of cyclin D1 expression either by antisense methodology or antibody microinjection extends the duration of the G1 phase, resulting in the blockade of proliferation [59, 60].

1.4.3 Thrombin activates the secretion and release of growth factors

Thrombin also activates the secretion and release of growth factors, like vascular endothelial growth factor (VEGF) [61], fibroblast growth factor (FGF) family members [62], and platelet-derived growth factor (PDGF) [63], which are suggested to interact in cell growth. Treatment of human RPE cells with thrombin results in dose and time-dependent increases in VEGF mRNA levels and protein secretion. Thrombin- caused VEGF expression is correlated predominantly with PAR-1. Moreover, inhibitory assays reveal that MAPK,

protein tyrosine kinase (PTK), PI3K, PKC, NF-κB, and ROS are involved in VEGF expression induced by thrombin [64].

FGF family members are demonstrated to have a variety of biological activities including angiogenesis, tissue regeneration, inflammation, and pathogenesis of some tumours. Thrombin, through activation of the PAR-1, rapidly induces FGF1 expression and its release [62].

PDGF is one of the numerous growth factors regulating cell growth and division. Enzyme immunoassay and RT-PCR demonstrated that thrombin induced the secretion and expression of PDGF from bronchial and alveolar epithelial cells. This cellular effect of thrombin is demonstrated to occur via a PAR-1-mediated mechanism, since PAR-1 agonist peptide is found to induce PDGF secretion from epithelial cells [63]. Thrombin significantly stimulates the proliferation of human A172 glioblastoma cells, and the increased growth of the cells primarily depends on the enhanced secretion of PDGF by thrombin. The effects of thrombin completely depend on its proteolytic activity, which is consistent with a PAR-mediated mechanism [65].

Endothelins, including Endothelin-1 (ET-1), Endothelin-2 (ET-2), and Endothelin-3 (ET-3), are vasoactive peptides found in brain endothelial cells, neurons and astrocytes. ET-1 works as a growth factor to promote proliferation of astrocytes [66]. Moreover, thrombin is capable of inducing the synthesis and secretion of ET-1 in RPE cells via PAR-1 [67]. Thrombin-caused ET-1 release to the cell culture medium contributes to the proliferation of rat gingival fibroblasts [68].

1.4.4 Thrombin triggers the glucose metabolism signaling cascades to mediate cell proliferation

As described in the paragraphs above, ET-1 behaves like a growth factor to stimulate astrocytes proliferation [66]. The mechanisms accounting for ET-1-induced cell proliferation are linked to the increased rate of glucose uptake, which is targeted for the nucleic acids synthesis required for cell proliferation. ET-1 is able to increase the rate of glucose-6-phosphate utilization through the pentose phosphate pathway [69], which supplies the ribose phosphate to synthesize nucleic acids for astrocytes proliferation [70]. Another explanation for the increased glucose uptake occurring in responses to ET-1 is that ET-1 up-regulated the glucose transporter type 1 (GLUT-1) and induced the expression of the glucose transporter type 3 (GLUT-3), an isoform not found in astrocytes in normal situation. As a result, intracellular glucose is phosphorylated by hexokinases (HKs) to glucose-6-phosphate, which is a charged molecule that cannot pass back through the plasma membrane, and therefore

glucose-6-phosphate is trapped within the cell. In this situation, both type I (HK1) and type II (HK2) hexokinases are found to be unregulated by ET-1 in astrocytes [71]. Thrombin is able to induce the secretion and release of ET-1 in primary astrocytes [72]. Moreover, thrombin is reported to stimulate glucose uptake in rat thoracic aortic smooth muscle cells *via* Src and subsequent p38 MAPK activation [73]. As a result, it can be proposed that thrombin is able to promote the secretion of ET-1, which subsequently upregulates the HKs to increase glucose uptake. Therefore, the cell proliferation is accelerated.

Hypoxia inducible factor-1 (HIF-1), a heterodimer composed of the constitutively expressed HIF-1β subunit and the highly regulated HIF-1α subunit, plays a critical role in glucose uptake, angiogenesis, glycolysis, pH balance, and metastasis. Moreover, HIF-1 as transcription factor mediates transcription of multiple genes, such as GLUT-1, GLUT-3, HK1 and HK2 [74]. HIF-1 was primarily identified because of its response to low O_2 concentrations, which led to the stabilization of HIF-1α in the intracellular environment. However, it is now apparent that HIF-1α can be accumulated under normoxia situation. For example, activation of the PI3K pathway results in HIF-1α accumulation in normoxia [75]. In spite of this, oncogene activation or losses of tumour suppressors also mediate HIF-1 accumulation. For example, HIF-1 accumulates in tumour cells after activation of oncogenes, such as Ras, SRC and PI3K [76]. In addition, HIF-1α is responsive to hormones such as insulin [77], growth factors such as IGF [78], thrombin [79], and vasoactive peptides such as angiotensin II [80].

HIF-1 regulated-genes are largely associated with glucose metabolisms, which is well described and reviewed by Denko [74]. The following table lists genes which are important for glucose metabolism regulated by HIF-1.

Product(s) of HIF-1 target genes	Metabolic Functions
Glucose transporters (GLUT-1 and -3)	Glucose uptake by cells
HK2	Phosphorylation of glucose
PGI, PFK1, aldolase, TPI, GAPDH, PGK	
PGM, enolase, PK, PFKFB1-4	Glycolysis
LDHA	Conversion of pyruvate to lactate
MCT4	Removal of lactate from the cell
PDK1, MXI1	Decreased mitochondrial activity
COX4i2, LON protease	Increased O_2 consumption in hypoxia

Table 1.4.4. Gene regulated by HIF-1 [74]**. For the abbreviations, please refer to the abbreviations list.**

It has also been proposed that ROS generated as by-products of electron transport at the mitochondria can stabilize HIF-1α in hypoxia [81-83]. The interaction of mitochondrial superoxide with the HIF-1 degradation machinery is not well-established, but it has been reported that hydrogen peroxide can oxidize the Fe^{2+} that is required as a cofactor for prolyl 4-hydroxylase (PHD) activity. The resulting Fe^{3+} cannot function in hydroxylation and the loss of PHD activity, in turn, results in HIF-1α stabilization [84]. However, this still remains to be confirmed.

In addition, there are still some open questions that need to be answered. It is not clear whether thrombin-induced ROS will work as signaling molecule to trigger the MAPK and PI3K/Akt signaling cascades to promote the proliferation of astrocytes. Further, it needs to be clarified whether mitochondrial ROS are involved in the regulation of glucose uptake signaling transduction to promote proliferation of astrocytes.

1.5   PAR-2 signal transduction and interaction partners

The human PAR-2 gene codes for a protein with 397 amino acids, sharing 30% amino acid identity with the human PAR-1 protein. PAR-2, ubiquitously expressed receptor found in every tissue and organ is activated by multiple trypsin-like serine proteases including trypsin, tryptase, and coagulation proteases. It is known that PAR-2 mediates the cellular effects through activation of heteromeric G-proteins. Other studies revealed that the predominant α subunit involved in mediating PAR effects are the pertussis-toxin-insensitive Gαq/G11 and G12/G13 subunits [85]. The response to activation of these G-proteins is the elevation of intracellular Ca^{2+} via the Cαq phospholipase C /IP3 pathway, as has been shown for PAR-2 in cultured hippocampal neurons [86].

The activated PAR-2 communicates mainly through two separate signaling arms, one is through Gαq with Ca^{2+} mobilization, and another is through the recruitment of β-arrestins (β-arrestin 1 and β-arrestin 2) scaffolds. β-Arrestins act as molecular switches which are capable of modifying the signals generated by the receptor. On the one hand, downstream targets of the Gαq/Ca^{2+} signaling arm are directly inhibited by β-arrestins; on the other hand, the two pathways are synergistic; For example, PAR-2 activates adenosine monophosphate-activated protein kinase (AMPK), a key regulator of cellular energy balance, through Ca^{2+}-dependent kinase kinase b (CAMKKb), while it inhibits AMPK through interaction with β-arrestins [87].

Recently, neuronal PAR-2 has been linked to the stimulation of the ERK subfamily of MAPK following middle cerebral artery occlusion [88]. The increase in ERK activity was neuron-specific and was significantly inhibited in PAR-2 knock-out mice, which is beneficial to neuronal survival, suggesting that the neuroprotective role of PAR-2 is directly connected

to ERK activation. The activation of ERK via PAR-2 is thought to rely on the β-arrestins-dependent internalization of the receptor and the formation of a complex to conduct the signaling cascades [89].

PAR-2 also couples to a number of signaling pathways usually stimulated strongly by cytokines, such as NF-κB pathway and the stress-activated protein kinases, p38 MAP kinase and JNK which has been demonstrated in transfected cells, human blood eosinophils, and rat pancreatic stellate cells. However, the exact mechanisms involved in these signaling pathways remained unclear.

It has been reported that phosphorylation plays a role in desensitization of activated PAR-2 signaling [90]. Previous studies showed that pharmacological inhibitors of PKC enhance PAR-2-mediated calcium responses in transformed rat kidney epithelial (KNRK) cells and Berkeley rat intestinal (hBRIE 380) cells, indicating a role for phosphorylation in PAR-2 regulation [91]. Other studies also displayed that PAR-2 activation caused a rapid and robust increase in phosphorylation of PAR-2 wild type, rather than mutants in which all serines and threonines in the cytoplasmic tail were converted to alanines. This result indicated that the major sites of PAR-2 phosphorylation occur within the cytoplasmic tail [90]. Phosphorylation is important for PAR-2 coupling to β-arrestins, since mutants of PAR-2 in which all serines and threonines in the cytoplasmic tail were converted to alanines, lose the capacity of desensitization, implying that β-arrestins mediate activated PAR-2 desensitization, presumably through phosphorylation, internalization and signaling to downstream effectors.

However, less is known how β-arrestins regulate the PAR-2 downstream signaling upon the activation of receptors under different stimuli. Moreover, it is not well elucidated what are the functional roles of the cluster of serines/threonines located in the cytosolic carboxyl tail in controlling the downstream signaling of PAR-2 receptor and cellular functions.

1.5.1 PAR-1 and PAR-2 interaction partners: β-arrestins

Several partner-proteins of PAR were identified in our laboratory over the past 10 years. For example, α-crystallin interacts with PAR-2 to rescue astrocytes from cell death, and the PAR-2-interacting protein Jab1 controlled PAR-2-induced activation of activator protein-1 to regulate c-Jun activation [92]. β-Arrestins were confirmed interacting with PAR-1 and PAR-2. There was strong evidence indicating that β-arrestin 1 was essential for PAR-1 desensitization, but dispensable for receptor internalization [93]. The situation was different for PAR-2, since both β-arrestin 1 and β-arrestin 2 have been confirmed to be crucial for receptor internalization as well as signaling desensitization [94].

Over the last decade, β-arrestins, the two members of the arrestin family with ubiquitous distribution have emerged as pleiotropic scaffold proteins mediating numerous diverse responses to multiple receptor agonists. The GPCR-stimulating β-arrestin signals are sometimes synergistic with, and sometimes independent from the heterotrimeric G-protein signals. Previous studies confirmed that β-arrestins are involved in PAR-2 receptor internalization [95] and mediated downstream cascades of PAR-1 stimulated by thrombin [96].

β-Arrestins have been demonstrated to be coupled to many signaling proteins, such as MAPKs and PI3K. β-Arrestins mediate the long-lasting ERK activation, which is quite different from the rapid and transient ERK activation mediated by G-proteins. The MAPK signaling pathways ERK, JNK3 and p38 are regulated by β-arrestins. It is worth to mention that protein kinase B (Akt) activation is either up-regulated or down-regulated by β-arrestins-dependent mechanisms, depending on the types of stimuli and receptors involved. Stimulation of the insulin receptor leads to β-arrestin 2-dependent phosphorylation of Akt at Thr 308 and Ser 473, respectively [97]. On the other hand, β-arrestin 2 can deactivate Akt by the formation of a β-arrestin 2/protein phosphatase 2A/Akt complex under the challenge of the dopamine D2 receptors [98]. Since activation of PI3K/Akt signaling pathways plays a pivotal role in cell proliferation, differentiation and survival, important studies have put emphasis on these signaling pathway-related molecular effectors. For example, it was found that β-arrestin 2 mediated phosphorylation of BAD through the PI3K/Akt signaling pathway, which protected cells from apoptosis [99]. β-Arrestins are involved in PAR-induced cellular protection. For instance, APC-activated PAR-1 cyto-protective signaling is mediated by β-arrestins recruitment and activation of the dishevelled-2 scaffold but not by Gαi [100].

Accumulating studies emphasized the functional role of β-arrestins, especially when they work as the signaling adaptors. β-Arrestins were reported to mediate cytoprotection in different kinds of cell types through stimulation of various signaling pathways. For example, in β-arrestin $1/2^{-/-}$ mouse embryonic fibroblasts, the apoptosis happened because without β-arrestins, the stimulation of the N-formyl peptide receptor initiated cell apoptosis followed by cell death. The reintroduction of either β-arrestin 1 or β-arrestin 2 inhibited the apoptosis [101]. Moreover, PAR-1 receptor stimulated by APC promoted cytoprotection through β-arrestin-mediated Ras-related C3 botulinum toxin substrate 1 signaling in human endothelial cells [100]. Activation of insulin-like growth factor 1 receptor initiated β-arrestin-dependent activation of Akt, and therefore protected the cells from apoptosis. The overexpression of β-

arrestin 2 significantly inhibited opioid-induced apoptosis, and β-arrestins prevented cell apoptosis through ERK1/2 and p38, Akt pathways [102, 103].

However, there is still limited information about the functional roles of β-arrestins in regulating PAR signaling cascades which block cell death in CNS cells. Here, we intend to investigate the potential role of β-arrestins in survival signaling pathways located downstream of PAR-1 and PAR-2 receptors in astrocytes.

1.5.2 PAR-2 interaction partner α-crystallin

α-Crystallin is the major structural protein of the mammalian lens, comprising two subunits, αA-crystallin and αB-crystallin. These two subunits belong to the small heat shock protein family of molecular chaperones, which has multiple functional effects on retinal diseases, multiple sclerosis, and cell apoptosis [104]. Accumulating studies over the past 15 years have confirmed the expression of α-crystallin in brain, spleen, lung, kidney, cornea, and skin and their roles in regulation of cell survival, and functions in the central nervous system.

α-Crystallin was demonstrated to interact only with PAR-2 among the PAR. αB-crystallin is one of the interaction partners of PAR-2 identified in our laboratory [105]. The functional role of α-crystallin is mainly focused on the chaperone activity. In the past five years, the intracellular protective effects of α-crystallin have been confirmed.

As the molecular chaperones, α-crystallin plays the functional roles not only in the extracellular matrix, and cell membrane, but also in some intracellular organelles including the nucleus. For example, α-crystallin targets extracellular components decreasing the damage to cells [106]. Extracellular application of α-crystallin promotes rat olfactory ensheathing cells survival and proliferation [107]. Apart from this, α-crystallin was pointed out that it can keep the cell membrane from rupturing induced by several stimuli [108]. Intracellular α-crystallin was believed to stabilize and prevent denaturation of proteins under the stimulation of stress through binding to the target protein [109]. Later it was confirmed that α-crystallin binds to the denatured proteins to promote the recovery of protein activity [110]. Other studies provided evidence to show that α-crystallin translocates from cytosol to nucleus and regulates gene expression [111, 112].

αB-Crystallin has been reported to colocalize or interact with the mitochondria [113] and protect retinal pigment epithelium cells against endoplasmic reticulum stress by restoring mitochondrial functions [114]. The astrocytes from inflammatory mice showed a decreased level of ROS when mice were pre-treated with α-crystallin, emphasizing that α-crystallin might serve as a potent pharmacological reagent in neuroinflammation [115]. Besides,

upregulation of α-crystallin was found during the early phase of experimental autoimmune uveitis against mitochondrial oxidative stress and stress-mediated apoptosis [116].

Signaling pathways are well documented that are integrated in physiological effects mediated by α-crystallin *in vitro* and *in vivo*. For instance, αB-crystallin prevented lens epithelial cells from ultraviolet A (UVA)-induced apoptosis through repression of UVA-induced activation of the Raf/MEK/ERK pathway, whereas αA-crystallin activated the Akt survival pathway to block the UVA-induced apoptosis. Beside this, it was found that calcium-activated Raf/MEK/ERK signaling pathway mediated p53-dependent apoptosis which was suppressed by αB-crystallin-activated Ras [117]. *In vivo* investigation showed that α-crystallin decreased the Ras homolog gene family member A (RhoA) protein activity and the phosphorylation of both cofilin and myosin light chain, and therefore promoted the axonal growth in rat [118]. Furthermore, α-crystallin has been shown to bind the proapoptotic molecules p53, Bax and Bcl-XS to inhibit these proapoptotic molecules translocating from cytoplasm to mitochondria. As a result, release of cytochrome c from mitochondria to activate apoptosis was blocked [118-121].

It was previously confirmed that overexpression of α-crystallin and the phosphorylation status of α-crystallin are important for protecting astrocytes from cell death induced by C2-ceramide and staurosporine [122, 123]. Compared to the large amount of reports on the functions of α-crystallin in the intracellular environment, there is still limited information to help understanding the functional role of α-crystallin when applied as extracellular protein.

The interaction of β-arrestins with sHSP was implied to be associated with cytoprotective effects. For instance, Formation of β-arrestins/HSP27 complex was confirmed to confer cytoprotective consequence of β-adrenergic receptor activation [124]. Similarly, phosphorylated HSP27 interacting with β-arrestin 2 to regulate TRAIL-triggered activation of Src-Akt/ERK pro-survival signaling in Hela cells [125]. As the interaction partners of PAR-2, we are interested in exploring whether β-arrestins and αB-crystallin will interact to each other upon the activation of PAR-2 receptor and whether some of the biological effects will be produced by these two protein interactions.

1.6 Aim of study

The aim of this project was to investigate how activation of PAR-1 and PAR-2 will initiate the intracellular signaling transductions to mediate astrocytes proliferation and cytoprotection. Moreover, we are interested in how β-arrestins and αB-crystallin as the interaction partners of PAR-1 and PAR-2 are involved in the protective and/or proliferative signaling pathways induced by activation of these two receptors. Our specific aims of this project are divided into four parts:

Part 1. Study of the possible cytoprotective effects induced by activation of PAR-1 and PAR-2.

(1). Scheme for the study of cytoprotection
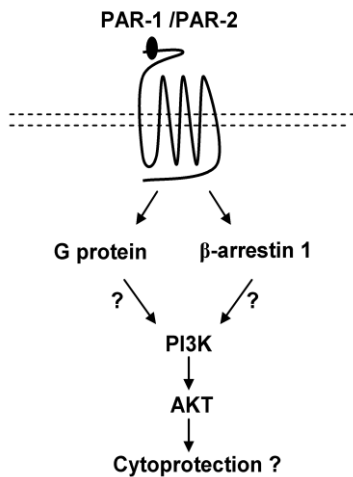
1 Investigation of the role of β-arrestins in astrocytes apoptosis and how β-arrestins are involved in PAR-1 and PAR-2 signaling.

2 Elucidating the signaling pathways which account for protection of astrocytes possibly induced by thrombin-activated PAR-1. The PI3K/Akt signaling pathways will be the focus in this issue.

Part 2. Investigation of the signaling pathways responsible for the proliferation of astrocytes induced by thrombin-activated PAR-1.

(2). Scheme for the study of proliferation
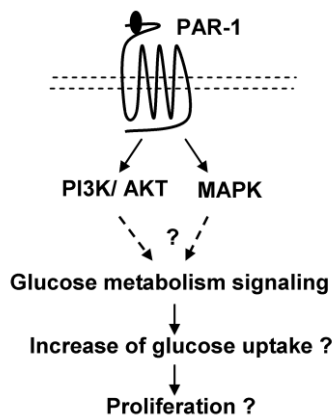
1. To find out whether thrombin triggers the glucose metabolism signaling pathway to accelerate the proliferation of astrocytes.
2. To clarify how MAPK, PI3K/Akt are involved in regulation of glucose metabolism in astrocytes.

Part 3. Functional study of the phosphorylation sites located in C-terminus of PAR-2.

1.   In this part we will generate a series of PAR-2 truncation mutants as depicted in scheme (3). Our purpose of generation these mutants is to identify the functional roles of the phosphorylation sites in controlling intracellular Ca^{2+}, ERK, Akt signaling pathways.

2.   Find out whether the truncations of PAR-2 carboxyl-tail will influence the receptor localization, expression and cell survival.

(3). Scheme for the functional study of PAR-2 carboxyl terminus

Receptor expression, localization, internalization; Ca^{2+}/ERK, Akt signaling; Cell death
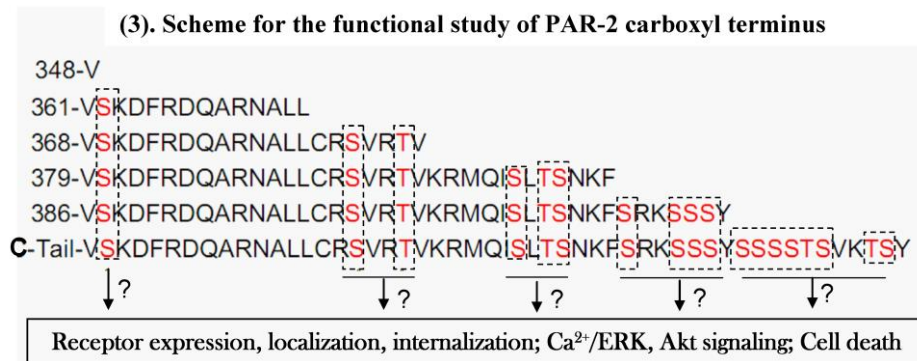
Part 4. Functional study of αB-crystallin in cytoprotection and proliferation of astrocytes induced by PAR-2.

(4). Scheme for the study of the role of αB-crystallin in protection and proliferation of astrocytes
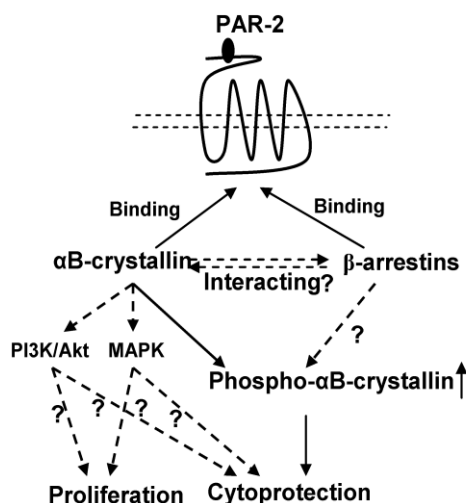
1. We will find out if β-arrestin 1 and 2 interact with αB-crystallin under the sitmulation of PAR-2 by trypsin.

2. We will investigate whether α-crystallin exerts protective and proliferative effects on astrocytes through activating MAPK and PI3K/Akt signaling pathways.

2. Materials and Methods

2.1 Materials

2.1.1 Chemicals and reagents

Name of chemicals	Company
Bio-Rad protein assay dye reagent concentrate	Bio-Rad
Ammonium peroxodisulfate, sodium azide paraformaldehyde (PFA)	Fluka
Fura-2 AM	Molecular Probes
lipofectamine ^{TM} 2000	Life Technologies Invitrogen
Bovine thrombin	Sigma, Steinheim, Germany
Typsin	Sigma, Steinheim, Germany
Staurosporine	Sigma, Steinheim, Germany
Nitrocellulose Transfer Membrane	Whatman, Dassel, Germany
Roti block buffer and Roti-PVDF	Carl Roth, Karlsruhe, Germany
Syto 59	Invitrogen, Karlsruhe, Germany
Dulbecco's modified Eagle's medium	Biochrom, Berlin, Germany
fetal calf serum	Biochrom, Berlin, Germany
penicillin and streptomycin	Biochrom, Berlin, Germany
Accutase	PAA, Pasching, Austria
DOTAP	Roche, Mannheim, Germany
Antimycin A	Sigma, Steinheim, Germany
siRNA of β-arrestin 1	Qiagen, Hilden, Germ
Non-specific target siRNA of control	Qiagen, Hilden, Germ
Protein G sepherose beads	Sigma, Deisenhofen, Germany
PAR-2 agonist (SLIGAL)	Polypeptide laboratories France
Amplex Red	Invitrogen, Eugene, Oregon, USA
Horse radish peroxidase	Invitrogen, Eugene, Oregon, USA
Antimycin A	Sigma, Steinheim, Germany

2.1.2 Experimental Assay kits

Kits	company
Accu Prime	Invitrogen, Karlsruhe,Germany
Cell Proliferation Reagent WST-1 assay kit	Roche, Dassel, Germany
Fluorescein (FITC) annexin V/ Dead cell apoptosis kit	Invitrogen , Eugene, USA
Glucose uptake assay kit	Cayman Chemical Company
HotStarTaq™ Master Mix kit	Qiagen,Hilden,Germany
HiSpeed Plasmid Midi kit	Qiagen,Hilden,Germany
MinElute PCR Purification kit	Qiagen,Hilden,Germany
MinElute Gel Extraction kit	Qiagen, Hilden, Germany
Magnet Assisted Transfection (MATra)	IBA GmbH, Göttingen, Germany
Supersignal West Pico Chemiluminescent Substrate	Pierce, Rockford, IL, USA
Site-directed mutagenesis kit	Stratagene, Amsterdam Netherlands
Taq Master Mix kit	Qiagen, Hilden, Germany

2.1.3 Inhibitors and antagonist

Inhibitors	company
BAPTA (cellular Ca^{2+} chelator)	Tocris, Bristol, UK
TcY-NH2 (PAR-4 antagonist)	Tocris, Bristol, UK
RWJ 56110 (PAR-1 antagonist)	Tocris, Bristol, UK
Rapamycin (mTOR inhibitor)	Selleckchem, München, Germany
AG1478 (inhibitor of EGF receptor tyrosine kinase)	Calbiochem, Nottingham, UK
AG1296 (inhibitor of PDGF receptor)	Calbiochem, Nottingham, UK
PD98059 (ERK inhibitor)	Tocris, Bristol, UK
SB203580 (p38 MAP kinase inhibitor)	Tocris, Bristol, UK
SP600125 (JNK inhibitor)	Calbiochem, Nottingham, UK
LY294002 (PI3K inhibitor)	Sigma, Steinheim,Germany
Diphenyleneiodonium (mitochondrial ROS inhibitor)	Sigma, Steinheim,Germany
protease inhibitor	Roche, Mannheim,Germany

<center>**Materials**</center>

Primary antibodies and secondary antibodies

Primary Antibodies	company
Rabbit p42/44 MAPK antibody	Cell signaling, Frankfurt, Germany
Rabbit β-arrestin 1 antibody	Cell signaling, Frankfurt, Germany
Rabbit β-arrestin 2 antibody	Cell signaling, Frankfurt, Germany
Phospho-Akt (Ser473) antibody	Cell signaling, Frankfurt, Germany
Rabbit total Akt antibody	Cell signaling, Frankfurt, Germany
Rabbit Caspase 3 antibody	Cell signaling, Frankfurt, Germany
Rabbit GAPDH antibody	Cell signaling, Frankfurt, Germany
Mouse monoclonal antibody against myc	Invitrogen, carlsbad, CA, USA
Mouse Hexokinase I (HK1)	LifeSpan Bioscience, Inc
Rabbit Hexokinase 2 (HK 2)	Cell signaling, Frankfurt, Germany
Rabbit phospho -p38 (Thr180/ Thr182) antibody	Cell signaling, Frankfurt, Germany
Rabbit (phospho) p42/44 MAPK	Cell signaling, Frankfurt, Germany
Rabbit polyclonal antibody against phospho-αB-crystallin (Ser59)	Stressgen, Victoria, Canada
Rabbit phospho-SAPK/JNK antibody (Thr183/Thr185)	Cell signaling, Frankfurt, Germany
Rabbit HIF-1α	BIOZOL, Eching, Germany
Rabbit Cyclin D1 antibody	Cell signaling, Frankfurt, Germany
Rabbit affinity isolated antibody against HA tag	Sigma, St Louis, MO, USA
Rabbit affinity isolated antibody against GAPDH tag	Santa Cruz Biotechnology
Mouse antibody against GAPDH tag	Millipore, Temecula, CA

Seconday antibodies	company
Alexa Fluor 555 goat anti-mouse IgG	Invitrogen Molecular Probes
Goat anti-Mouse IgG	Jackson Immuno Researc
Goat anti-Rabbit IgG	Jackson Immuno Researc

2.1.4 Experimental facilities and instruments

Instruments	company
T3 Thermocycler from Biometra	Biometra, Göttingen, Germany
Electrophoresis power supply,	Bio-Rad, Munich, Germany
Semi-dry Transfer Cell	Bio-Rad, Munich, Germany
GS-800 Calibrated Densitomete	Bio-Rad, Munich, Germany
Gel document system and Gene pulser II	Bio-Rad, Munich, Germany
Chemi Doc ^{TM} XRS , Molecular imager	Bio-Rad, München, Germany
Cell culture incubator	IBS, Fernwald, Germany
Gel-blotting-papers	Schleicher & Schuell, Dassel, Germany
LSM510 laser scanning confocal microscope	Carl Zeiss, Jena, Germany
Axiovert 135 fluorescence microscope	
Microplate reader	Molecular Devices, CA, USA
Thermomixer comfort	Eppendof
UV/visible Spectrophotometer	Pharmacia Biotech
Biofuge pico and 13 R centrifuges,	
Megafuge 1.0 R centrifuge,	
Sorvall$^{®}$ RC-5B Refrigerated Superspeed Centrifuge,	Hanau, Germany
Sorvall$^{®}$ discovery^{TM} 90 ultraspeed centrifuge	
UV/visible Spectrophotometer	Pharmacia Biotech

2.1.5 Buffers

Modified 1× RIPA buffer:

50 mM Tris, 150 mM NaCl, 0.25% Na-deoxycholate, 1 mM NaF, 1 mM Na_3VO_4 and protease inhibitor cocktail tablets (pH=7.4)

TBST

20 mM Tris/HCl, pH 7.6, 137 mM NaCl, 0.1% Tween 20

NaHBS buffer

145 mM NaCl, 5.4 mM KCl, 1 mM $MgCl_2$, 1.8 mM $CaCl_2$, 25 mM glucose, 20 mM HEPES, pH 7.4 adjusted with Tris (hydroxymethyl) aminomethane

PBS

137 mM NaCl, 2.6 mM KCl, 8.1 mM Na_2PHO_4, 1.4 mM KH_2PO_4, pH 7.4

Puck's D1 solution

137 mM NaCl, 5.4 mM KCl, 0.2 mM KH_2PO_4, 0.17 mM Na_2HPO_4, 5.0 mM glucose, 58.4 mM sucrose, pH 7.4

HBSS buffer

50 mM KCL, 0.44 mM KH_2PO_4, 0.34 mM $Na_2HPO_4 \cdot 2H_2O$, 0.41 mM $MgSO_4 \cdot 7H_2O$, 87.4 mM NaCl, 10 nM HEPES, 1.25 mM $CaCl_2$, 4.2 mM $NaHCO_3$, 5.6 mM Glucose, pH=7.3

1 × TAE buffer

40 mM Tris, 20 mM acetic acid, 1 mM Na_2EDTA

Resolving buffer (SDS-PAGE-Laemmli)

750 mM Tris/HCl, pH 8.8

SDS solution

10% (w/v) SDS in H_2O

PER solution

10% (w/v) Ammoniumperoxodisulfat in H_2O

1× Transfer buffer

100 ml of 10 × Transfer buffer (Bio-Rad, München, Germany), 200 ml of Methnol and 700 ml of H_2O

1× Running buffer

100 ml of 10 × Running buffer (Bio-Rad, München, Germany) in 900 ml of H_2O

Membrane stripping buffer

Membrane stripping buffer is from Thermo, Rockford, USA.

2.1.6   Molecular mass markers

2.1.6.1   *Nucleic acid standard marker*

GeneRuler DNA Ladder Mix (100bp, 1kb and 10 kb) were from MBI Fermentas, Germany.

2.1.6.2   *Protein standard marker*

Precision Plus (All Blue) (250-10 kDa) Bio-Rad, München, Germany.

LMW-SDS marker GE Healthcare, München, Germany.

PageRuler Plus Prestained Protein Ladder was from Fermentas.

2.1.7   Primers

Gene	species	Paris of Primers for amplification (5' → 3')	Tm
β-arrestin 1 (HindIII/SacII)	Human	Fw:GAC AAG CTT GCC ACC ATG GGC GAC AAA GGG ACC Re: TCC CCG CGG TCT GTT GAG CTG TGG AGA GC	56°C
β-arrestin 1 (HindIII/XhoI)	Human	Fw:GAC AAG CTT GCC ACC ATG GGC GAC AAA GGG AC Re:CCG CTC GAG CGT CTG TTG AGC TGT GGA GAG C	56°C
β-arrestin 1 (NotI/ XbaI)	Human	Fw: ATA AGA AT G CGG CCG CTA GCC ACC ATG GGC GAC AAA GGG ACC Re: CTA GTC TAG ATC TGT TGT TGA GCT GTG GAG	56°C
β-arrestin 2 (NotI/ XbaI)	Bovine	Fw: CGG GCG GCC GC AAG CCA CCG TCT TCA AG AAA TCG AGT CCT AAC Re: CCG TTC TAG A CTA GCA GAA CTG GTC GTC ATA GTC	58°C
β-arrestin 2 (BgLII/HindIII)	Bovine	Fw: CCA AGA TCT CGC CAC CAT GGG GGA GAA ACC CGG GAC Re: CTT AAG CTT GCA GAA CTG GTC ATA GTC CTC G	58°C

2.1.8   Plasmid Vectors

pEGFP-N1 and ptdTomato-N1 were from Clontech.

pcDNA3.1-Myc-His (B), and pVL1392 were from Invitrogen.

2.1.9   Enzymes and Buffer*s*

T4 DNA Ligase was from Invitrogen, Carlsbad, CA, USA.

T4 DNA Polymerase was from Invitrogen, Carlsbad, CA, USA.

All of the restriction enzymes were from MBI Fermentas, Germany.

The digestion reactions were done by different restriction enzymes corresponding to the suggested buffers.

2.2 Methods

2.2.1 Methods of molecular biology

2.2.1.1 RNA extraction and RT-PCR

Total RNA was extracted from cultured cells using RNeasy Mini kit (Qiagen, Hilden). 1 µg of the harvested RNA was reverse-transcribed by Omniscript™ Reverse Transcription kit (Qiagen), and the resulting cDNA was used as template to amplify the indicated gene.

2.2.1.2 DNA amplification

As for the PCR reaction, the pairs of primers were used which are listed in (Table 2.1.8). The PCR reaction mixture was prepared:

10×Accu Prime ™ pfx Reaction mix	5 µl
Primer FW	1 µl
Primer RV	1 µl
Template DNA	200 ng
Accu Prime ™ DNA Polymerase	0.5 µl
H_2O	X µl
Final volume of reaction mixture	50 µl

The program applied to amplify the gene of β-arrestin 1 and β-arrestin 2 as follows:

95°C -----1 min
↓
95°C ----- 30 sec
↓
56°C / 58°C -----40 sec ⎫
↓ ⎬ **30 × cycles**
72°C-----1 min ⎭
↓
72°C-----5 min
↓
4°C----- pause
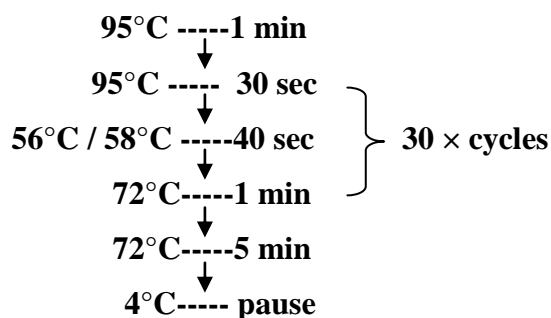
The PCR products were analyzed by electrophoresis with 1% agarose gel containing ethidium bromide, and visualized by Bio-Rad gel document system (Bio-Rad).

2.2.1.3 Plasmid constructs

The cDNA fragments of human β-arrestin 1 and Bovine-β-arrestin 2 containing upstream of restriction enzyme sites and the initiator ATG were amplified by PCR and cloned into the vectors with different tags indicated in the following table respectively.

No.	Inserted DNA	vector	Tag
1	Human-β-arrestin 1	pEGFP	GFP
2	Human-β-arrestin 1	pEYFP	YFP
3	Human-β-arrestin 1	pCDNA3.1(+)	His-myc
4	Human-β-arrestin 1	pvL1392	GST
5	Bovine-β-arrestin 2	ptdTomato-N1	Tomato-red
6	Bovine-β-arrestin 2	PvL1392	HA

2.2.1.4   Generation of the mutated gene

Site-directed mutagenesis kit was used to generate truncations of PAR-2 receptor. Two complimentary oligonucleotides containing the desired gene fragment coding the indicated mutants were synthesized. PAR-2 wild type gene inserted into pEGFP vector was used as template to amplify the target gene. Reaction was performed in a T3 Thermocycler (Biometra), using the following programme:

Initial denaturation at 98 °C for 30 sec

↓

Denaturation at 95°C for 30 sec

↓

Annealing at 55-57 °C for 40-60 sec   **18 × cycles**

↓

Extension for x min at 72°C (2 min/kb)

↓

Extension at 72°C for 5 min

↓

4°C pause
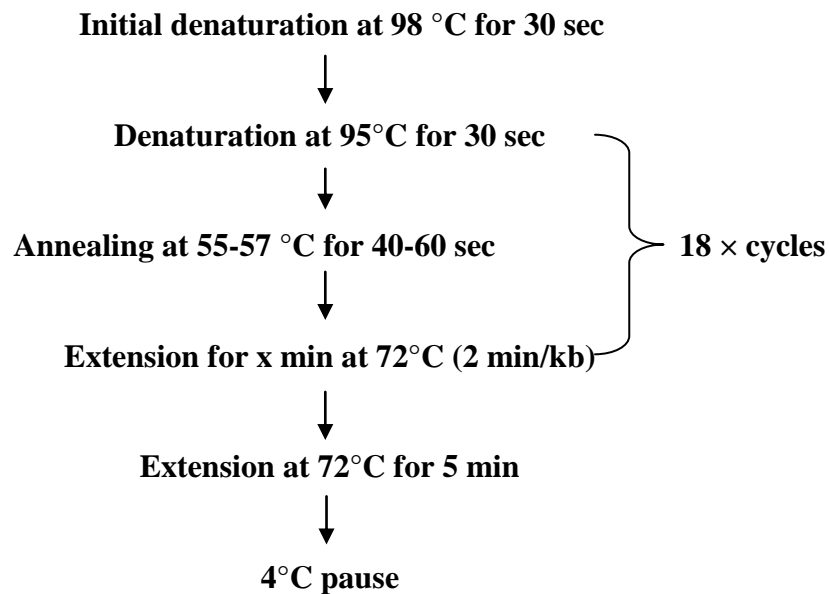
The primers used in the PCR reaction are listed in the follow table

Name	Species	Sequences of the paired primers
S348Z	Rat	5'-TTTGTCTACTACTTTGTTAAGCTTCGAATTCTGCAG-3'
		5'-CTGCAGAATTCGAAGCTTAACAAAGTAGTAGACAAA-3'
C361Z	Rat	5'-GCCAGAAACGCGCTCCTCAAGCTTCGAATTCTGCAG-3'
		5'-CTGCAGAATTCGAAGCTTGCAGGAGCGCGTTTCTGGC-3'
K368Z	Rat	5'-CGAAGCGTCCGCACCGTGAAGCTTCGAATTCTGCAG-3'
		5'-CTGCAGAATTCGAAGCTTCACGGTGCGGACGCTTCG-3'
S379Z	Rat	5'- TCGCTCACTCCAACAAGAAGTCTTCGAATTCTGCAG-3'
		5'-CTGCAGAATTCGAAGCTTCGTGTTGGAGGTGAGCGA-3'
S386Z	Rat	5'TCCAGGAAATCCAGCTCTAAGCTTCGAATTCTGCAG-3'
		5'-CTGCAGAATTCGAAGCTTAGAGCTGGATTTCCTGGA-3'

After the PCR reaction, 1 µl of the *Dpn* I restriction enzyme (10 U/µl) were added to each tube of PCR production. The mixture was immediately incubated at 37°C for 1 h to digest (Adeno) methylated GATC sites, which was useful for removing plasmid template from PCR samples.

For the selection of the positive mutated plasmid, 10 µl of the reaction were used for transformation of DH5α competent cells. Positive clones were selected using Kan[r] or Amp[r] LB agar plates.

2.2.1.5   *Isolation and purification of DNA fragment from agarose gel*

The prospected DNA fragments amplified from PCR reactions were identified by electrophoresis with 1% agarose gel. The specific bands of the target genes embedded in gel were harvested by MinElute Gel Extraction kit (Qiagen, Hilden, Germany) and purified by MinElute PCR Purification kit (Qiagen, Hilden, German).

The purified DNA fragments and selected vectors were digested by the pairs of restriction enzymes (Table 2.1.8) with the suggested buffers from MBI Fermentas Company. The programme used to digest DNA fragments and vectors as follow:

DNA	1 µg
Enzyme A (10 U/µl)	2 µl
Enzyme B (10 U/µl)	2 µl
Buffer (10x)	2 µl
H$_2$O	variable
Final volume	20 µl

2.2.1.6 Ligation reaction

Plasmid vector	1x
DNA	3x
T4 DNA Ligase (1 U/µl)	1 µl
Ligase buffer (5x)	4 µl
H_2O	variable
Final volume	20 µl

2.2.2 Methods of cell biology

2.2.2.1 Preparation and culture of primary astrocytes

Primary astrocytes-enriched cell cultures were obtained from newborn rats, as described previously [126]. In brief, the newborn rats were decapitated; total brains were removed and collected in ice-cold Puck's-D1 solution (137 mM NaCl, 5.4 mM KCl, 0.2 mM KH_2PO_4, and 0.17 mM Na_2HPO_4, 5.0 mM glucose, 58.4 mM sucrose, pH 7.4). The brains were gently passed through nylon mesh (256 µM and 136 µm diameter) and centrifuged at 400 g for 5 min. The cells were collected and resuspended in DMEM containing 10% heat-inactivated FCS, 100 U/ml of penicillin and 100 µg/ml of streptomycin. Astrocytes were seeded in flasks and kept in culture for 10-13 days; thereafter the cells were detached by accutase and reseeded on 6-well plate at the density of 1.95×10^6 cells/well, or 10,000 cells/well of 96-well plates for 24 h before the functional induction or transfection. All of the cell culture and sub-culture were kept in the humidified incubator with 10% CO_2 at 37°C. The medium was changed for the first time after 5 days and thereafter every 2 or 3 days.

2.2.2.2 HEK 293 cell culture

HEK 293 (Human embryonic kidney, epithelial) cells were cultured in DMEM (Dulbecco minimum essential medium) / HAM'S F12 (1:1) with 2 mM Glutamine, 10% FCS (fetal calf serum), 100U/ml Penicillin and 100 µg/ml of Streptomycin (Biochrom, Berlin, Germany). HEK 293 cells were cultured in the incubator with humidified atmosphere of 95% air, 5% CO_2 at 37°C.

2.2.2.3 Synthesis of small Interfering RNA (si-RNA) and Transfection

The pre-validated double-stranded siRNA sequences targeting rat β-arrestin 1 (NM - 012910.1): 5'-AGCCUUCUGUGCTGAGAAC-3'corresponding to positions 441–459 and the non-silencing siRNA duplex: 5'-UUCUCCGAACGUGUCACGU-3' with 2-nucleotide 3'-dtdt overhangs were from QIAGEN GmbH (Hilden, Germany).

2.2.2.4   Transfection of astrocytes with lipofectamine ^{TM} 2000

One day before transfection, astrocytes were reseeded in 6 well plates with 1.95×10^6 cells/well. Astrocytes were transfected with the mixture containing 60 nM siRNA and 6 µl of lipofectamine^{TM} 2000 in 500 µl of FCS-free medium. Thereafter, astrocytes were kept in culture for 48 h after transfection before checking the knocking down efficiency of specific genes by Western blot.

2.2.2.5   Transient Transfection of HEK 293 cells with MATra

HEK 293 cells were split in 60 mm dishes and grown until a cell density of 50-60%. 6 µg DNA was mixed with FCS-free media and 6µl of MATra-solution. The mixture was incubated for 30 min at room temperature. During incubation of the mixture, cell complete medium was changed to 4 ml of serum-free medium; thereafter the DNA/MATra-Mix was added and incubated for 30 min on a magnetic plate at 37°C in incubator. 8 h later, complete media was added to replace with the serum-free medium. 24-48 h post transfection, cells were subsequently used for functional treatments.

2.2.2.6   Stable transfection of HEK 293 cells with DOTAP

To generate the stable cell lines of PAR-2 truncations, the plasmids carrying with PAR-2 mutated genes were transfected into HEK 293 cells with DOTAP liposomal transfection reagent according to the manufacturer's protocol (Roche Diagnostics, Germany). 24 h post transfection, G418 were added to select the positively transfected cell lines.

2.2.2.7   SDS-PAGE

Astrocytes or HEK-293 cells were homogenized in 1×RIPA buffer. After the measurement of protein concentration by the Bradford method, 30-50 µg of protein were separated by 10% to 12.5% sodium dodecyl sulfate polyacrylamide gel electrophoresis (SDS-PAGE) and followed by electro-transfer to nitrocellulose membranes or polyvinyliden difluoride membranes. The membranes were probed with respective primary antibodies overnight at 4°C after blocking by 10% Roti-block for 1 h at room temperature. Further, membranes were incubated with different secondary antibodies corresponding to the sources of primary antibodies for 1 h at room temperature, and proteins were visualized by enhanced chemiluminescence. Membranes were developed by Fuji images and the OD values of bands were quantified by Quantity One quantification software (Bio-Rad) with normalization to the control (GAPDH or total Akt). Or membranes were visualized by molecular imager system (Bio-Rad, München, Germany).

2.2.3 Methods of cellular functional studies

2.2.3.1 Induction of cell death or cell protection

Astrocytes were detached by accutase and reseeded on 6-well plate at the density of 1.95×10^6 cells/well for 24 h. Then astrocytes were deprived of serum overnight before transfection of siRNAs. Astrocytes were transfected with control siRNA or siRNA of β-arrestin 1 for 48 h. Thereafter, the transfected cells were going to deprivation of serum overnight before the treatments.

For the cell death induction, cells were incubated with 0.5 µM staurosporine in fetal calf serum-free DMEM in the absence or presence of thrombin to induce the possible protection through activating PAR-1 for 24 h. The staurosporine and thrombin were added at the same time in the cases of the co-treatment. For Western blot, equal amount of protein were loaded to 12.5% SDS-PAGE gel. Cell apoptosis or protection was checked by quantification of cleaved caspase 3 under the indicated treatments.

2.2.3.2 Cell viability / proliferation assay

Astrocytes were incubated in 96-well plates (10,000 cells / well) with complete medium for 48 h, thereafter the medium was replaced by serum-free medium for another 24 h. After that, astrocytes were treated in the presence of either staurosporine or thrombin plus staurosporine for 48 h. Cell viability was measured by WST-1 assay. In brief, 10 µl WST-1 solutions with 90 µl serum-free medium was added to each well containing astrocytes without disturbance of cells. After 2 h incubation in a humidified atmosphere (37°C, 10% CO_2), the absorbance at 450 nm was measured using a microplate reader. The wells only with medium and WST-1 solution were set as blank.

2.2.3.3 Glucose uptake assay

Astrocytes were seeded in 96 black-clear bottom plates with the density of 10,000-50,000 cells / well. Cells were kept culture for 24 h. After that, astrocytes were deprived of serum over night. The next morning, serum-free medium were replaced by glucose- and serum- free medium for 6 h. Thereafter, astrocytes were treated with or without thrombin at the presence of 2-[N-(7-nitrobenz-2-oxa-1,3-diazol-4-yl) amino]-2-deoxy-D-glucose (2-NBDG, 150 µg/ml) dissolved in glucose- and serum- free medium. The plate was incubated for 10 min in incubator. 10 min later, the assay buffer was applied to wash cells twice. Immediately after washing, 100 µl of assay buffer were added and 2-NBDG taken up by cells was read by microreader at excitation of 485 nm and emission of 535 nm.

2.2.3.4 *Preparation of rat whole brain mitochondria and ROS determination*

Mitochondria (RBM) was isolated from 5 months old Rat brain according the method described before [127]. Protein concentration was measured by Bradford assay. ROS generation was estimated as release of H_2O_2 using the Amplex Red (AR) Invitrogen (Eugene, Oregon, USA)/horse radish peroxidase (HRP) (Sigma-Aldrich Chemie GmbH, Sternheim, Germany) system. The fluorescence was determined in standard black 96 well plates with 50 µg RBM and 1 µM of Antimycin A (Sigma, Steinheim, Germany) in the presence of glutamate and malate (5 mM respectively) as substrate. Besides, each well also contains 2 U/ml HRP and 5 µM Amplex Red. Then the different concentrations of αB-crystallin were added to evaluate the possible inhibitory effects on ROS release from RBM. The signal from the wells which contained RBM and Antimycin A without Glutamate and Malate were set as control. Before reading the data, αB-crystallin was incubated with mitochondria for 20 min.

2.2.3.5 *Intracellular ROS production measurements*

Astrocytes were seeded in 96 black-clear bottom plates with the density of 10,000 - 50,000 cells / well for 24 h. Then astrocytes were incubated in serum-free medium overnight. The next day, astrocytes were incubated with 25 µM $DCFH_2$-DA dissolved in 200 µl of HBSS buffer in the presence or absence of different concentrations of thrombin for 15 min at 37°C. 15 min later, the basal level of ROS production were read immediately by microreader at 504 nm excitation, 530 nm emission. Then the plate was kept at 37°C in the drawer of the microplate reader for 30 min to obtain the data of the ROS production in this period.

$DCFH_2$-DA is a stable non-fluorescent cell permeable compound. When astrocytes uptake this reagent, $DCFH_2$-DA is hydrolyzed to $DCFH_2$ by intracellular esterases and rapidly oxidized to the highly green fluorescent component, 2,7-dichlorofluorescein (DCF) by endogenous hydroperoxides. As a result, the ROS production level can be measured by DCF fluorescence. The formula used to calculate ROS production as follow:

$$ROS = \frac{Ft_{30} - Ft_0}{Ft_0} \times 100$$

Ft_0 = basal level of ROS, Ft_{30} = 30 min of ROS production

2.2.3.6 *Immunoprecipitation (IP)*

HEK-293 cells were transiently co-transfected with human β-arrestin 1 or Bovine β-arrestin 2 genes inserted into pcDNA 3.1(+) vector with myc-his tag and αB-crystallin inserted into PEAK 10 vector with HA tag. The cells transfected only with αB-crystallin-HA

were set as negative control. 36 h after transfection, cells were incubated with serum-free medium for another 30 min, and then 100 nM of trypsin was added to activate PAR-2 for another 30 min. Agonist was removed after 30 min through aspirating medium immediately, and cell lysates were prepared by 1×RIPA buffer and quantified by the Bradford method. Equal amounts of lysates were rotated with the anti-myc antibody (1:200, Invitrogen) together with protein G beads at 4 °C overnight. The next morning, beads were centrifuged (4800 rpm) for 3 min and washed by 1×RIPA buffer without protease inhibitor three times. The protein bound beads were boiled in Laemmli buffer for 10 min at 96°C, then separated by SDS-PAGE, and immunoblotted with the anti-HA antibody (1:5000, Sigma).

2.2.3.7 *Immunostaining*

HEK-293 cells were seeded on the cover slides 24 h before transient co-transfection of β-arrestin 1/2 with GFP or YFP tag and αB-crystallin with myc tag. 36 h post transfection, cells were deprived of serum for 30 min. Then the transfected cells were exposed to 100 nM trypsin to activate the PAR-2 receptor for different time periods. Cover slides were washed by cold PBS twice after the treatment of trypsin. Cells were fixed with 4% paraformaldehyde solution (PFA)(4% sucrose, 120 mM Na-Phosphate buffer, pH 7.4) for 30 min at RT, after removal of PFA, fetal serum blocking buffer (FSBB; 6% FCS, 20 mM Na-phosphate buffer, 0.45 M NaCl, 0.1% Triton-X100, pH 7.4) was added for 20 min to block unspecific binding. Coverglasses were washed three times in low salt (0.15 mM NaCl and 10 mM phosphate), three times in high salt (0.5 mM NaCl and 20 mM phosphate) buffer. Cells were then incubated with primary myc antibody (1:500) overnight.

After the incubation of primary antibody, cells were washed again by high salt buffer three times (10 min for each washing). Cells were exposed into the FBSS solution with secondary antibody (goat anti-mouse alexa 555; 1:200) for 90 min at RT without light exposure.

After incubation with secondary antibodies, cells were washed once with high salt buffer, once with 120 mM Na-phosphate, and once with 5 mM Na-phosphate. After washing with PBS (pH 8.9), cover slides were drained and mounted onto microscope slides. Fluorescence images were captured sequentially at excitation of 488 nm, and 543 nm with a LSM510 laser scanning confocal microscope (Carl Zeiss, Jena, Germany).

2.2.3.8 *Fluorescence imaging analysis*

Astrocytes were seeded on the 35 mm disposable dishes with the optical quality of glass for superior high resolution microscopy image. Astrocytes were seeded at the density of 1.5×10^5 cells/well and cultured for 24 h. After the cell death inducement, cold PBS was used

to wash cells three times. Then the cells were dyed with 500 µl of 1× annexin-V dye solution containing 5 µl annexin V-conjugated to fluorescence (excitation of 488 nm), 1 µl (100 µg/ml) of PI (excitation of 543 nm), 10 µl RNase, 1:20,000 of Syto 59 (excitation of 633 nm). Among them, annexin V recognizes the apoptotic cells with green fluorescence, PI is incorporated into the late apoptotic /dead cells with red fluorescence and Syto 59 stains the RNA and DNA in both live and dead cells displaying blue fluorescence. After 15 min of incubation with dye solution at room temperature, cells were gently washed by 1×PBS for three times. After that, 1 ml of 1×annexin-V binding buffer was added to the cells. Cell death or protection were immediately examined by a Zeiss inverted LSM 510 laser scanning confocal microscope. The percentage of dead cells was the ratio of PI positive cells to Syto 59 positive cells. The proportion of apoptotic cells was evaluated by the ratio of annexin-V positive cells to Syto 59 positive cells. For each treatment, two areas were randomly selected and counted.

2.2.3.9   *Cytosolic Ca^{2+} measurement*

To monitor the Ca^{2+} mobilization in different PAR-2 truncations, the stable transfected HEK-293 cells carrying different mutants of PAR-2 were challenged under a series of different concentrations of trypsin. For experiments, cells were loaded with the Ca^{2+} sensitive Fura-2AM (2 µM, 0.02% Pluronic, 30 min at 25 °C). The dye remains intracellular after cleavage by non-specific esterase activity. Fluorescence signals were acquired at 510 nm emission during alternate excitation at 340 nm (Fura-2AM bound to free Ca^{2+}) and 380 nm (unbound Fura-2AM molecule) every 3 sec. The intracellular Ca^{2+} concentrations were measured with an imaging system (Agilent Technologies/TILL Photonics, Gräfelfing, Germany) attached to a Zeiss Axioscope microscope (Carl Zeiss, Jena, Germany).

The data were obtained from at least three independent experiments. Only cells with a clearly membrane-localized GFP-signal and with the typical calcium response kinetics upon challenge of agonist were included in the data analysis.

2.3.   Statistical analysis

Data were expressed as means ± SEM and analyzed for statistical significance by using one-way analysis of variance (ANOVA), followed by Dunnett's test to evaluate the data with comparison of control, or by Newman–Keuls test to assess the statistical meaning between different experimental groups. The criterion for statistical significance was $p < 0.05$.

3   Results

3.1   Activation of PAR-1 rescues β-arrestin-1-silenced astrocytes from apoptosis through PI3K/Akt signaling pathway.

3.1.1   Knock-down of β-arrestin 1 reduces resistance to staurosporine-induced apoptosis in astrocytes.

To clarify the role of β-arrestin 1 plays in apoptosis of astrocytes, the cells were transfected with specific siRNA to reduce the endogenous β-arrestin 1 level (Fig. 3.1.1a). Thereafter, the apoptotic process was induced through incubation of astrocytes with 0.5 μM of staurosporine for 24 h. The level of cleaved caspase 3 was monitored by Western blot of astrocytes transfected with the siRNA of β-arrestin 1 or control siRNA. Application of staurosporine to astrocytes caused apoptosis, which was demonstrated by the increased production of cleaved caspase 3 (Fig. 3.1.1b).

An increased level of cleaved caspase 3 was detected in β-arrestin 1-siRNA-transfected astrocytes compared to non-silenced astrocytes (Fig. 3.1.1b). Quantitative analysis revealed that in β-arrestin 1-lacking astrocytes, a level of 324% of cleaved caspase 3 as compared to non-silenced astrocytes with the same treatment (Fig. 3.1.1c). Thus, under the challenge of staurosporine, β-arrestin 1-lacking astrocytes displayed a higher level of apoptosis compared to non-silenced cells.
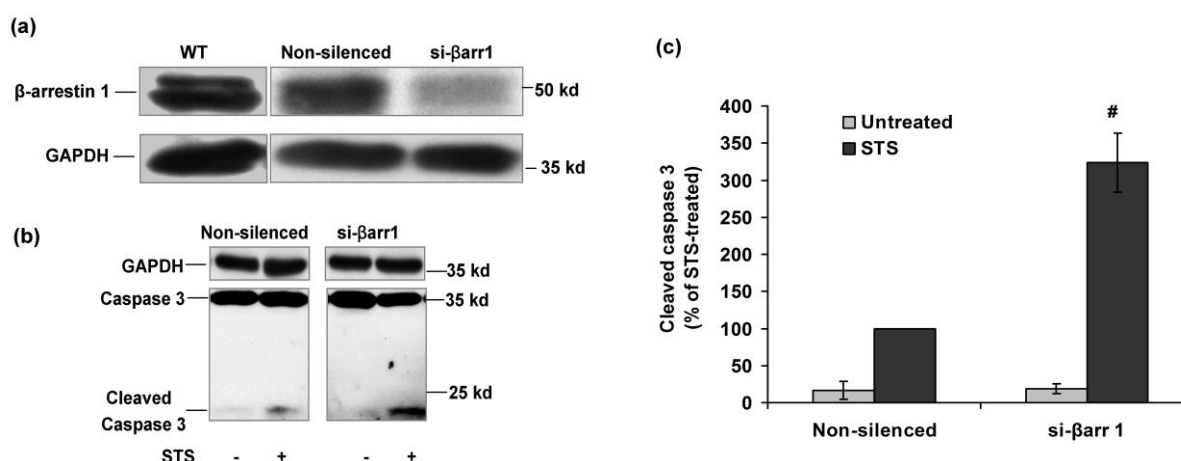
Fig. 3.1.1 Down regulation of β-arrestin-1 in astrocytes exacerbates apoptosis in astrocytes.
Astrocytes were transfected with non specific targeted sequence of siRNA (Non-silenced) or siRNA of β-arrestin-1 for 48 h (a). The gene knock down efficiency were evaluated by Western blot. (b) For the apoptosis induction, the transfected astrocytes were deprived of FCS over night and then the transfected astrocytes were incubated with 0.5 μM staurosporine (STS) in FCS- free DMEM medium for 24 h. 50 μg of protein were loaded for each lane. The experiments were repeated for at least three times independently and the representative blots were shown. (c) The level of cleaved caspase 3 under the different conditions as described and normalized to the value of GAPDH. The level of cleaved caspase 3 in non-silenced astrocytes under the treatment of staurosporine was set as control (100%). Data shown in Fig. 3.1.1c represents the mean ±SEM of three independent experiments. # p <0.001 as compared with control (n=3).

3.1.2   Concentration dependence for thrombin to protect astrocytes.

Staurosporine (STS; 0.5 μM) was used to induce cell death in astrocytes and cell viability was checked by the WST-1 assay as shown in Fig. 3.1.2. Compared to the cells treated with STS, the untreated cells showed 40% higher in viability. On the other hand, 0.1 U/ml to 10 U/ml of thrombin were added in the simultaneous presence of STS to the astrocytes. Upon treatment with 0.5 U/ml and 1 U/ml of thrombin, the viability of astrocytes was significantly increased from 100% to 154% and 159%, respectively. When the concentration of thrombin was increased to 5 U/ml and 10 U/ml, the viability of astrocytes failed to show any significant protection. STS-treated astrocytes displayed a dose-response curve for thrombin. Thus, 1 U/ml of thrombin was used in the following experiments as the optimal concentration for cytoprotection.
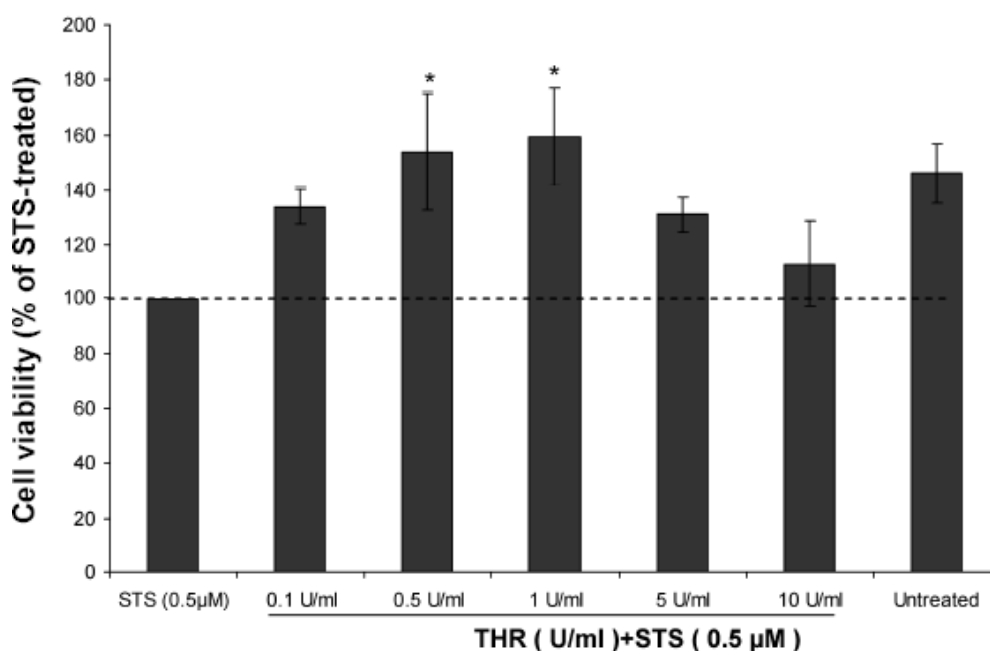
Fig. 3.1.2 The concentration dependence of thrombin to protect astrocytes from apoptosis. Astrocytes were incubated with 0.5 μM staurosporine (STS) or 0.5 μM STS plus various concentrations of thrombin (THR), or serum-free medium (Untreated) for 48 h. Protection by thrombin against treatment with STS in astrocytes was checked by WST-1 assay. The viability of cells treated only with 0.5 μM STS was set as 100%. The bars show the mean value ± S.E.M. (* $p < 0.05$, compared to 100%, n=4).

3.1.3 Thrombin decreases the levels of cleaved caspase 3 and cell death in β-arrestin 1-deficient astrocytes.

Thrombin protects astrocytes from staurosporine-induced cell death. It promoted the survival of astrocytes, as shown in the cell protection assay above in Fig. 3.1.2. We examined whether thrombin also rescued the astrocytes from apoptosis caused by staurosporine in β-arrestin 1-siRNA-transfected astrocytes. In the experiments, we used 1 U/ml thrombin which was identified as the optimal concentration to exert cytoprotection applied to astrocytes. Western blot results showed that the level of cleaved caspase 3 induced by the apoptotic stimulus staurosporine was reduced by thrombin treatment in β-arrestin 1-silenced astrocytes (Fig. 3.1.3a and b, lane 7 *vs* lane 8). However, the reduction was only slightly apparent in β-arrestin 1 non-silenced astrocytes (Fig. 3.1.3b, lane 3 *vs* lane 4).

Furthermore, astrocytes were monitored the proportions of early apoptotic and late apoptotic thrombin annexin V and PI staining with methods described in 2.2.3.6. The data from fluorescence imaging analysis showed that staurosporine caused a significantly higher percentage of PI-positive cells (dead cells) in β-arrestin 1-deficient astrocytes than in non-silenced astrocytes (45% *vs* 24 %). Interestingly, the percentages of dead cells in β-arrestin 1-silenced astrocytes were largely decreased (from 45% to 10 %) as compared to that in non-silenced astrocytes (24% to 11%) when the cells were co-treated with STS and thrombin (Fig. 3.1.3c). However, there were no significant differences in the percentages of apoptotic cells detected by annexin V staining between β-arrestin 1-silenced and non-silenced astrocytes. In addition, thrombin treatment failed to reduce the number of apoptotic astrocytes in both β-arrestin 1-silenced and non-silenced astrocytes (Fig. 3.1.3d).
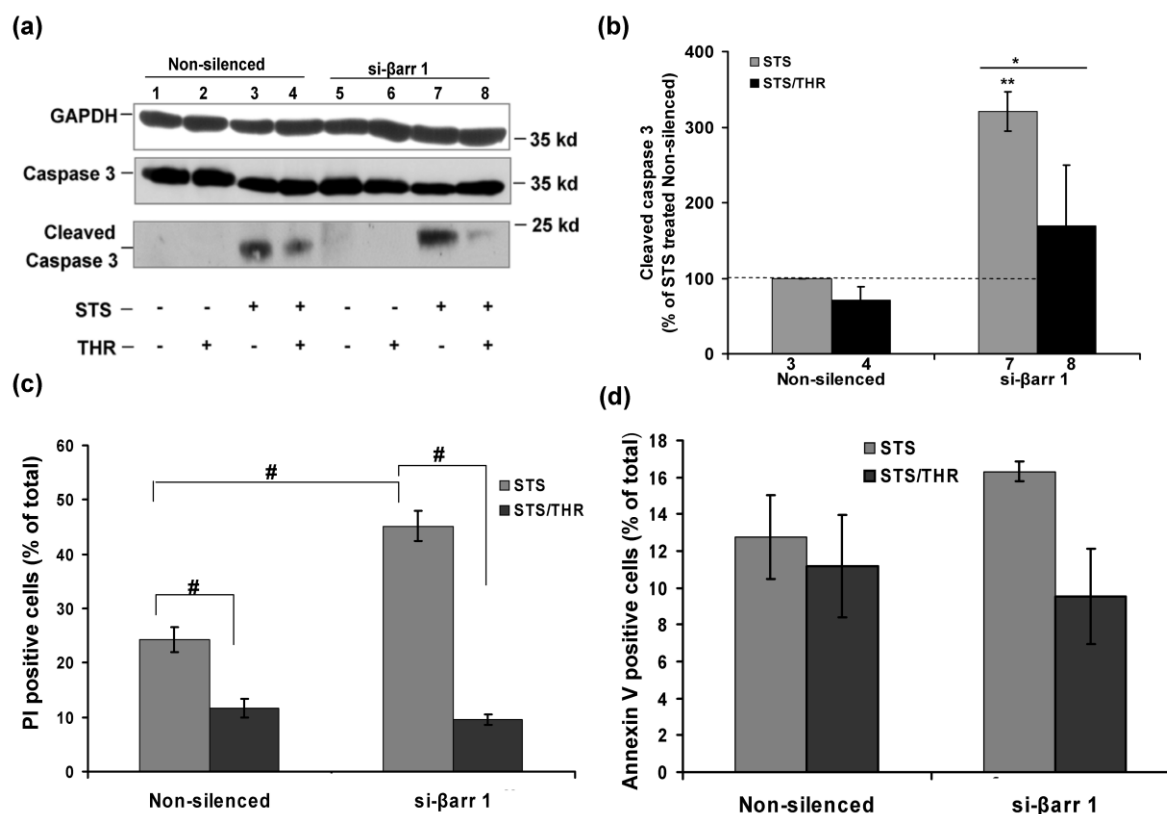
Fig. 3.1.3. Thrombin potently protects β-arrestin 1-deficient astrocytes from cell death.

(a) Thrombin reduced the cleaved caspase 3 protein level in control si-RNA-transfected (Non-silenced) and si-β-arrestin 1 (si-βarr1) astrocytes. Apoptosis or protection was induced by staurosporine (STS, 0.5μM) without or together with thrombin (THR; 1 U/ml) treatment for 24 h. The cells treated with buffer were used as control (lane 1). (b) The quantification of cleaved caspase 3 was normalized to GAPDH and STS-treated non-silenced cells were taken as 100% (n=3). (c) Astrocytes were stained with PI after each treatment indicated to get the ratio of late apoptotic cells to total cells. STS induced significant higher percentage of PI-positive astrocytes in β-arrestin 1-deficient astrocytes as compared to that in non-silenced astrocytes. And thrombin significantly reduced the percentage of PI positive cells in both non-silenced astrocytes and β-arrestin 1 lacking astrocytes (# p <0.001). (d) After the indicated treatments, astrocytes were stained with annexin V to evaluate the ratio of early apoptotic cells to total cells. There were no differences in the percentages of annexin-V positive cells in both non-silenced astrocytes and β-arrestin 1-lacking astrocytes under STS treatment. At the same time, thrombin failed to show any significant effects on decreasing the number of annexin-V positive cells in both non-silenced astrocytes and β-arrestin 1 lacking astrocytes. The numbers under the X-axis in (b) correspond to the respective lane numbers given in the Western blot in (a).

35

3.1.4 Downregulation of β-arrestin 1 enhances the long-term Akt (Ser 473) phosphorylation stimulated by thrombin.

The PI3K/Akt signaling pathway is the most important pathway related to cell survival, as revealed in many studies. We wanted to find out whether the protection effects of thrombin treatment was connected to activation of the PI3K/Akt signaling pathway in both non-silenced and β-arrestin 1-deficient astrocytes. Cells were incubated in the absence or presence of 1 U/ml thrombin together with staurosporine for long time periods lasting up to 24 h. Interestingly, after long time incubation with thrombin (24 h), β-arrestin 1-deficient astrocytes showed a higher level of Akt phosphorylation, as compared to the control siRNA-transfected astrocytes. This indicated that β-arrestin 1 has a negative control over the thrombin-activated long-term Akt (Ser 473) phosphorylation (Fig. 3.1.4a).

We quantified the thrombin-stimulated phosphorylation of Akt after long time stimulation (Fig. 3.1.4b). It can be seen from the quantification of phosphorylation of Akt that only the β-arrestin 1-silenced cells exposed to the combined treatment of thrombin and staurosporine (lane 10) showed a significant increase in phosphorylation of Akt compared to the untreated control cells. The non-silenced untreated cells were set as control, which was taken as 100% (lane 1). Moreover, in β-arrestin 1-silenced astrocytes, in the presence of staurosporine, the 24-h application of thrombin significantly stimulated the phosphorylation of Akt, as compared to the cells treated with staurosporine alone (lane 10 *vs* lane 9). Strikingly, in β-arrestin 1-deficient astrocytes, co-treatment with staurosporine and thrombin for 24 h significantly enhanced the Akt phosphorylation as compared to that in the control si-RNA transfected astrocytes with the same co-treatment with staurosporine and thrombin (lane 10 *vs* lane 5).

Taken together, in staurosporine-treated astrocytes, β-arrestin 1 negatively regulates the long-term Akt (Ser 473) phosphorylation under the challenge of thrombin. The inhibition exerted by β-arrestin 1 apparently disappears in the absence of this protein. This causes the positive overshoot in Akt (Ser473) phosphorylation seen in Fig. 3.1.4b.

(a)

(b)
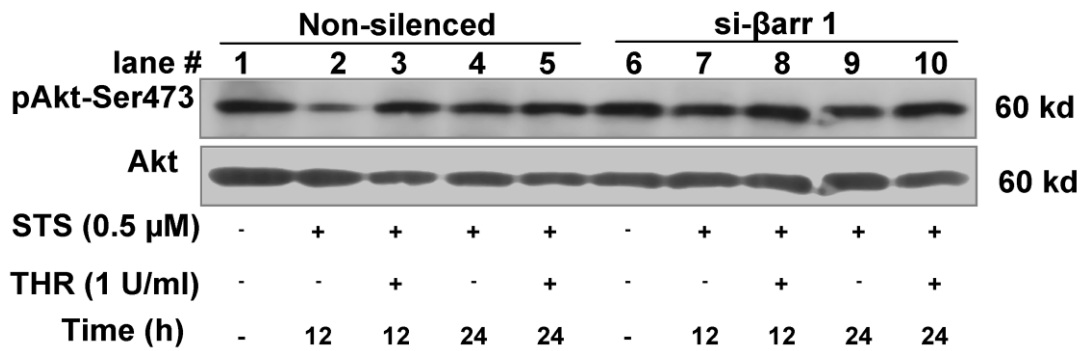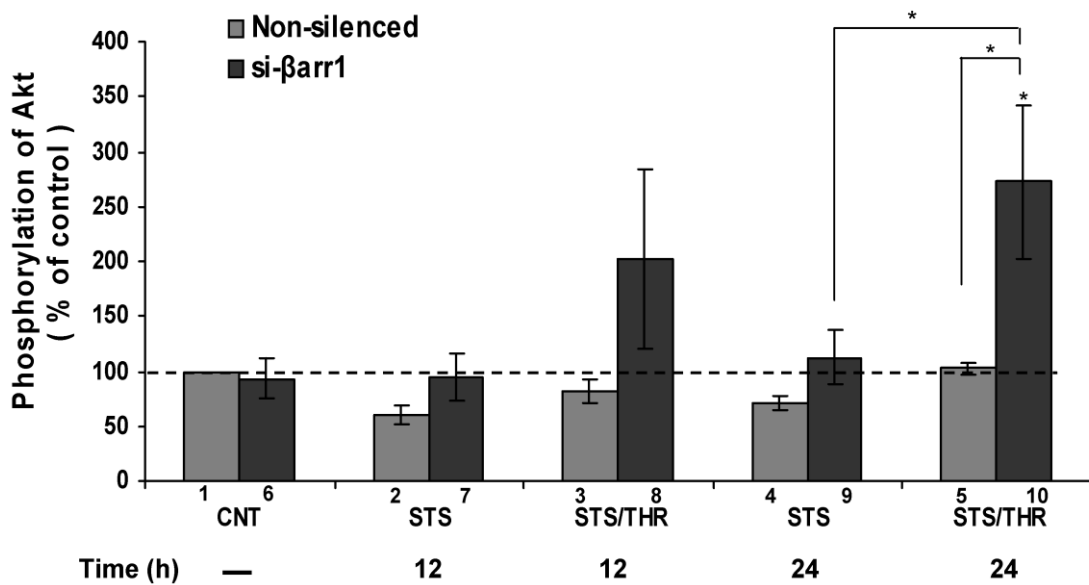
Fig. 3.1.4 β-Arrestin 1 inhibits thrombin-activated long-term Akt phosphorylation in astrocytes. (a) Astrocytes were transfected with control si-RNA (Non-silienced) and si-β-arrestin 1 (si-βarr1) for 48 h. Then the transfected cells were treated with the STS or the combination of staurosporine (STS) and thrombin (THR). Phosphorylation of Akt (Ser 473) was determined by Western blot and total Akt was used to verify equal loading. (b) Quantification of phosphorylation of Akt (Ser 473). Quantity One Densitometry software was used to determine the values for the ratio of phosphorylated Akt to total Akt at 12 h and 24 h. The value of phosphorylated Akt (Ser 473) from non-silenced si-RNA-astrocytes without any treatment was set as 100%. Data are shown as the means ± S.E.M from 4 independent experiments. The significances were got from the comparisons between different bars signified by lines otherwise the comparison were made to 100% (* $p < 0.05$, n=4). The numbers under the X-axis correspond to the respective lane numbers given in the Western blot in (a).

3.1.5 Blockade of the PI3K/Akt signaling pathway by specific inhibitor abolishes the cytoprotection through thrombin.

To evaluate whether the PI3K/Akt signaling pathway plays an important role in the cytoprotection caused by thrombin, the compound LY294002 was used as an inhibitor to block the PI3K/Akt signaling pathway. Astrocytes transfected with control siRNA or siRNA of β-arrestin 1 were incubated with 20 μM of LY294002 together with 1 U/ml of thrombin. The inhibitory effects exerted by LY294002 on phosphorylation of Akt were studied to confirm the potency of the inhibitor. In a time series we determined the change of phosphorylation of Akt at Ser 473. Results from the Western blot demonstrate that LY294002 potently blocks the PI3K signaling pathway. LY294002 significantly inhibits the phosphorylation of Akt (Ser 473). After 10 min, the phosphorylation was clearly reduced and after longer stimulation (up to 2 h), the phosphorylation of Akt was nearly undetectable (Fig. 3.1.5a). This confirms that LY294002 is an effective inhibitor of the PI3K/Akt signaling pathway in astrocytes. Therefore, we used it for our further experiments.

The inhibitor LY294002 was applied to astrocytes to block the PI3K/Akt signaling pathway to verify whether the PI3K/Akt signaling pathway is crucial for survival of astrocytes. Cell death was induced with staurosporine both in the non-silenced control and β-arrestin 1-lacking astrocytes. We stimulated these cells with 1 U/ml of thrombin in the absence or presence of LY294002. The apoptosis was checked by the quantification of cleaved caspase 3 level under the respective treatments. Examples, as given in Fig. 3.1.5b, were used for the quantitative analysis displayed in Fig. 3.1.5c. The latter shows that staurosporine caused more than three times higher level of cleaved caspase 3 in β-arrestin 1-lacking astrocytes compared to control siRNA-transfected astrocytes (lane 8 *vs* lane 3). This confirms that β-arrestin 1 is necessary for astrocytes to resist the apoptosis induced by staurosporine.

In addition, thrombin treatment in the presence of staurosporine significantly inhibited the formation of cleaved caspase 3 in β-arrestin 1-deficient astrocytes (lane 9 *vs* lane 8). Furthermore, in β-arrestin 1 siRNA-transfected astrocytes, blockade of the PI3K/Akt cascade by LY294002 caused an about 400% higher level of cleaved caspase 3 than in the control siRNA-transfected cells under staurosporine treatment (lane 10 *vs* lane 3). The latter was taken as 100%. Thus, the decreased cleavage of caspase 3 resulting from the thrombin co-treatment was dramatically reversed by the application of LY294002 ((lane 9 *vs* lane 10) and (lane 4 *vs* lane 5). Also in the non-silenced astrocytes, application of staurosporine / thrombin

/ LY294002 leads to 270% increase in cleaved caspase 3 level, as compared to the control non-silenced siRNA-transfected cells under staurosporine treatment (lane 5 *vs* lane 3).

(a)

(b)

(c)
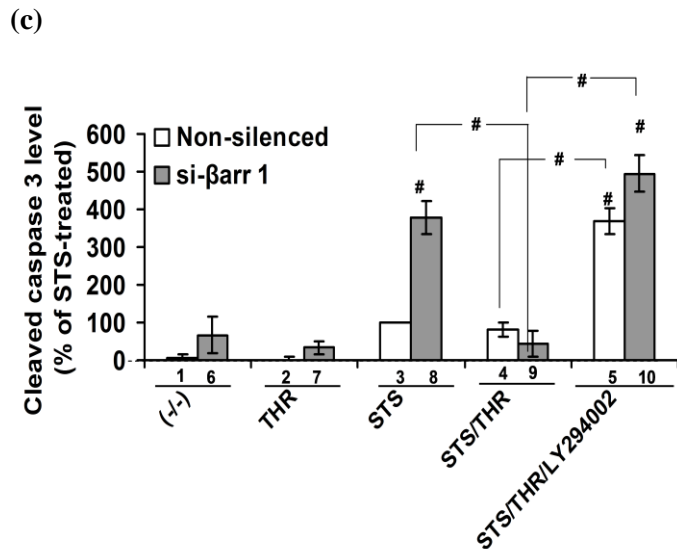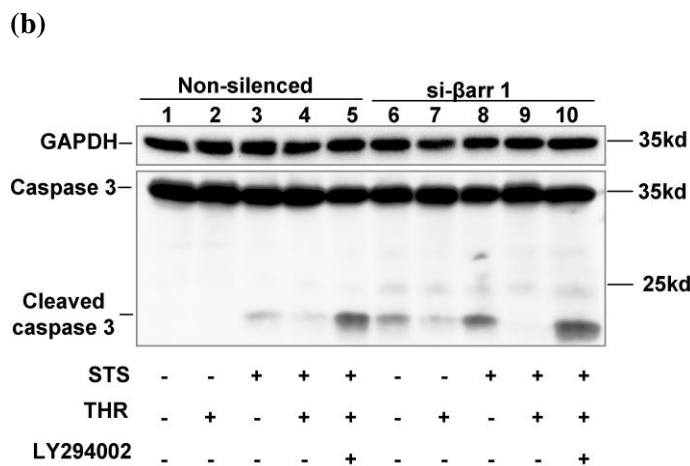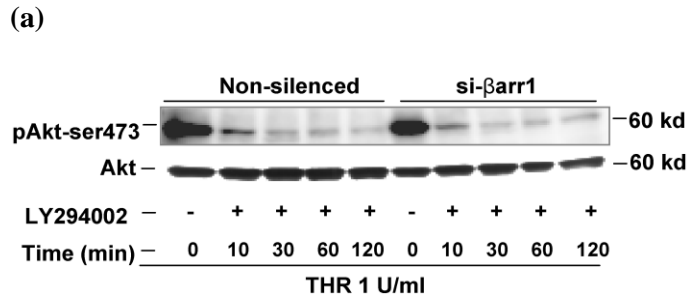
Fig. 3.1.5 The PI3K inhibitor LY294002 blocks the protection by thrombin in both non-silenced and β-arrestin 1-depleted astrocytes.

(a) Astrocytes were transfected with control siRNA (Non-silenced) or si-β-arrestin 1 (si-βarr1) under incubation with inhibitor of PI3K (LY294002) and thrombin (THR) for different times, the phosphorylation of Akt (Ser 473) was determined by Western blot. 10 min after application of LY294002, the phosphorylation of Akt (Ser 473) stimulated by thrombin was effectively inhibited. A representative Western blot of phosphorylation of Akt (Ser 473) is shown here (n=3). The numbers above the pAkt blot indicate the different lanes in the blot.

(b) Representative Western blot of cleaved caspase 3 in astrocytes treated with staurosporine (STS) or STS / THR or STS / THR / LY294002 for 24 h. GAPDH was used to verify the equal amount of protein loaded.

(c) Quantification of cleaved caspase 3 values is given as the ratio of cleaved caspase 3 to GAPDH. The value of cleaved caspase 3 from control siRNA transfected astrocytes, which were treated by 0.5 μM staurosporine was normalized and taken as 100%. Statistical analysis for difference of cleaved caspase 3 values from staurosporine-treated cells are compared between the two different bars delineated by lines otherwise the comparison was made to 100% with the indication by # $p < 0.001$ (n=7). The numbers under the X-axis correspond to the respective lane numbers given in the Western blot in (b).

3.1.6 Thrombin-induced transactivation of PDGF and EGF receptors contributes to the Akt (Ser 473) phosphorylation in β-arrestin 1-silenced astrocytes.

The transactivation by thrombin of the EGF receptors rather than of the PDGF receptors initiates the Akt signaling pathway. This connection was established in retinal psigment epithelium cells [58]. To investigate whether thrombin induced-transactivation of EGF or PDGF receptors contributed to Akt activation which protects astrocytes from cell death, we tested the effects of specific PDGF receptor and EGF receptor inhibitors on thrombin-induced Akt (Ser 473) phosphorylation. The representative blots are shown in Fig. 3.1.6a. First, thrombin induced a significant increase of Akt (Ser 473) phosphorylation in β-arrestin 1-lacking astrocytes as compared to that in non-silenced astrocytes under the combined treatment of staurosporine for 24 h. On the other side, the application of LY294002 completely abolished the phosphorylation of Akt (Ser 473) in astrocytes transfected with both kinds of siRNA (lane 3 and 8).

Blockade of the activity of EGF receptors by AG1478 or PDGF receptors by AG1296 reduced the phosphorylation level of Akt (Ser 473) activated by thrombin in the β-arrestin 1-deficient astrocytes (lane 9 and 10). However, neither the blockade of EGF receptors nor of PDGF receptors had an effect on thrombin-stimulated Akt (Ser 473) phosphorylation in non-silenced astrocytes. In conclusion, thrombin-induced transactivation of EGF receptors and PDGF receptors contributes to thrombin-induced Akt (Ser 473) phosphorylation in β-arrestin 1-silenced astrocytes (Fig. 3.1.6a and b).

(a)

(b)
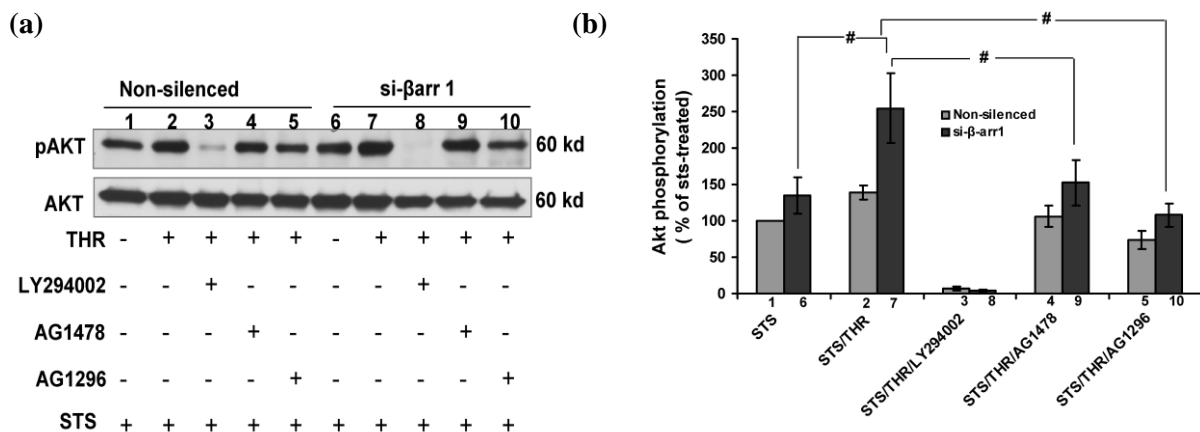
Fig. 3.1.6 Blockade of EGF and PDGF receptors decreased the level of phosphorylation of Akt (Ser 473) caused by thrombin in β-arrestin 1-deficient astrocytes. The control siRNA (Non-silenced) and si-β-arrestin 1 (si-βarr1)-transfected astrocytes were stimulated as indicated for 24 h. AG1478 (10 μM) is used to inhibit EGFR tyrosine kinase activity and AG1296 (10 μM) is used to block the PDGF receptor. (a) Astrocytes were incubated with the respective inhibitors throughout the experiments. A representative Western blot is shown. (b) Quantification of the Akt (Ser 473) phosphorylation normalized to total Akt. The value of phosphorylation of Akt (Ser 473) from control astrocytes or si-β-arrestin 1-transfected astrocytes which were treated with staurosporine (STS) alone was normalized and set to 100%. Significant differences of phosphorylation of Akt (Ser 473) levels under various treatments are analyzed between the two different bars delineated by lines or compared to 100% (n=4, # p<0.001). The numbers under the X-axis correspond to the respective lane numbers given in the Western blot in (a).

3.1.7 β-arrestin 2 is not involved in regulation of apoptosis in astrocytes.

In order to investigate whether β-arrestin 2 plays cytoprotective functional role in astrocytes, β-arrestin 2 was downregulated in astrocytes with the same method used to silence β-arrestin 1. After the confirmation of the knockdown efficiency (Fig. 3.1.7a), the cells were incubated with staurosporine 24 h or combination of staurosporine, thrombin and LY294002. The cleaved caspase 3 were firstly checked as the apoptotic marker protein by Western blot (Fig. 3.1.7b), and the cleaved caspase 3 were quantified. The quantification value was got by the ratio of cleaved caspase 3 to GAPDH and then normalized to staurosporine-treated (Fig. 3.1.7c). According to the quantification data, STS in the β-arrestin 2-deficient astrocytes failed to induce a significant higher cleavage of caspase 3 than that seen in the control siRNA transfected astrocytes (lane 8 *vs* lane 3). The application of thrombin was able to decrease the level of cleaved caspase 3 in β-arrestin 2-silenced astrocytes slightly (lane 9 *vs* lane 8). When inhibiting the PI3K signaling pathway by LY294002, the cleaved caspase 3 was significantly increased in both non-silenced astrocytes and β-arrestin 2-silenced astrocytes (lane 5 and lane 10), but the levels of cleaved caspase 3 show no significant differences between these two groups. To sum up, unlike β-arrestin 1, β-arrestin 2 is unimportant for antiapoptosis in astrocytes.

(a)

(b)

(c)
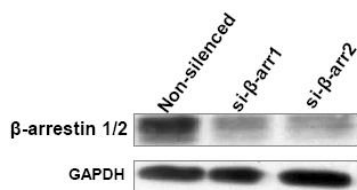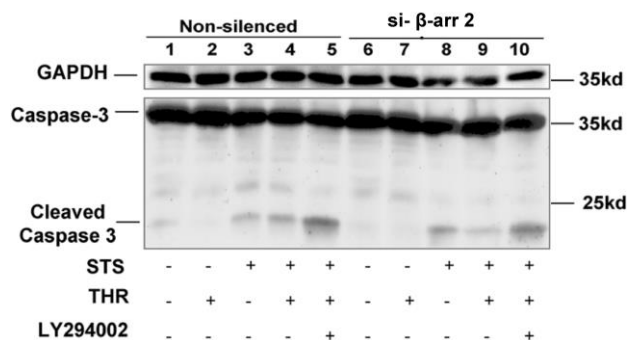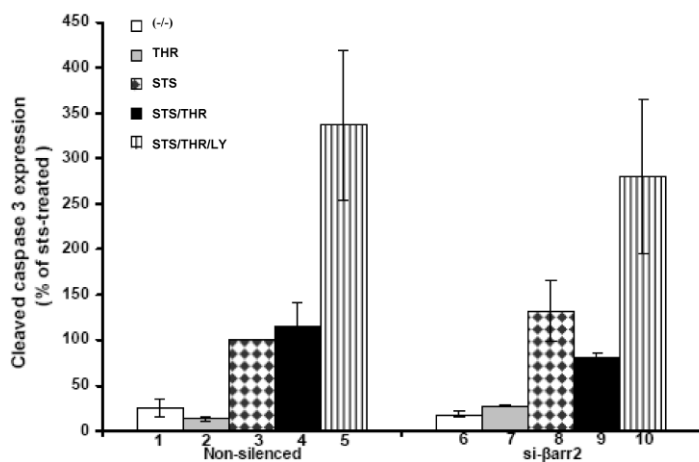
Fig. 3.1.7. β-arrestin 2 is dispensable for astrocytes to resist apoptosis.

(a) Down regulation of β-arrestin 1 and 2 in astrocytes for 48 h, then the knockdown efficiency was evaluated by Western blot, and the representative Western blot was shown to confirm the knock down efficiency.

(b) Astrocytes were transfected with the non-silenced si-RNA and β-arrestin 2-silenced siRNA for 48 h, and then cells were incubated with FCS free medium over night. The next morning, astrocytes were incubated with staurosporine (STS), or the combination of thrombin (THR) and STS, or the mixture of STS, THR and LY294002 (LY) for 24 h. All of the reagents were added to the cells at the same time and incubated during the whole procedure. Western blot were done to detect the levels of cleaved caspase 3 to assess the apoptosis and protection, and the house-keeping protein GAPDH was used as loading control. The representative blot is shown here.

(c) The quantification of the cleaved caspase 3 under the various treatments from two independent experiments. The data from non-silenced astrocytes with STS treatment was set as 100% (n=3). The numbers under the X-axis are corresponding to the respective lane numbers given in the Western blot in (a).

3.2 Thrombin-activated PAR-1 promotes the proliferation of astrocytes by multiple mechanisms

3.2.1 The concentration dependence of thrombin-promoted proliferation of astrocytes.

Thrombin was demonstrated to promote astrocytes proliferation [128]; however, there is no evidence showing the optimal concentration of thrombin to increase astrocytes proliferation. Here we used a series of concentrations of thrombin from 0.1 U/ml up to 5 U/ml to determine which will be the optimal concentration for inducing astrocytes proliferation. According to the data, 0.5 and 1 U/ml significantly increased the cell proliferation with 174% and 175%, respectively, as compared to the control (100%). When the concentration of thrombin was increased to 5 U/ml, the percentage of the proliferation declined to 149% (Fig. 3.2.1). Consequently, the optimal concentration of thrombin to stimulate astrocytes proliferation is between 0.5 U/ml to 1 U/ml. We used 1 U/ml for the further experiments.
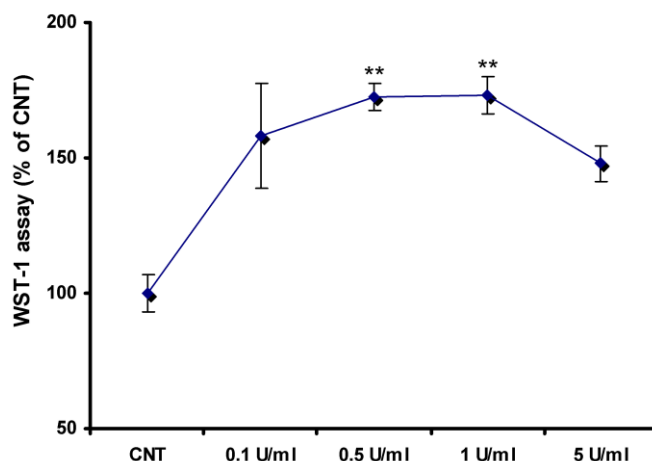
Fig. 3.2.1 **Proliferation of astrocytes induced by different concentrations of thrombin**. Astrocytes were seeded on 96 well plates one day before the induction of proliferation by thrombin. Then astrocytes were deprived of FCS overnight. The next morning, astrocytes were incubated with different concentration of thrombin in serum free medium. 48 h later, cell proliferation were estimated by WST-1 assay. The cells only with FCS-free medium incubation were set as control (100%). (n=3, * $p<0.05$, ** $p<0.01$)

3.2.2 Thrombin induces intracellular Ca^{2+} increase in astrocytes

Thrombin was reported coupling to Ca^{2+} signaling through activation of thrombin-receptors [129]. That means thrombin-induced intracellular Ca^{2+} increases correlate with activations of PAR-1, PAR-3 and PAR-4 receptors. To make it clear which is the most important receptor involved in thrombin-induced intracellular Ca^{2+} increases, we monitored the Ca^{2+} responses under different concentrations of thrombin in the absence or presence of the antagonists for PAR-1 (RWJ) and / or PAR-4 (tcY) (PAR-3 antagonist is not available currently). Briefly, astrocytes were preincubated with antagonists for 1 h in FCS-free

medium. Then astrocytes were loaded with Fura-2AM in HBSS buffer with the same concentration of antagonists used in the last step. Astrocytes were challenged by different concentrations of thrombin. Ca^{2+} was detected at the respective 510 nm emission intensity of the ratiometric calcium-sensitive dye Fura-2AM after excitations at 340 nm and 380 nm. The ratio of the emission intensities of 340 nm and 380 nm excitations indicates the intracellular calcium concentration.

As data show in Fig. 3.2.2, with treatment of 0.1 U/ml of thrombin, the maximum value of the ratio of F340/F380 was 0.9. Under the same concentration of thrombin, the ratio was only slightly decreased when the astrocytes were incubated with thrombin in the presence of PAR-1 antagonist (column 2 *vs.* 1). Interestingly, when PAR-4 receptors were blocked by tcY, the ratio was largely increased to 2.1 (column 3). However, inhibition of PAR-1 and PAR-4 together resulted in the dramatic decrease of the Ca^{2+} response caused by thrombin (column 4). The data indicate that the PAR-4 receptor may play an inhibitory role in Ca^{2+} responses, since without activation of PAR-4, the maximum of the Ca^{2+} responses was observed (column 3). Moreover, it may also imply that co-activation of PAR-1 and PAR-3 contributes to the maximum Ca^{2+} responses (column 3). Blockade of PAR-1 and PAR-4 together eliminates the possibilities of collaboration between PAR-1 and PAR-3, or the collaboration between PAR-4 and PAR-3 to couple to the Ca^{2+} signaling, resulting in the dramatic decrease of Ca^{2+} level (column 4).

Similarly, upon 0.5 U/ml and 1 U/ml of thrombin, the Ca^{2+} responses were quite similar to each other under the same experimental conditions (column 5 *vs* 9, column 6 *vs* 10, column 7 *vs* 11, and column 8 *vs* 12). In detail, the ratio of thrombin caused maximum value of Ca^{2+} responses was 2.1 to 2.15 (column 5 and 9). More interesting phenomena was that the level of Ca^{2+} response induced by thrombin in the presence of PAR-1 receptor antagonist was lower than the ratio obtained under PAR-1 plus PAR-4 antagonists (column 6 *vs* 8; column 10 *vs* 12), suggesting that PAR-1 played an important role in inducing the maximum Ca^{2+} responses under 0.5 U/ml and 1 U/ml of thrombin (column 5 and 9). Furthermore, treatment of PAR-4 antagonist failed to decrease the maximum Ca^{2+} response induced by thrombin (column 7 and 11), indicating that PAR-4 played a dispensable role in coupling Ca^{2+} signaling under 0.5 U/ml and 1 U/ml of thrombin treatment. Overall, the data manifested that under 1 U/ml of thrombin challenge, thrombin increased the intracellular Ca^{2+} signaling mainly through activation of PAR-1 receptor.

Under the stimulation with 5 U/ml of thrombin, the Ca^{2+} response was increased to 2.7 (column 13), which was the largest value among the different concentrations of thrombin-

caused Ca^{2+} responses. It is thought that PAR-1 and PAR-4 are responsible for this maximum ratio, since blockade of PAR-4 receptor is capable of lowering this maximum value (column 15 *vs* 13). Inhibition of PAR-1, the Ca^{2+} response was decreased to the lowest value (column 14).

In conclusion, thrombin is able to increase intracellular Ca^{2+} level under different concentrations of thrombin. The maximum of Ca^{2+} responses induced by 1 U/ml of thrombin is mainly through PAR-1 activation. However, the highest Ca^{2+} response caused by lower concentration (0.1 U/ml) of thrombin is attributed to the stimulation of PAR-1 and PAR-3. Ca^{2+} responses caused by 5 U/ml of thrombin are because of the activation of PAR-1 and PAR-4 receptors.
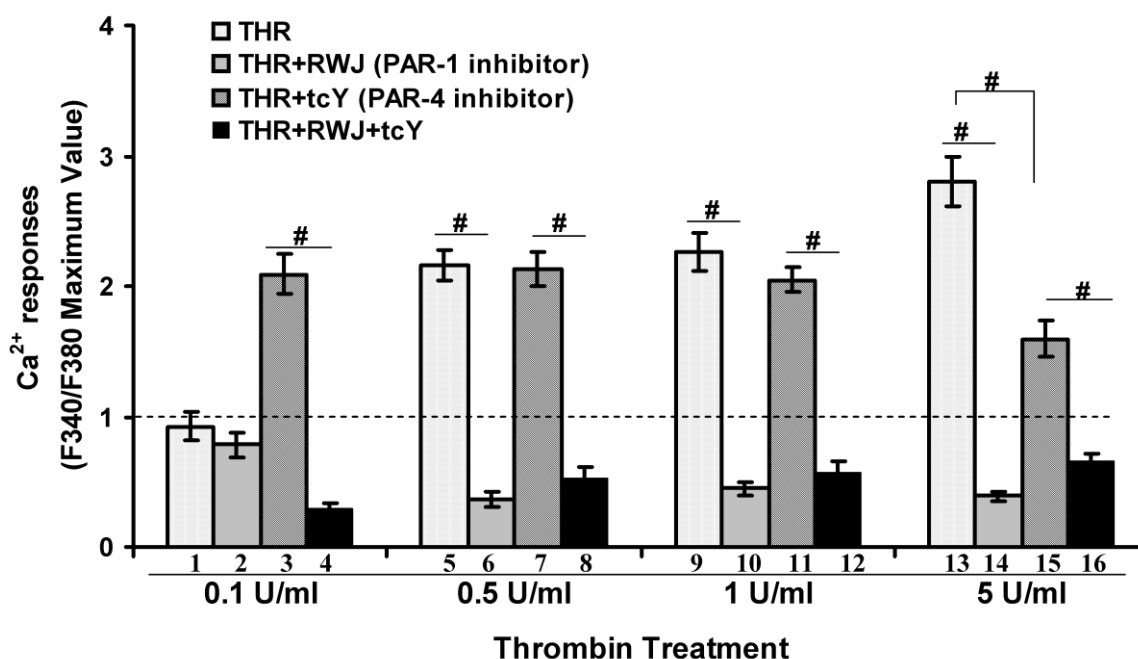
Fig. 3.2.2. The Ca^{2+} responses under different concentrations of thrombin. Astrocytes were cultured on the coverslides. 10 µM of PAR-1 inhibitor (RWJ) or PAR-4 antagonist (tcY) dissolved in FCS-free medium were incubated with astrocytes for 1 h. After that cells were prepared as described above to evaluate intracellular Ca^{2+} responses. The numbers under the X-axis are corresponding to the respective bar's number. The experiments were repeated 3 times and each time more than 15 cells were selected to analyze (# $p<0.001$).

3.2.3 Thrombin causes intracellular ROS production in astrocytes

Thrombin was reported to produce ROS release in microglia and activate the NADPH oxidise, which contributed to thrombin-induced loss of hippocampal neurons [50]. To check whether thrombin induced intracellular ROS production also in astrocytes, astrocytes were treated with different concentrations of thrombin, and then the ROS production was monitored for 30 min and measured by the method described in 2.2.3.4. Fig. 3.2.3 shows that 1 U/ml and 5 U/ml of thrombin significantly induce ROS production in astrocytes.
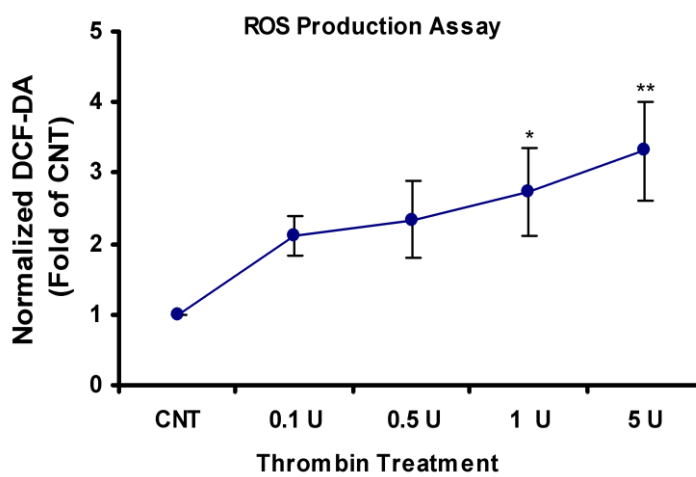
Fig. 3.2.3 Thrombin-induced intracellular ROS release in astrocytes. Astrocytes were prepared and the ROS releases induced by thrombin were measured according to the methods described in 2.2.3.4. Then the different value of ROS production were collected and calculated according to the formula shown in 2.2.3.4. Data from the control cells which are treated with HBSS buffer without thrombin was taken as 1. (n=4, * $p<0.05$, ** $p<0.01$)

3.2.4 Thrombin-induced intracellular Ca^{2+} and ROS contribute to astrocytes proliferation

We are aiming at investigating whether intracellular Ca^{2+} elevation and ROS release produced by thrombin will be beneficial for the astrocytes proliferation. The inhibitor Diphenyleneiodonium (DPI) which has been frequently used to inhibit ROS production mediated by flavoenzymes, particularly NADPH oxidase was used here. DPI was also demonstrated to block mitochondrial ROS production through inhibiting NADH-ubiquinone oxidoreductase (complex I) [130]. At the same time, we used BAPTA-AM as the chelator of intracellular Ca^{2+}.

From WST-1 assay Fig. 3.2.4 (see also in Fig. 3.2.1), it can be seen that thrombin significantly induces astrocytes proliferation (bar 2). With the cotreatment of thrombin plus DPI (bar 3) or the cotreatment of thrombin and BAPTA (bar 4), the cell proliferation caused by thrombin is significantly decreased (bar 3 *vs* bar 2, and bar 4 *vs* bar 2). Astrocytes

incubated with DPI or BAPTA-AM alone displays a lower proliferation as compared to the control (bar 5 *vs* bar 1 and bar 6 *vs* bar 1). In consequence, we conclude that thrombin-initiated intracellular Ca^{2+} and ROS production make contributions to astrocytes proliferation.
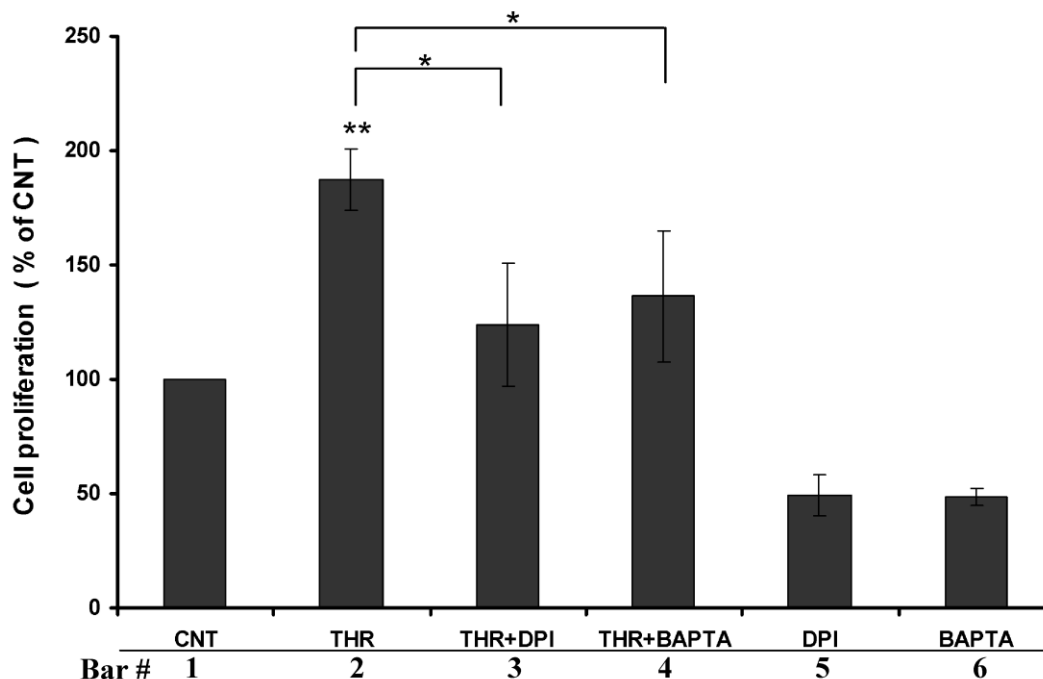
Fig. 3.2.4. Inhibition of thrombin-caused intracellular Ca^{2+} increases or ROS production abolishes thrombin-induced astrocytes proliferation, respectively. Astrocytes were seeded and prepared for WST-1 assay according to the description of the method in 2.2.3.2. After the starvation of astrocytes overnight, astrocytes were treated with 1 U/ml of thrombin (THR) with or without 500 nM of Diphenyleneiodonium (DPI) or 50 μM of BAPTA-AM (BAPTA) for 48 h. Thereafter, WST-1 assay were done and the data were collected. The cells without treatment were set as control (CNT). (n=4 * $p<0.05$, ** $p<0.01$).

3.2.5 Thrombin increases the astrocytes proliferation through ERK and JNK rather than p38 signaling pathways

It is reported that thrombin enhanced astrocytes proliferation through the ERK signaling pathway [35]. We study whether JNK and p38 will be also involved in thrombin-induced astrocytes proliferation. We did Western blot after treating astrocytes with 1 U/ml of thrombin for different times. As a result, thrombin significantly increases the level of the phosphorylation of ERK and JNK at 1 h and 24 h (Fig. 3.2.5a and b). However, thrombin failed to significantly activate the phosphorylation of p38 in these time scales (Fig. 3.2.5c).

(a)

(b)

(c)
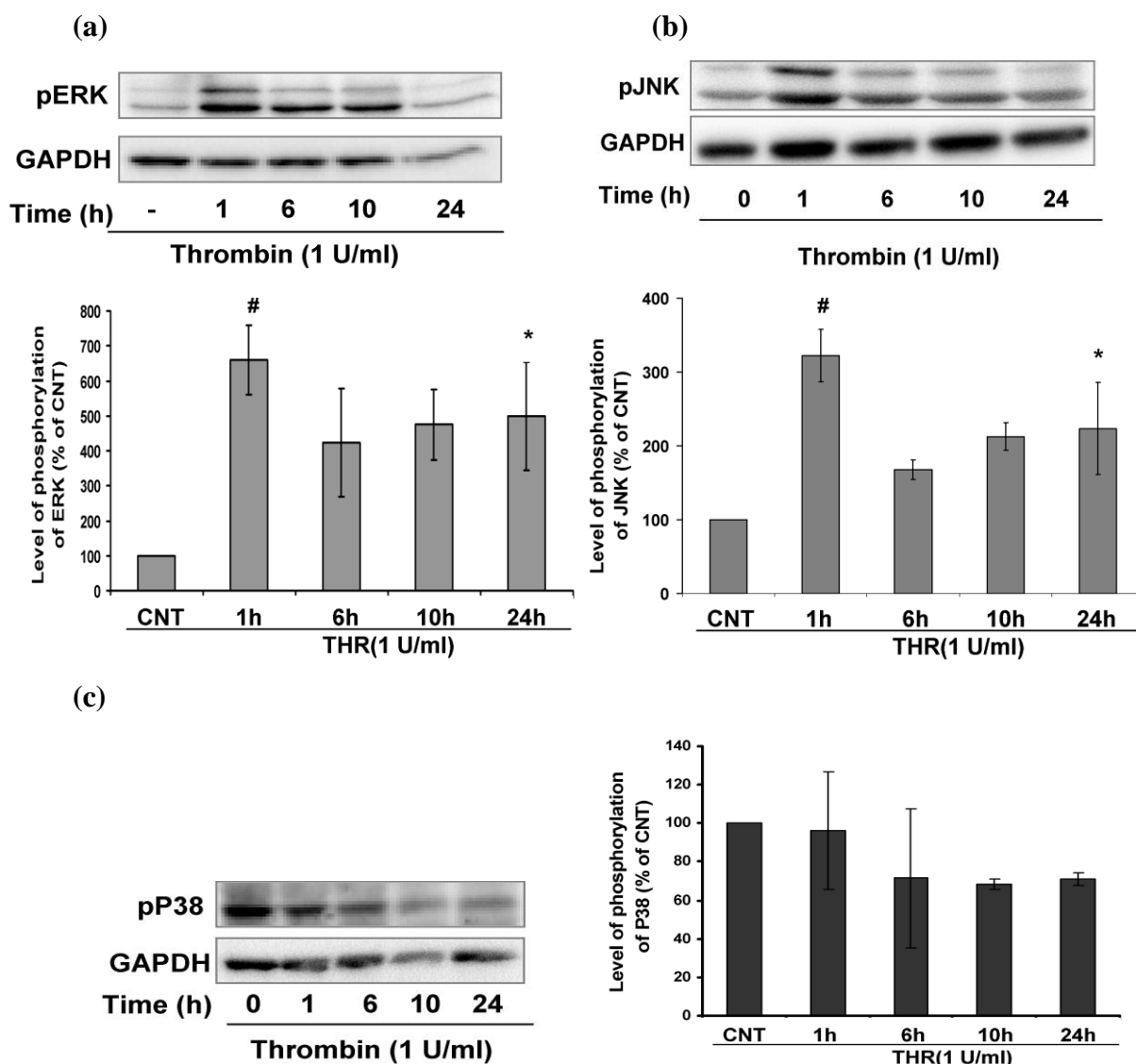
Fig. 3.2.5 Thrombin stimulates the phosphorylation of ERK and JNK rather than p38. Astrocytes were cultured on the 6-well plates with the density of 1.95×10^6 cells/well one day before the treatment. Then astrocytes were deprived of FCS overnight. For the induction, 1 U/ml of thrombin (THR) were added into the serum-free medium to astrocytes and kept in culture for time scales indicated in the figures. 50 μg of proteins were obtained and loaded for Western blot experiments. The representative blot and the quantifications of the protein level were shown. Statistical analysis was made comparison to control (CNT). (n=4, * $p<0.05$, # $p<0.001$)

3.2.6 Blockade of ERK and JNK signaling pathways eliminates thrombin-induced proliferation in astrocytes

It is shown that thrombin enhanced the phosphorylation level of ERK and JNK rather than p38 (Fig. 3.2.5). In order to make clear if thrombin-stimulated ERK and JNK signaling cascades mediate astrocytes proliferation, we used a series of inhibitors to block the relative signaling cascades as indicated in Fig. 3.2.6. Our data clearly show that blockade of thrombin-activated ERK and JNK signaling pathways significantly decrease astrocytes proliferation triggered by thrombin (Fig. 3.2.6). Interestingly, the combination of thrombin and p38 inhibitor does not change the proliferation rate of astrocytes, suggesting that thrombin is able

to accelerate astrocytes proliferation through ERK and JNK rather than p38, which is in accordance with our result showing that thrombin failed to stimulate p38 phosphorylation (Fig. 3.2.5).
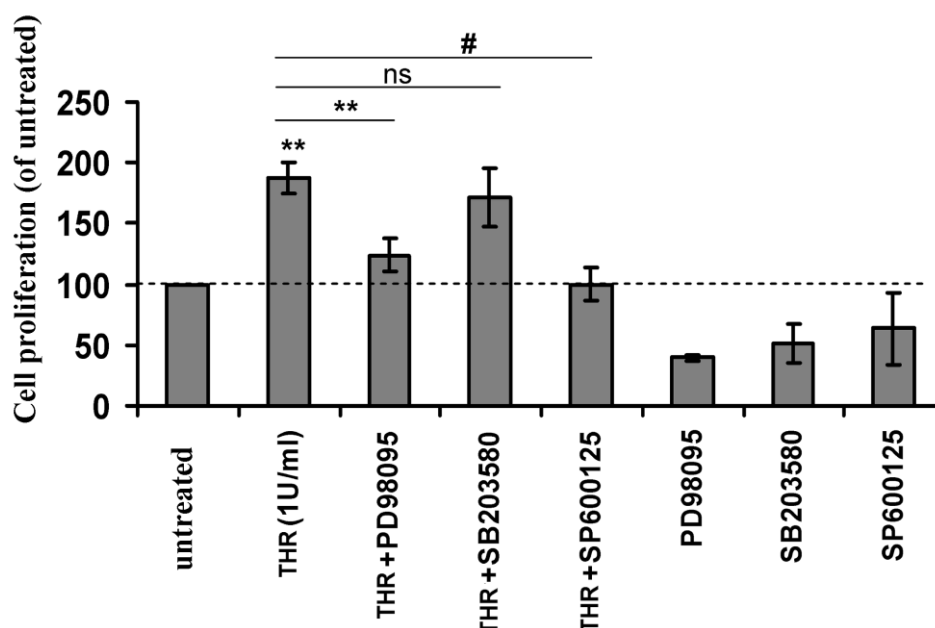
Fig. 3.2.6 Thrombin-initiated ERK and JNK activation contributes to astrocytes proliferation. Astrocytes were prepared as mentioned in cell proliferation assay in 2.2.3.2. Then astrocytes were incubated with 1 U/ml of thrombin (THR) in the presence or absence of 20 μM of ERK inhibitor (PD98095); or p38 inhibitor (SB203580) or JNK inhibitor (SP600125) or with inhibitors alone for 48 h. Cell viability was determined by the WST-1 assay, astrocytes without thrombin and inhibitors treatment were set as control, and the proliferation data from it were taken as 100%. (n=4, ** $p<0.01$, # $p<0.001$, ns=not significant)

3.2.7 Thrombin activates PI3K signaling pathway to increase phosphorylation of Akt, which needs transactivation of EGF and PDGF receptors

Thrombin was demonstrated to protect β-arrestin 1-lacking astrocytes from apoptosis through activation of Akt signaling pathway (Fig. 3.1.5). We are wondering whether thrombin stimulates Akt signaling pathway to accelerate astrocytes proliferation. Moreover, we want to elucidate whether blockade of the transactivation of EGF and PDGF receptors will affect the phosphorylation of Akt. We first treated astrocytes with thrombin for different times, and then the Western blot method was used to detect the changes of phosphorylation of Akt. According to the data shown in Fig. 3.2.7, thrombin significantly induced phosphorylation of Akt. Blockade of transactivation of EGF and PDGF receptor by AG1478 and AG1296 attenuated thrombin-induced Akt phosphorylation. When LY294002 was used to inhibit the PI3K, the thrombin-caused Akt phosphorylation was completely abolished. The results strongly support that thrombin induces phosphorylation of Akt which needs transactivation of EGF and PDGF receptors.

(a)   **(b)**
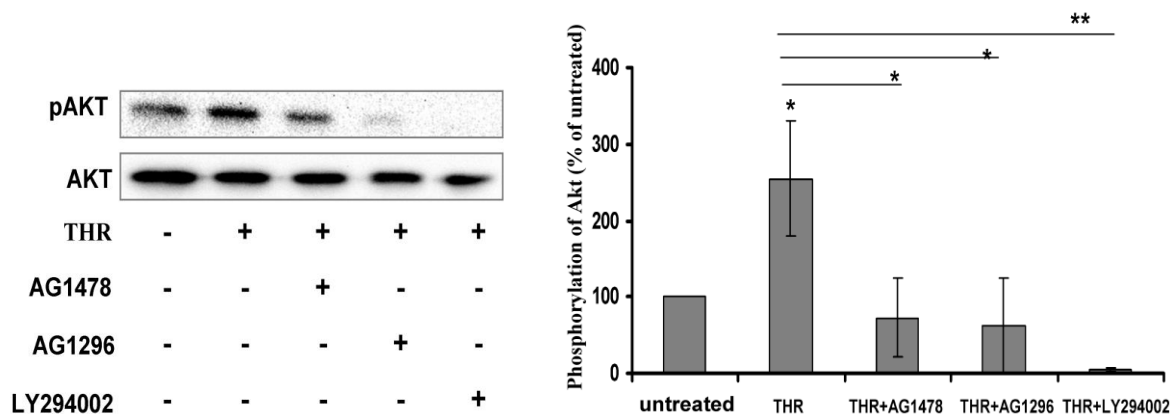
Fig. 3.2.7 Thrombin activates PI3K/Akt signaling pathway and induces transactivation of EGF and PDGF receptors. Astrocytes were treated by 1 U/ml of thrombin (THR) in the absence or presence of 10 μM of AG1478, 10 μM of AG1296, or 20 μM of LY194002 to block the transactivation of EGF receptor, PDGF receptor and PI3K signaling pathway for 24 h. the untreated cells (untreated) were set as control. (a) The representative Western blot and (b) the quantification of the band density of phosphorylation Akt are shown. (n=3, * $p < 0.05$, ** $p < 0.01$).

3.2.8 Thrombin caused-phosphorylation status of Akt determines the level of cyclin D1

Akt was indicated to regulate cyclin D1 to promote β-cell proliferation [131]. To explore whether thrombin-induced Akt phosphorylation will regulate cyclin D1, we used the Western blot method to monitor the protein level of cyclin D1 upon the stimulation of thrombin in astrocytes at different time points. At the same time, to make it clear whether thrombin caused-phosphorylation status of Akt determines the level of protein cyclin D1, AG1478 and AG1296 were used to block transaction of EGF and PDGF receptors to attenuate Akt phosphorylation, and LY294002 was used to block phosphorylation of Akt. Under this situation, we checked whether cyclin D1 expression was affected or not. The data showed that thrombin successfully and significantly upregulated intracellular cyclin D1 after 10 h and 24 h incubation with thrombin (Fig. 3.2.8a). With the attenuation of thrombin-induced phosphorylated Akt by AG1478 and AG1296, the level of cyclin D1 was also significantly decreased. Strikingly, blockade of PI3K signaling pathway not only abolished Akt phosphorylation (Fig. 3.2.7), but also dramatically decreased the protein level of cyclin D1 induced by thrombin (Fig. 3.2.8b).
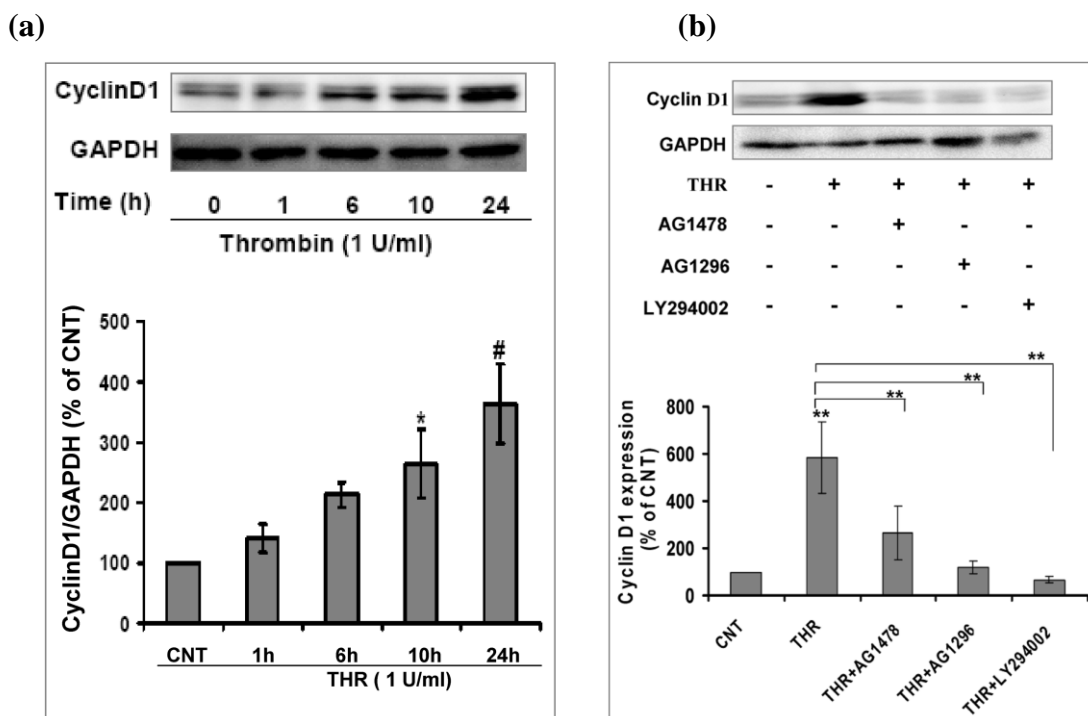
Fig. 3.2.8 Thrombin-caused phosphorylation status determines cyclin D1 accumulation. Astrocytes were treated without or with thrombin (THR) in the absence or presence of 10 μM of AG1478, 10 μM of AG1296, or 20 μM of LY194002 to block the transactivation of EGF receptor, PDGF receptor and PI3K signaling pathway for 24 h. The untreated cells were set as control (CNT). (a) Thrombin upregulated the protein level of cyclin D1. (b) Inhibition of Akt phosphorylation decreased the upregulation of cyclin D1 induced by thrombin. All of the comparisons were made to control (CNT) (n=4, * p<0.05, ** p<0.01, # p<0.001).

3.2.9 Blockade of Akt signaling pathway influences thrombin-induced astrocytes proliferation

We already confirmed that cyclin D1 was unregulated by thrombin-stimulated Akt phosphorylation (Fig. 3.2.8a). We next wanted to check whether the phosphorylation of Akt contributes to astrocytes proliferation induced by thrombin. Since it was already found that thrombin-induced Akt activation was related with the transactivation of PDGF and EGF receptors [58], the inhibitors of PDGF, EGF receptors and inhibitor of PI3K were applied in the presence of thrombin.

Our data showed that thrombin generated 101% of increases of cell proliferation as compared to the control (Fig. 3.2.8, column 2 *vs.* column 1), see also Fig. 3.2.1. Moreover, the application of inhibitors (AG1296) of the PDGF receptors and PI3K (LY294002) significantly decreased the rate of astrocytes proliferation, the percentage was reduced from 201% to 140% (Fig. 3.2.8, column 2 *vs.* column 3) and 60% (Fig. 3.2.8, column 2 *vs.* column 5) respectively. However, thrombin was capable of accelerating astrocytes proliferation in the presence of inhibitor (AG1478) of EGF receptor. The obtained cell proliferation results strongly indicate that astrocytes proliferation induced by thrombin is correlated to the

phosphorylation status of Akt, suggesting that the axis of PI3K/Akt/cyclin D1 plays a key role in thrombin-mediated astrocytes proliferation. Surprisingly, blockade of transactivation of EGF receptor did not affect cell proliferation induced by thrombin. However, thrombin-induced transactivation of PDGF receptor contributes to astrocytes proliferation.
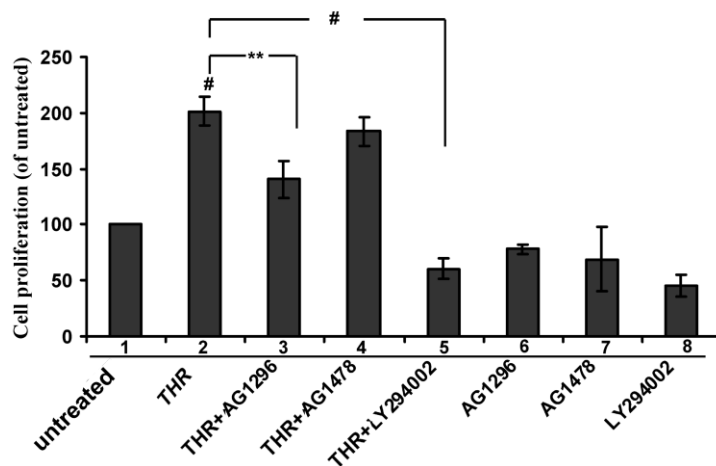
Fig. 3.2.9 Inhibition of the phosphorylation of Akt decreases the rate of astrocytes proliferation induced by thrombin. Astrocytes were seeded on 96 well-plates to measure cell proliferation rate as described in 2.2.3.2. Astrocytes were treated with 1 U/ml of thrombin (THR) in the presence or absence of 10 μM of AG1478 to block the activation of EGF receptor, or 10 μM of AG1296 to block the activation of PDGF receptor, or 20 μM of LY294002 to inhibit the activation of PI3K/Akt signaling pathway. The WST-1 assay was done 24 h post addition. Cells without thrombin or/and inhibitors treatment were set as control. (n=4, ** p<0.01, # p<0.001). The numbers under the X-axis represent the corresponding column.

3.2.10 Thrombin induced increase of intracellular glucose uptake, which is responsible for astrocytes proliferation

In order to find out whether thrombin-induced astrocytes proliferation occurs through stimulating glucose uptake or not, astrocytes were treated with 1 U/ml of thrombin for 10 min, then the D-glucose analog 2-[N-(7-nitrobenz-2-oxa-1,3-diazol-4-yl) amino]-2-deoxy-D-glucose (2-NBDG) uptake by astrocytes was evaluated. The assay is based on direct incubation of astrocytes with a fluorescent D-glucose analog 2-NBDG followed by measuring the intensity of fluorescence emitted by the cells, reflecting the amount of 2-NBDG taken up via GLUT.

The data from glucose uptake assay showed that thrombin may enhance the glucose uptake in astrocytes. Co-application of thrombin and Apigenin or Apigenin alone attenuated the rate of glucose uptake (Fig. 3.2.10a). Apigenin is a natural product belonging to the flavone class, which is demonstrate to inhibit GLUT-1 mRNA and protein expression to decrease glucose uptake in cancer cells [132]. The data with Apigenin were used as negative control for the assay, as indicated by the manual.

To further confirm that thrombin did increase glucose uptake in astrocytes, which promoted astrocytes proliferation, the Apigenin was used in the cell proliferation assay. Similarly, thrombin significantly induced astrocytes proliferation as compared to the cells without thrombin treatment. Strikingly, when astrocytes were incubated with thrombin in the presence of Apigenin, thrombin-induced increases of astrocytes proliferation were significantly eliminated, with the percentage declined from 180% to 80% (Fig. 3.2.10b). The WST-1 assay data strongly support our hypothesis that thrombin enhanced glucose uptake in astrocytes to accelerate astrocytes proliferation.

(a)   **(b)**
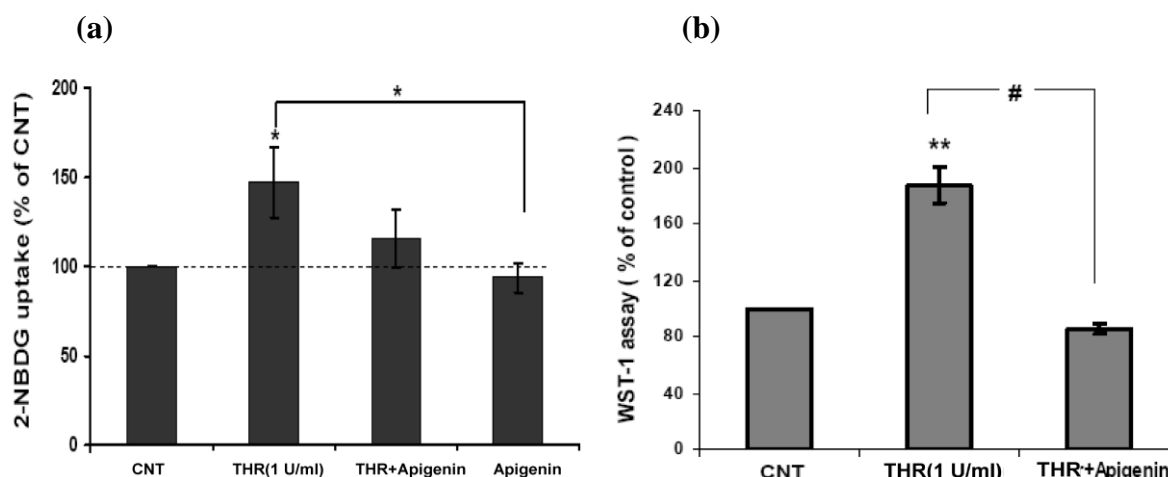
Fig. 3.2.10. Thrombin increased-glucose uptake contributes to astrocytes proliferation. Astrocytes were seeded according to the protocol described in 2.2.3.2 and 2.2.3.3. (a) Astrocytes were treated with 1 U/ml of thrombin (THR) in the absence or presence of Apigenin (50 μM) for 30 min, or cells were treated with Apigenin alone which was set as negative control. The cells without treatment were set as control and the data were taken as 100%, (n=3, * $p<0.05$). (b) Astrocytes were treated with 1 U/ml of thrombin in the absence or presence of Apigenin for 48 h, then the rate of proliferation were assessed by WST-1 assay (n=4, ** $p<0.01$, # $p<0.001$).

3.2.11 HK2 is up-regulated by thrombin, which manifests the enhancement of glucose uptake in astrocytes

Glucose plays a key role in producing ATP by all cells in both the presence and absence of molecular oxygen (O_2). The first step in glycolysis is the phosphorylation of glucose by hexokinases. The up-regulated glycolysis which is mediated by hexokinase confers accelerated proliferative effects in cells. To understand if thrombin-caused enhancement of glucose uptake is because of the upregulation of hexokinases, we treated astrocytes with 1 U/ml of thrombin for 24 h, then the protein levels of hexokinase 1 (HK1) and hexokinase 2 (HK2) are evaluated by Western blot. In parallel, we wanted to find out Apigenin also inhibits hexokinases protein expression to decrease glucose uptake.

According to Fig. 3.2.11a, application of thrombin led to increased protein level of HK2. The quantification data manifested that the level of HK2 is 2 times higher in thrombin-

treated astrocytes than that in the control cells (100%). Combination of thrombin and Apigenin decreased HK2 protein level to 80% (Fig. 3.2.11c). However, it seems that thrombin has little effects on regulation of HK1 in astrocytes (Fig. 3.2.11b). The consequences are that thrombin conferred to increase of glucose uptake in astrocytes mainly through upregulating HK2.

(a)
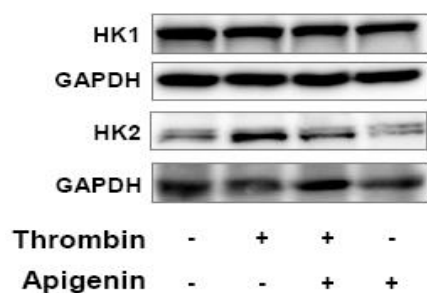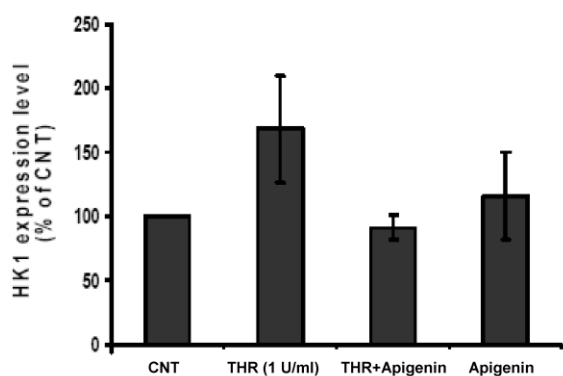
(b)   **(c)**
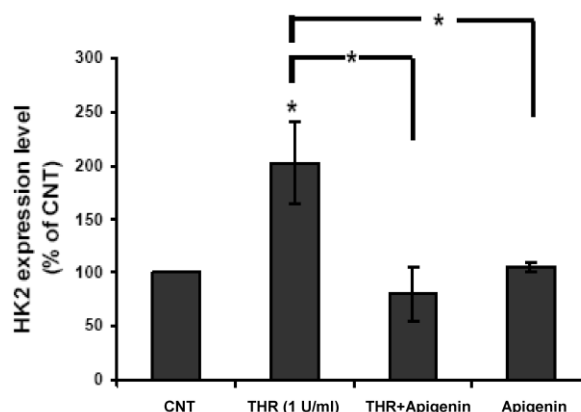
Fig. 3.2.11. Thrombin upregulates HK2 rather than HK1 in astrocytes. Astrocytes were treated with 1 U/ml of thrombin (THR) in the absence or presence of Apigenin for 24 h. Then the cells were harvested to do Western blot. 50 µg of protein for each lane were loaded. The primary HK1 and HK2 antibodies were used to detect the levels of respective protein. (a) The representative Western blot showed that HK1 and HK2 under the conditions indicated. (b) Quantification of the level of HK1 and (c) quantification of the level of HK2 under the indicated conditions (n=4, * p<0.05).

3.2.12 Thrombin-triggered MAPK/HIF-1α and PI3K/Akt/HIF-1α signaling pathways synergistically mediate HK2 in astrocytes

HIF-1α was reported to be incorporated in the ET 1-mediated signaling pathways to promote astrocytes proliferation through increasing glucose uptake [133]. Our hypothesis is that thrombin may also stimulate HIF-1α, which subsequently upregulates HK2 to promote glucose uptake in astrocytes. Moreover, we wondered if MAPK and PI3K/Akt are also integrated in thrombin-mediated HIF-1α stabilization. To examine the hypothesis, thrombin was applied to astrocytes in the absence or presence of inhibitors of ERK, JNK, and LY294002 in FCS-free medium for 24 h. Then the protein levels of HIF-1α and HK2 were examined by Western blot.

The data presented in Fig. 3.2.12a demonstrated that thrombin significantly stabilized HIF-1α in astrocytes. The quantified data of band density emphasized that thrombin induced accumulation of HIF-1α was almost 3 times higher than that in the untreated cells, which were used as control (100%). In addition, blockade of ERK, JNK and PI3K signaling cascades by the specific inhibitors decreased the accumulation of HIF-1α caused by thrombin. The percentages of thrombin-induced HIF-1α accumulation declined from 290% to 140%, 73%, and 87% by inhibition of ERK, JNK and PI3K, respectively, suggesting that these signal transduction pathways are very important for thrombin stabilizing HIF-1α.

We next checked the protein levels of HK2 under the same conditions. Coincidently, the HK2 level correlated to the HIF-1α level. Thrombin significantly upregulates HK2 (Fig. 3.2.12c) which was also demonstrated by Fig. 3.2.11a and c, and inhibitors of ERK, JNK, and PI3K significantly decreased the protein level of HK2 induced by thrombin. The OD value of HK2 was decreased from 220% to 122%, 146% and 82%, respectively (Fig. 3.2.12c). Our data support that thrombin activated HIF-1α / HK2 signaling cascade to mediate glucose metabolism in astrocytes.

(a)
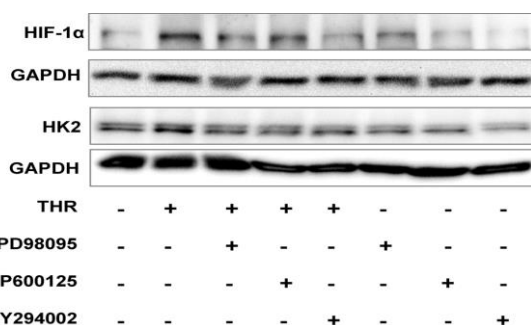
(b)
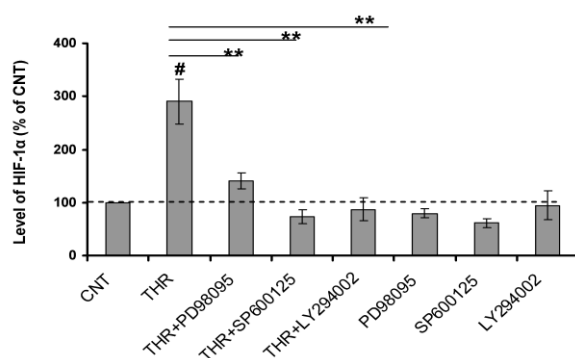
(c)
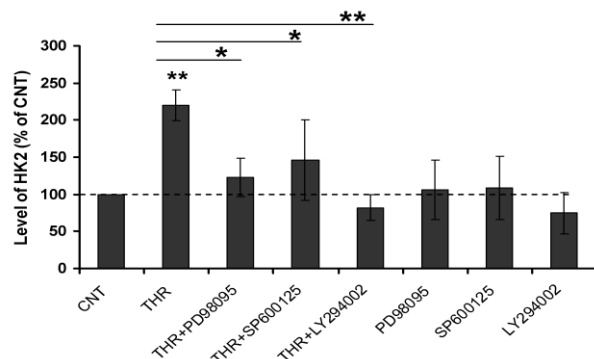
Fig. 3.2.12. ERK, JNK and PI3K signaling cascades is important for thrombin-induced HIF-1α accumulation and HK2 upregulation.

Astrocytes were treated with 1 U/ml of thrombin (THR) in the absence or presence of 10 μM of PD98095, which is the ERK inhibitors (THR+PD98095), or 20 μM of SP600125 which is the JNK inhibitor (THR+SP600125) or 20 μM of LY294002 (THR+LY294002) which blocks PI3K or these inhibitors alone for 24 h. After the induction, astrocytes were harvested to do Western blot to probe protein level of HIF-1α and HK2. The untreated cells were set as control (CNT); the ratio of HIF-1α and HK2 to GAPDH were taken as the relative value of each protein level.

(a) The representative blot showed the thrombin-stimulated HIF-1α and HK2 in astrocytes under the indicated conditions.

(b) The quantification data showed the relative level of HIF-1α.as compared to the CNT (n=4, ** p<0.01, # p<0.001).

(C) The quantification data of HK2 under the indicated conditions as compared to the CNT (n=5, * p<0.05, ** p<0.01).

3.2.13 Thrombin-induced mitochondrial ROS has no effects on signaling of ERK, JNK and Akt.

ROS, as a "second messenger" in intracellular signaling cascades was demonstrated to regulate cell proliferation or cell differentiation through MAPK and Akt cascades [134] [135]. To explore whether thrombin-activated ROS work as signaling molecule to target on the ERK, JNK, or Akt signaling pathways, we treated astrocytes with thrombin in the absence or presence of the ROS inhibitor DPI and ROS inducer Antimycin A. Then we monitored the changes of phosphorylation of ERK, JNK and Akt. The data from Western blot demonstrated that thrombin plus Antimycin A significantly induced the hyper phosphorylation of ERK and

JNK as compared to that level in thrombin-treated cells. However, when DPI was used to block thrombin-induced ROS production, there were no significant changes in phosphorylation of ERK and JNK. Moreover, phosphorylation of Akt was also failed to be affected by blockade of ROS by DPI (Fig. 3.2.13).

(a)

(b)

(c)

(d)
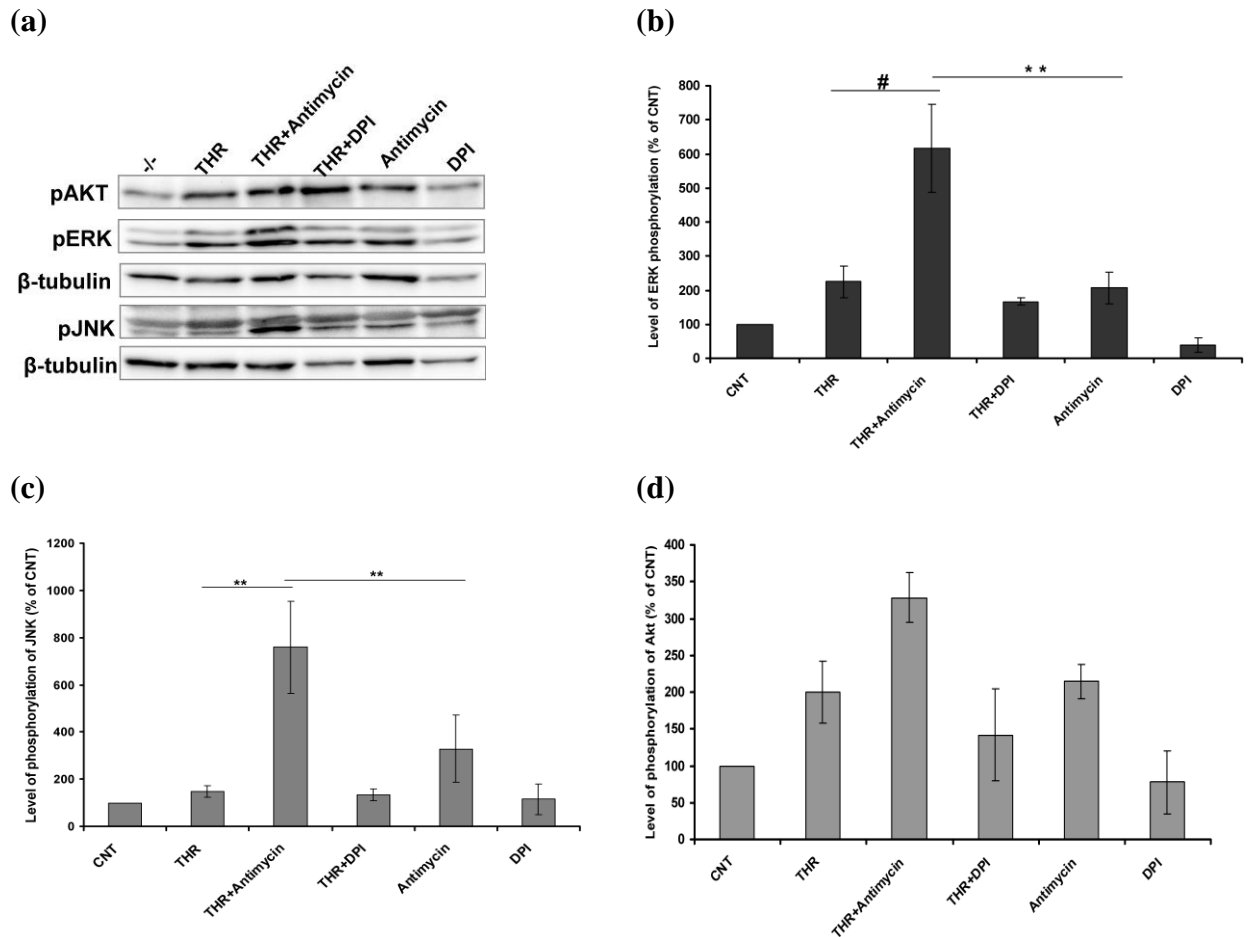
Fig. 3.2.13. Thrombin-induced ROS production was not responsible for activation of ERK, JNK, and Akt in astrocytes. Astrocytes were treated with 1 U/ml of thrombin without or with the cotreatment of Antimycin A (10 mM) or DPI (500 nM) for 24 h. Then astrocytes were harvested for Western blot. β-tubulin was used to control the equal loading of protein in each lane. (a) The representative blot was shown here and (b) quantification of phosphorylated ERK, (c) quantification of phosphorylated JNK and (d) quantification of phosphorylated Akt were shown, respectively (n=4, ** $p<0.01$,# $p<0.001$).

3.3 The functional studies of PAR-2 carboxyl tail in intracellular signaling and cell death

3.3.1 Constructions of PAR-2 truncated mutants

To examine the functional role of PAR-2 carboxyl tail in receptor internalization, and to find out which cluster of serine/threonine is important for signaling and cell survival, the various truncated mutants were generated by PCR mutagenesis as described in the methods. Briefly, the template DNA used to amplify the PAR-2 truncated mutants is the rat wild type PAR-2 receptor inserted into the pEGFP-N1 vector. The GFP tag was linked to the C-terminal of PAR-2. The template DNA was generously supplied by Dr. Rongyu Li. PAR-2 carboxyl tail truncation mutants were generated by deletion of certain gene fragments from the indicated residues. The detailed serine/threonine clusters contained in C-terminal truncations are shown as Fig. 3.3.1. The mutants were named 348-Del, 361-Del, 368-Del, 379-Del, and 386-Del.
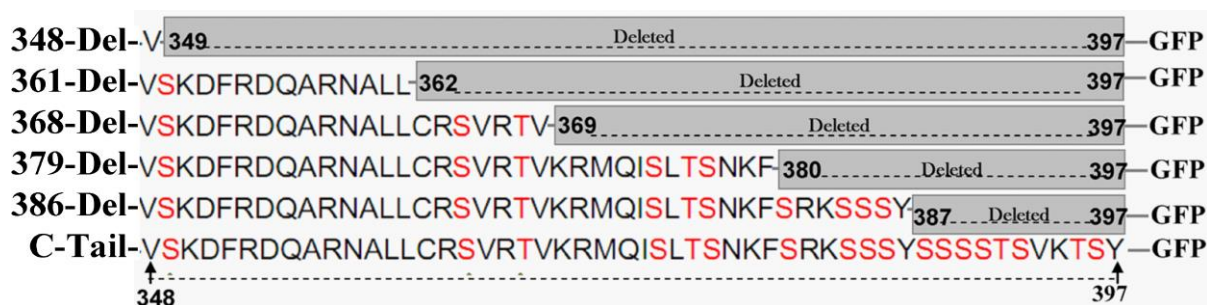
Fig. 3.3.1 The serine/threonine residues contained in the carboxyl-tail of PAR-2 in the different truncation mutations. The red characters point out the cluster of the serine/threonine included in the different mutations. The grey boxes indicate the residues deleted in each mutant. At the same time, in the carboxyl-terminus of each mutant, the GFP tag was attached.

3.3.2 The expression and internalization of PAR-2 carboxyl-tail mutants

To investigate whether the phosphorylation sites of serines and threonines located in the carboxyl tail of PAR-2 are essential for the receptor internalization, the truncation mutants of PAR-2 were treated with 100 nM trypsin for 30 min.

In unstimulated cells, the major portion of the truncated receptors was expressed nicely on the cell membrane, except for 348-Del, in which all the serine and threonine phosphorylation sites were deleted. Without the whole carboxyl-tail, the truncation 348-Del lost one of the important and typical characters of membrane receptor which is expressed mainly in the cell plasma membrane. It can be seen that 348-Del distributes mainly in the cytosol with low level of expression in the cell membrane. Under the challenge of trypsin, the 348-Del receptor failed to show any obvious changes in receptor localization. Unlike 348-Del, PAR-2 carboxyl tail truncation mutants, 361-Del, 368-Del, 379-Del, and 386-Del, which

were lacking different phosphorylation sites of serine or threonine at the carboxyl tail region, were expressed mainly on the cell membrane as wild type receptors do. Importantly, the expression level of these mutants was comparable with that of the wild-type receptor. Interestingly, under the stimulation with trypsin for 30 min, a similar internalization pattern for carboxyl tail mutants was observed as for PAR-2 wild type receptor. The internalized receptors with green fluorescence were nicely colocalized with lysosome tracker with red fluorescence, as indicated by white arrows. At the same time, with the receptor going into the cytoplasm upon the stimulation by trypsin, decreasing numbers of PAR-2 truncation mutants were observed on the cell membrane in Fig. 3.3.2. The results of truncation mutants internalization and expression are summarized in Table. 3.3.2. Taken together, these findings imply that a short peptide present in 361-Del was sufficient for preserving the membrane-expressed pattern and internalization, highlighting that Ser 349 may play a key role in maintaining the receptor on the cell membrane or Ser 349 is important for receptor internalization.

Table. 3.3.2 The expression and internalization of PAR-2 mutant truncations.

Name of receptor	Expression	Internalization
348-Del	Cell membrane and cytoplasma	No
361-Del	Cell membrane	yes
368-Del	Cell membrane	yes
379-Del	Cell membrane	yes
386-Del	Cell membrane	yes
PAR-2 (wild type)	Cell membrane	yes

Time (min)
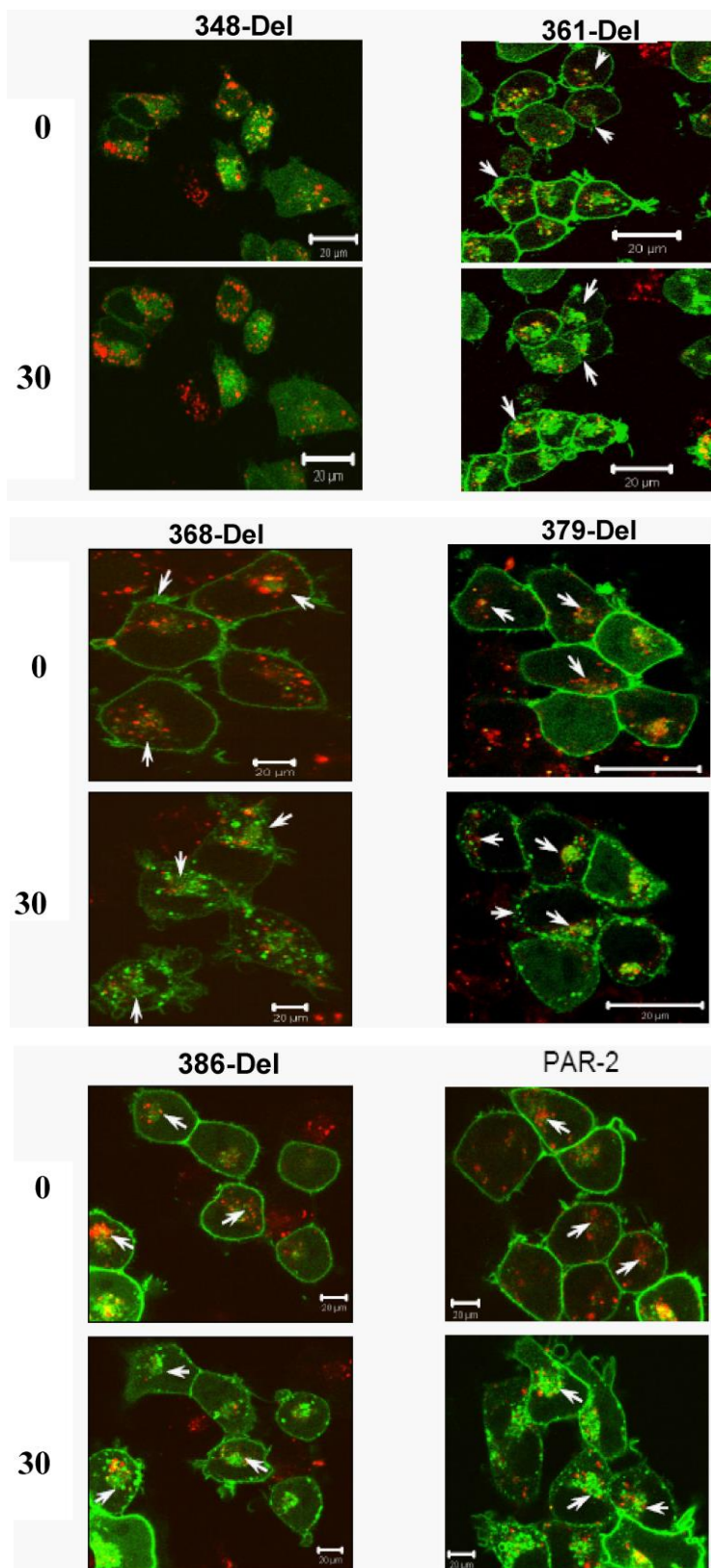
Fig.3.3.2. The internalization assay of PAR-2 truncations.
HEK 293 cells were stably transfected with PAR-2 mutants with GFP tag, (green fluorescence), designated as 348-Del, 361-Del, 368-Del, 379-Del, 386-Del, and PAR-2 (wild type receptors).
The transfected cells were cultured until 70% confluence, and then the cells were used for receptor internalization assay. Briefly, the transfected cells were incubated with 0.5 mg/ml of lysosome tracker (red fluorescence) for 30 min in serum free medium at 37°C. After washing cells with pre-heated HBSS twice, cells were exposed in 100 nM trypsin dissolved in HBSS at 37°C; the targeted cells were selected and monitored for 30 min to visualize receptor's trafficking. Images were processed with Zeiss confococal microscopy software. The experiments were repeated at least three times, and similar results were obtained (Scale bar = 20 µm).

3.3.3 Calcium Responses of PAR-2 mutants under the challenge with different concentrations of trypsin

To determine whether the constructed PAR-2 mutants have different abilities to trigger the intracellular Ca^{2+} release, we measured the Ca^{2+} mobilization under the challenge of different concentrations of trypsin. Intriguingly, Ca^{2+} responses in mutants 348-Del, 361-Del, and 368-Del showed little differences as compared to the HEK-GFP cells under all the different concentrations of trypsin treatments, but lower than that in PAR-2 wild type receptor-transfected cells. The initiation of comparable Ca^{2+} responses was found in 368-Del upon higher concentration of trypsin treatment (100 nM). In contrast, the initiation of comparable Ca^{2+} responses under the lower concentration of trypsin (0.01 nM, 0.1 nM and 1 nM) occurred in the mutant 386-Del. Compared to the wild type receptor, the mutants Del-379 and 386-Del showed comparable Ca^{2+} responses, which are higher than that in mutants 348-Del, 361-Del, and 368-Del under the corresponding concentrations of trypsin.
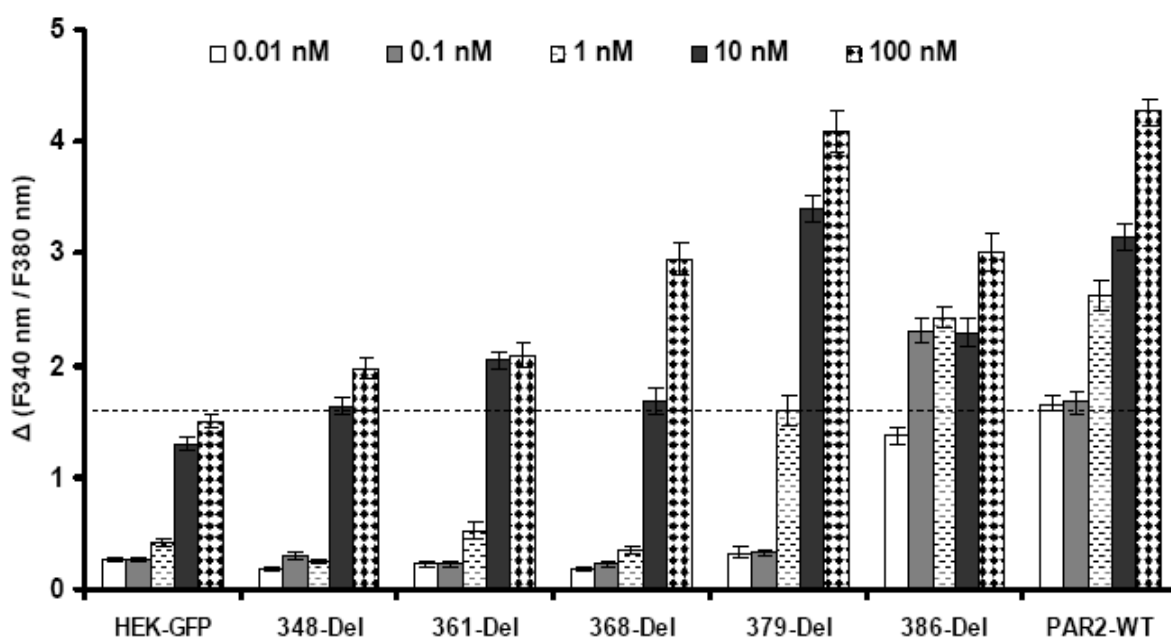
Fig. 3.3.3. The intracellular Ca^{2+} mobilization in different PAR-2 truncations. The stably transfected HEK293 cells expressing different mutants of PAR-2 were challenged by the indicated concentrations of trypsin. The intracellular Ca^{2+} responses were measured with Fura 2 dye by imaging system attached to a Zeiss Axioscope microscope. For experiments, cells were treated and the Ca^{2+} concentrations were analyzed as mentioned in method 2.2.3.8. The data are obtained and analyzed from three independent experiments. Only cells with the obviously membrane-localized GFP-signal and with the typical calcium response kinetics upon trypsin pulses were taken into account in the data analysis. For each measurement, at least 15 cells were selected for analysis and totally 60 cells were selected and analyzed for each measurement. Data shown here represent the mean ± SEM (n>3).

3.3.4 The capacity of PAR-2 mutants of activating the ERK and Akt phosphorylation

To assess whether loss of the different clusters of serine/threonine at the carboxyl tail affect PAR-2 signal transduction, we monitored the phosphorylation level of ERK and Akt under the stimulation with 100 nM trypsin for 30 min. As shown in Fig. 3.3.4, transient phosphorylation of ERK was completely abolished in the 348-Del mutant. Compared to the wild type receptor, the mutant truncations show the significant reduction in ERK phorphorylation upon the activation by trypsin. However, no significant differences in Akt phosphorylation were observed in different mutant truncations as compared to wild type receptors.
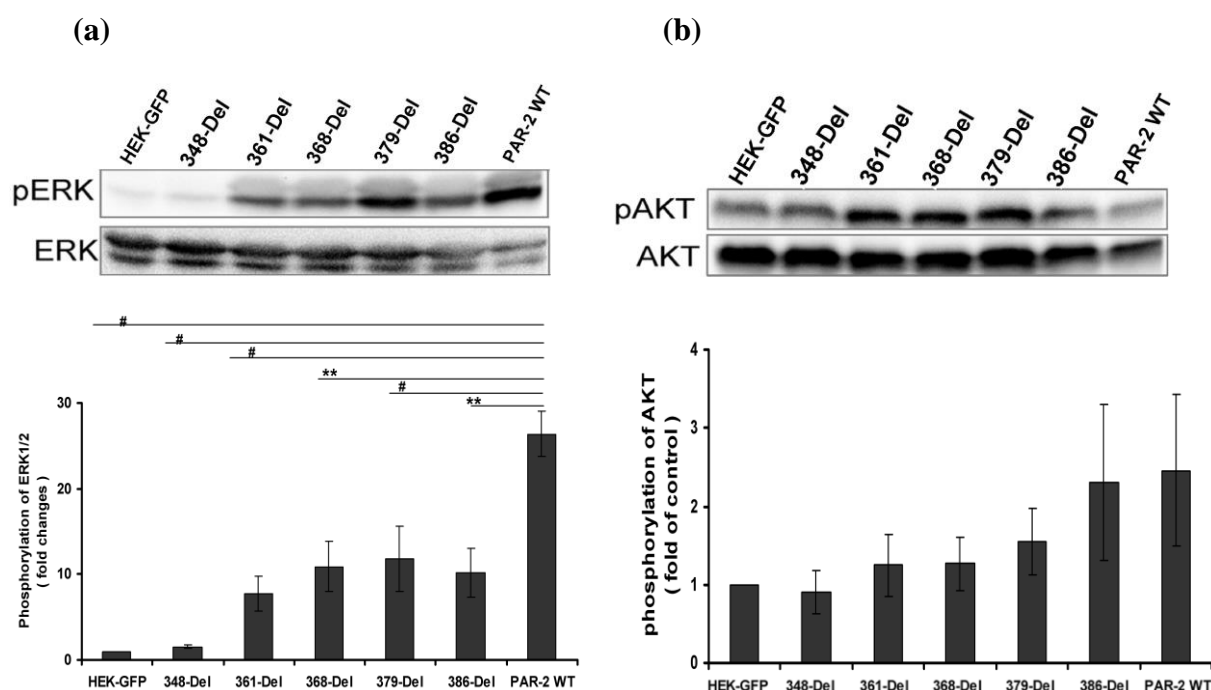
Fig. 3.3.4 Trypsin-stimulated levels of phosphorylation of ERK1/2 and Akt in truncation mutants. The transiently transfected HEK 293 cells were deprived of serum overnight. The next morning, cells were incubated with 100 nM trypsin dissolved in serum-free medium for 30 min. Thereafter, the cells were washed and lysed. The same amounts of extracted proteins were loaded to SDS-PAGE gel. (a) Western blots were done to monitor the level of phosphorylation ERK, and the quantified bars show the mean value ± SEM of four independent experiments (** $p<0.01$, # $p<0.001$). (b) The representative Western blot is shown here and the levels of phosphorylation of Akt in PAR-2 mutants, and the quantification of these levels show the mean value ± SEM of three independent experiments.

3.3.5 The cell viability of the HEK 293 cells transfected with different PAR-2 truncation mutants under the stimulation with PAR-2 agonist

Activation of endogenous PAR-2 receptor with the specific peptide agonist or trypsin was demonstrated to induce proliferation of the endometriotic stromal cells [136] and rat pancreatic stellate cells proliferation [137]. In this study, our hypothesis was that stimulation of HEK 293 cells with overexpression of different PAR-2 mutants might lead to cell death at different extents. The explanation of this hypothesis was that the receptor over-expressing cells would produce long-lasting signal transduction in the intracellular environment upon agonist treatment. The excess signaling might finally be harmful to the cells.

In order to examine our hypothesis, the various stably transfected PAR-2 mutants HEK 293 cells were treated with 50 μM of PAR-2 agonist for 48 h. Finally, the viabilities of differently transfected cell were evaluated by WST-1 assay. From the data shown in Fig. 3.3.5, we did not observed a difference in cell viability between the PAR-2 agonist-treated HEK-GFP cells and the untreated HEK-GFP cells. Similar results were observed in 348-Del cells, which is in agreement with the signaling investigation. The initiation of significantly decreased cell viability was observed in mutant 361-Del, which showed that 32% of cell death after 48 h incubation with PAR-2 agonist as compared to the HEK-GFP cells. The percentages of cell death were increased in the mutant truncations containing more serine/therione phosphorylation sites in the carboxyl tail. Especially in the cells expressing 386-Del, the cell death was similar as that in the cells carrying wild type receptors; around 74% of cell death was observed.
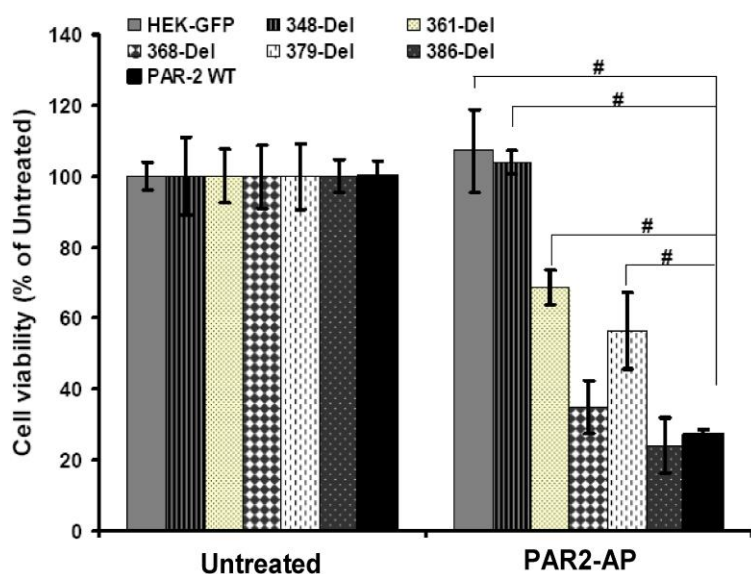
Fig. 3.3.5 Stimulation of PAR-2 mutant truncations induced cell death by PAR-2 AP. Stable-transfected PAR-2 mutants were seeded on the 96 well-plates at the density of 15,000 cells per well for 24 h. After that, cells were deprived of FCS overnight. The next morning, cells were treated with 50 μM of PAR-2 agonist for another 48 h. The untreated cells were set in parallel as control. The cell death was evaluated by WST-1 assay. Data shown here represent the mean ± SEM of at least three independent experiments. The one-way analysis of variance (ANOVA), followed by Newman–Keuls test to assess the statistical significances of the differences between the PAR-2 agonist-treated cells. There were no differences in cell viability between the untreated transfected cells (# p <0.001).

3.4 The possible interaction between αB-crystallin and β-arrestin 1/2, and their functional roles in the cell death

3.4.1 Colocalization of αB-crystallin and β-arrestin 1/2 without or with the activation of PAR-2

It was reported that formation of β-arrestin1/2 and Hsp27 complex in response to the selective β adrenergic receptor agonist isoproterenol was sufficient for protection against programmed cell death initiated by staurosporine in a human urothelial cell line [124]. β-arrestin was well studied as cytosolic protein associated with receptor desensitization and internalization of some 7 transmembrane receptors, including PAR-1 and PAR-2.

To make it clear whether the activation of PAR-2 will initiate the β-arrestin1/2 and αB-crystallin complex formation, we transiently co-expressed β-arrestin 1 with GFP tag or β-arrestin 2 with YFP tag and αB-crystallin with myc tag in HEK293 cells, which were seeded on coverslides. 36 h later, cells were deprived of FCS for 30 min, and then we incubated the transfected cells in 100 nM of trypsin to activate the PAR-2 receptor for different times. Thereafter cells were prepared for immunostaining, as described in 2.2.3.6. All specimens were examined with a confocal laser-scanning microscope. As for single scanning for detection of the fluorescence of YFP, a 488 nm laser wavelength filter was used. Single scanning for detection of the fluorescence of Alexa Fluor 555, a 546 nm laser was used.

Here we show the representative immunostaining pictures demonstrating the interaction between β-arrestin 2-YFP and αB-crystallin-myc. Moreover, the similar interaction was found between β-arrestin 1 and αB-crystallin (not show). Based on the results shown in Fig. 3.4.1, without trypsin treatment, a small number of αB-crystallin colocalized with β-arrestin 2 on the cell membrane (at 0 min). Similar results were observed after application of trypsin for 2 or 5 min. Upon the activation of PAR-2 by trypsin for 30 min, the increasing number of αB-crystallin and β-arrestin 2 were colocalized on the cytoplasm and cell membrane. The results support the idea that αB-crystallin and β-arrestin 1 and 2 interacted with each other not only on the cell membrane in the non-stimulation station, but also colocalized with each other under trypsin treatment.

Time (min)	β-arrestin 2	αB-crystallin	overlay
0			
5			
30			
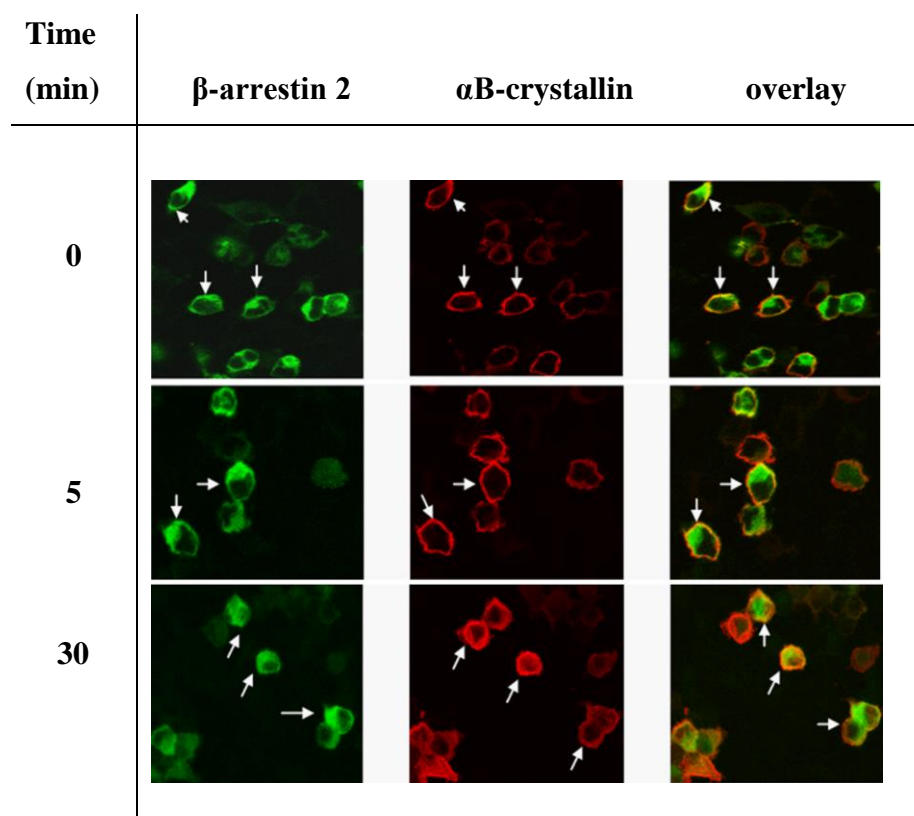
Fig. 3.4.1 The interaction between β-arrestin 2 and αB-crystallin.
HEK293 cells were cotransfected with β-arrestin 2-YFP and αB-crystallin-myc for 36 h. Thereafter, the transfected cells were deprived of serum for 30 min before treating cells with 100 nM of trypsin for different times as indicated in figures.
Fluorescence images were captured sequentially at excitation of 488 nm, and 543 nm with a LSM510 laser scanning confocal microscope.
The experiments were repeated at least twice with similar results for each.

3.4.2   Co-immunoprecipitation of β -arrestin1/2 with αB-crystallin

In order to confirm the interaction results obtained with the confocoal microscope, HEK293 cells were co-transfected with β-arrestin1/2 with myc tag and αB-crystallin with HA tag plasmids. The cells transfected with αB-crystallin-HA alone were set as negative control. 36 h after transfection, cells were incubated with FCS-free medium for another 30 min, and then 100 nM of trypsin was added to activate PAR-2 for another 30 min. Agonist was removed after 30 min through aspirating medium immediately, and cells lysates were quantified to ensure the same quantity of protein contained in each protein sample. For the immunoprecipitation experiments, cell lysates were incubated with protein A/G beads and the following steps were carried out as described in the methods 2.2.3.5.

From the IP results in Fig. 3.4.2, it can be found that β-arrestin 1 shows a strong expression level in HEK 293 cells (in lane 6) and β-arrestin 1 interacts with αB-crystallin when PAR-2 was activated by trypsin for 30 minutes (lane 1). In addition, we found low expression of β-arrestin 2-myc in HEK 293 cell lysates from cells that were co-transfected with β-arrestin 2-myc and αB-crystallin-HA (lane 7). However, the interaction between β-arrestin 2-myc and αB-crystallin-HA still can be detected slightly (lane 2, red box), indicating that β-arrestin 2 interacts with αB-crystallin either. The IP results favour our hypothesis that

β-arrestins interact with αB-crystallin under the stimulation of PAR-2 by trypsin, which is also in accordance with the results obtained from immunostaining of cells.

In the control (lane 3), when β-arrestins were absent in the HEK 293 cells, no immunoprecipitated protein were detected in 20 Kd. Lanes 4 and 5 show that αB-crystallin are well produced in HEK-293 cells which are co-transfected with αB-crystallin and β-arrestins.
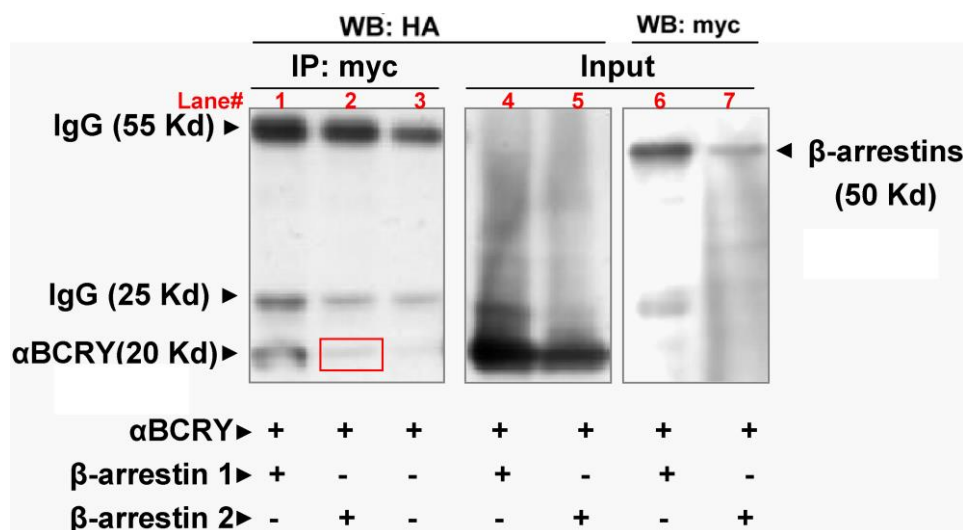
Fig. 3.4.2 Identification of the interaction between β-arrestins and αB-crystallin by IP experiments. HEK293 cells were cotransfected with with β-arrestin1/2 with myc tag and αB-crystallin with HA tag plasmids for 36 h. Then the cells were incubated with FCS-free medium for another 30 min, thereafter 100 nM of trypsin was added to activate PAR-2 for another 30 min. The whole cell lysates were prepared for IP experiments as described in 2.2.3.5. Lanes 4-7 show the input control of respective protein in the same cell lysates used for IP experiments. The experiments were repeated three times to get consistent results. The representative figure is shown here.

3.4.3　β-arrestin-1 is involved in the PAR-2-activated phosphorylation of αB-crystallin at Ser59

The phosphorylation of αB-crystallin at Ser 59 induced by agonist-induced PAR-2 activation is demonstrated to be important for protecting rat brain astrocytes from C2-ceramide- and staurosporine-induced cell death [123]. To understand deeply whether β-arrestin 1 is involved in regulation of αB-crystallin phosphorylation at Ser 59, β-arrestin 1 was down-regulated by transfection of astrocytes with siRNA of β-arrestin 1, the knockdown efficiency was shown in Fig. 3.1.7a. In the absence of β-arrestin 1, the specific PAR-2 agonist lost the capacity to transiently activate αB-crystallin phosphorylation at Ser 59. This phenomenon was clearly confirmed by Western blot data (Fig. 3.4.3a). With stimulation of PAR-2 agonist for 1 h, there is a relatively lower level of αB-crystallin phosphorylation at Ser 59 in β-arrestin 1-silenced astrocytes as compared with this level shown in the non-silenced astrocytes (Fig. 3.4.3 a and b). Interestingly, there are no differences observed in αB-crystallin

phosphorylation level of Ser 59 in the the long time activation of PAR-2 at 6 and 24 h. In conclusion, our data support that β-arrestin 1 is necessary for maintaining the transient αB-crystallin phosphorylation at Ser 59 under the challenge of PAR-2 activation.

(a)

(b)
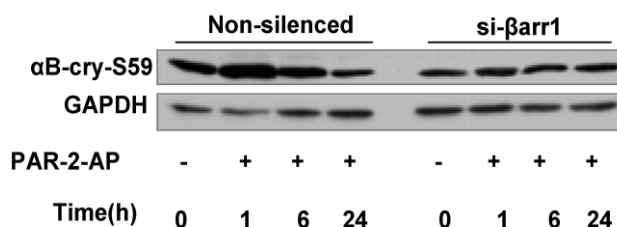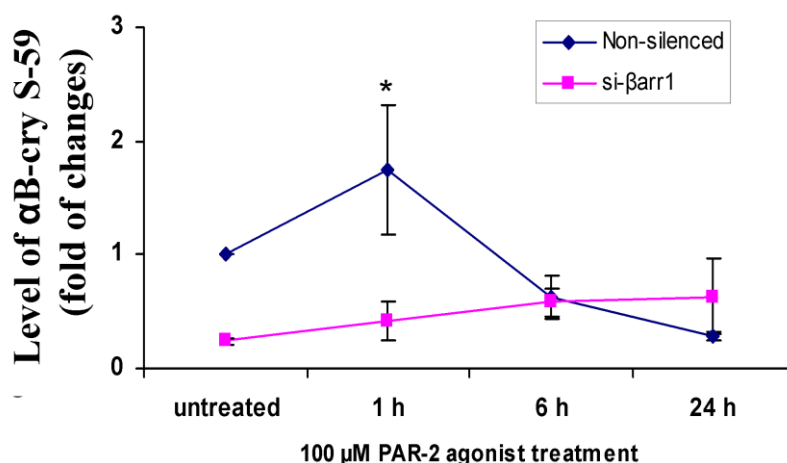
Fig. 3.4.3. β-arrestin-1 regulates the transient phosphorylation of αB-crystallin at Ser59 in astrocytes. (a) The β-arrestin-1-deficient astrocytes were deprived of FCS overnight, and then the astrocytes were incubated with 100 μM of PAR-2 agonist for indicated times. The representative blot is shown here to display the changes of phosphorylation at different time points. (b) The level of the phosphorylation αB-crystallin at Ser 59 was quantified and normalized to GAPDH. The value of phosphorylated αB-crystallin at Ser 59 in untreated non-silenced astrocytes was set as 1. The data show the mean value± SEM, n=5.

3.4.4 Activation of PAR-2 failed to save astrocytes from STS-induced apoptosis in β-arrestin-1-deficient astrocytes.

β-Arrestin-1 was demonstrated to negatively regulate PI3K/Akt signaling pathway upon thrombin-activated PAR-1, which played a pivotal role in cytoprotection in previous results (3.1.3). In order to investigate whether β-arrestin 1 played any functional roles in PAR-2 downstream signaling cascades, we checked the functional changes upon the activation of PAR-2 receptor in β-arrestin 1-deficient astrocytes. Similarly, to the experiments described in 3.1.3, the β-arrestin 1-deficient astrocytes were treated with staurosporine to induce cell death. At the same time, the specific PAR-2 agonist (PAR-2-AP) was given in the absence or presence of staurosporine.

From the data in Fig. 3.4.4b, quantification of the level of cleaved caspase 3 shows that staurosporine caused 2 times higher level of cleaved caspase 3 in β-arrestin-1-silenced astrocytes as compared to that in the non-silenced cells. However, it is not observed that activation of the PAR-2 receptor protected astrocytes from staurosporine-induced cell death in both non-silenced and β-arrestin 1-silenced astrocytes, because the level of cleaved caspase 3 in the co-treatment of PAR-2 agonist and staurosporine showed the similar level as in staurosporine-treated non-silenced and β-arrestin-1-silenced astrocytes. In contrast to the activation of PAR-1 which prevented apoptosis occurred in β-arrestin 1-deficient astrocytes (see Fig. 3.1.3); the activation of PAR-2 was incapable to rescue astrocytes from cell death in β-arrestin 1-deficient astrocytes.

(a)

(b)
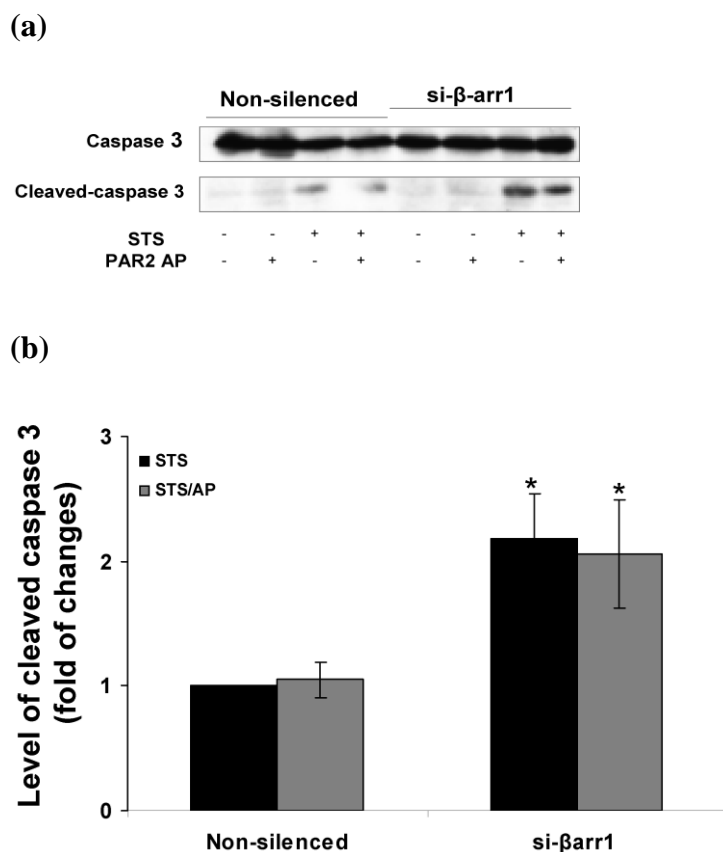
Fig. 3.4.4 PAR-2 activation failed to protect astrocytes from staurosporine-induced cell death.
(a) The FCS-starved non-silenced or β-arrestin 1-silenced astrocytes were treated with 0.5 μM staurosporine (STS) in the absence or presence of 100 μM of PAR-2 agonist (AP). 24 h later, the cells were harvested and Western blots were done to assess the level of cleaved caspase 3 under the indicated treatments. The representative blot of cleaved caspase 3 from one of three independent experiments is shown. (b) The value of cleaved caspase 3 is obtained by the ratio of cleaved caspase 3 divided to the sum of cleaved caspase 3 and caspase 3. The level of cleaved caspase 3 in non-silenced cells in the presence of STS was taken as 1. Data shown in b represent the mean ± SEM of three independent experiments.
*$p < 0.05$ as compared to the non-silenced cells treated with staurosporine, which was taken as 1.

3.4.5 αB-crystallin promotes astrocytes viability and facilitates the phosphorylation of MAPK and Akt

αB-crystallin was reported to have protective effects on astrocytes from chemically induced cell death [105]. Newly published data suggest that αB-crystallin applied in the extracellular environment will be absorbed by the cells, and then exert antiapoptotic effects as intracellular player [138]. However, compared to the large amount of data explaining the functions of endogenous αB-crystallin, the functions exerted by exogenous αB-crystallin on cells are largely unknown.

To evaluate whether exogenous αB-crystallin has any effects on astrocytes survival, the cell viability was evaluated after deprivation of serum in the absence or presence of αB-crystallin for 48 h. The viability of astrocytes was checked by WST-1 assay. It can be seen that extracellular application of different concentrations of αB-crystallin promotes astrocytes survival at different extents (Fig. 3.4.5a). In detail, application of 1 µg/ml of αB-crystallin to astrocytes yields a small elevation of astrocytes viability, while 10 µg/ml and 100 µg/ml of αB-crystallin lead to 1.6 times and 1.9 times higher viability of astrocytes, respectively, as compared to the control.

Since the MAPK and PI3K/Akt were implicated in cell survival and cell proliferation, we were wandering whether αB-crystallin works like a signaling molecule which activates these signal transductions in astrocytes. The primary astrocytes were incubated with 100 µg/ml of αB-crystallin in serum-free medium for 24 h or 48 h. After that, Western blots were done to monitor the activation of ERK1/2, p38, JNK and PI3K/Akt signaling pathways. It was shown that the phosphorylation of ERK, p38, JNK and Akt was enhanced after application of the exogenous 100 µg/ml of αB-crystallin for 24 h as well as 48 h (Fig. 3.4.5b).

(a)

(b)
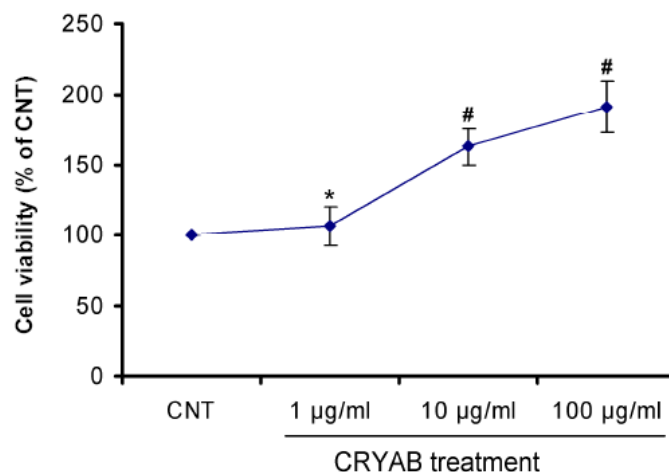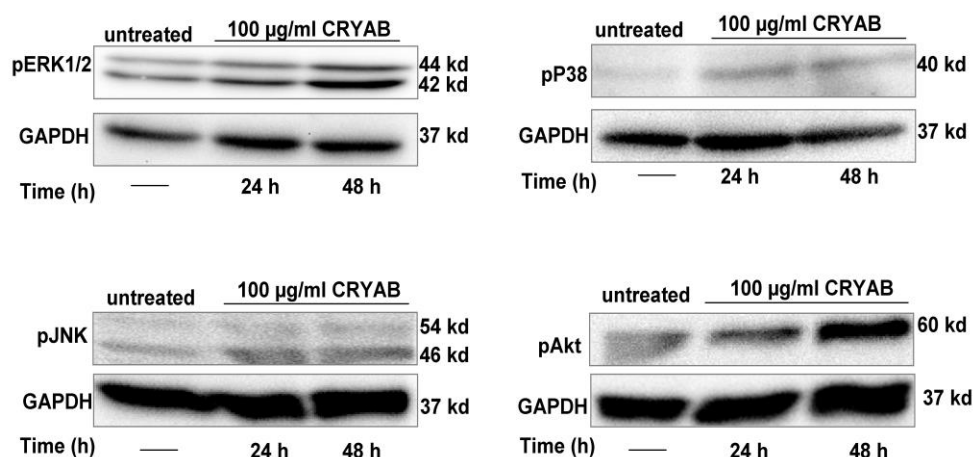
Fig. 3.4.5. αB-crystallin increases the viability of astrocytes and stimulates MAPK and Akt signaling pathways. (a) Astrocytes were exposed to FCS-free medium in the absence (control, CNT) or presence of 1 µg/ml, or 10 µg/ml, or 100 µg/ml of αB-crystallin for 48 h. The cell viability was analysed by WST-1 assay. The results show the percentage changes of cell viabilty upon treatment with different concentrations of αB-crystallin as compared to control cells (CNT), (* $p<0.05$, # $p<0.001$, n=3). (b) Astrocytes were incubated with 100 µg/ml of αB-crystallin for 24 h or 48 h in FCS-free medium, thereafter the phosphorylation of Akt, ERK1/2, p38 and JNK was detected by Western blot. The experiments were repeated for three times with similar results and representative Western blots are shown here.

3.4.6 Blockade of MAPK and Akt signaling pathways eliminates αB-crystallin-enhanced astrocytes survival.

In order to clarify if the stimulation of MAPK and PI3K/Akt signaling pathways by αB-crystallin are the potential mechanisms accounting for the improved survival of astrocytes, the cell viability induced by αB-crystallin in the presence of the following inhibitors was assessed. Inhibitors PD98095, SP600125, LY294002 and Rapamycin were used to block the ERK, p38, JNK, PI3K/Akt and mTOR signaling pathways, respectively.

As a result, all the inhibitors, when applied alone, induce decrease of cell viability, suggesting that inhibition of the MAPK and PI3K/Akt signaling pathways in FCS-free medium has harmful effects on astrocytes survival. Furthermore, αB-crystallin induced a higher percentage (160%) of cell viability as compared to the control (100%). The increases of cell viability were significantly hampered by the co-application of all the inhibitors used here. The percentage of cell viability in the presence of αB-crystallin declined from 160% to 103% or 100%, when inhibiting the ERK and p38, respectively. Moreover, restraining of the JNK and PI3K signaling pathways dramatically decreased the viability of αB-crystallin-treated astrocytes, with percentages of 64% and 57%, respectively. At the same time, when inhibiting mTOR, the suggested signaling cascade located downstream of PI3K/Akt, a significantly reduced cell viability was also observed.

To sum up, exogenous application of αB-crystallin triggers MAPK and PI3K/Akt/mTOR signaling pathways to accelerate the survival of astrocytes in the serum-starved situation.
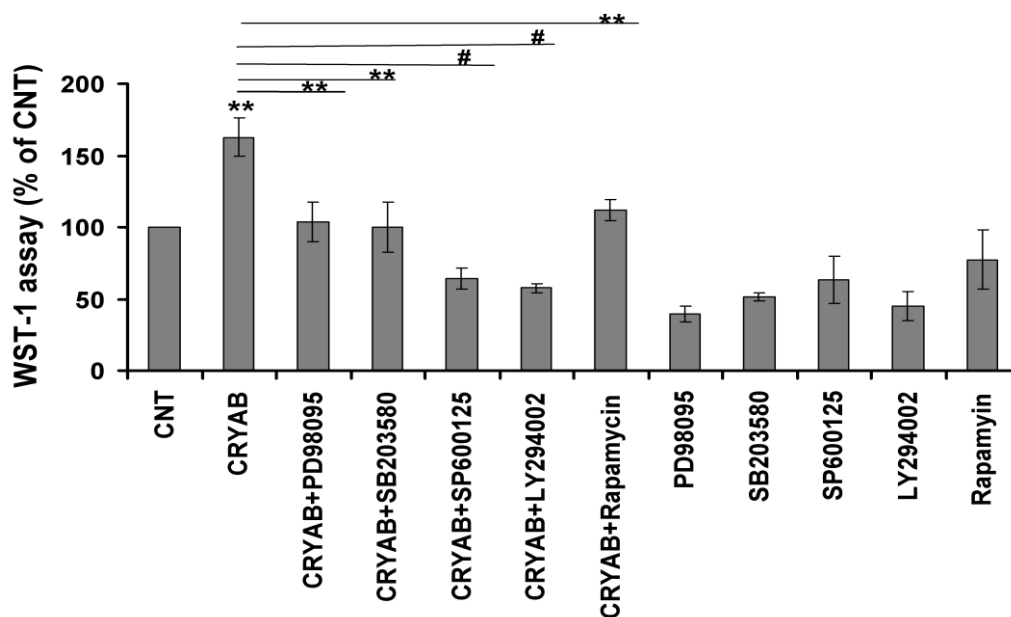
Fig. 3.4.6 MAPK and PI3K/Akt/mTOR signaling pathways are responsible for the viability of astrocytes promoted by αB-crystallin. Astrocytes were treated without or with 10 μg/ml of αB-crystallin (CRYAB) plus one of following inhibitors respectively: 2 μM mTOR inhibitor (Rapamycin), or 20 μM PI3K/ Akt inhibitor (LY294002), or 10 μM ERK1/2 inhibitor (PD98095), or 10 μM p38 inhibitor (SB203580), or 20 μM JNK inhibitor (SP600125) for 48 h. The cell viability was evaluated by WST-1 assay. The untreated cells were set as control which was viewed as 100%, (** p<0.01, # p<0.001, n=3).

3.4.7 Extracellular application of αB-crystallin protects astrocytes from apoptosis through stimulating the Akt signaling pathway.

It was previously well documented that overexpression of αB-crystallin and the increased level of specific phosphorylation of αB-crystallin at Ser 45 and Ser 59 protect astrocytes from cell death induced by C2-ceramide and staurosporine [122, 139]. Correspondingly, downregulation of αB-crystallin increased the astrocytes death. It was also proven that αB-crystallin was capable of promoting the survival of astrocytes under serum deprivation (Fig. 3.4.5). To understand whether αB-crystallin has antiapoptotic effects, we treated astrocytes with staurosporine for 48 h to induce apoptosis without or with extracellular application of 10 µg/ml or 100 µg/ml of αB-crystallin. The apoptosis was estimated by the protein level of cleaved caspase 3 in Western blots. Under the treatment with staurosporine, there was an increase of cleaved caspase 3. Interestingly, this level was significantly reduced after the co-treatment of astrocytes with αB-crystallin (10 µg/ml or 100 µg/ml) (Fig. 3.4.7).

The Akt signaling pathway is involved in cell survival and proliferation, which was seen in many studies. To investigate whether the phosphorylation status of Akt was correlated with the antiapoptotic effects of αB-crystallin, the level of Akt phosphorylation was probed in parallel. With staurosporine, there was a decreased level of phosphorylation of Akt. With the combination of 10 µg/ml or 100 µg/ml αB-crystallin, the level of phosphorylation of Akt was significantly increased as compared with the treatments only with staurosporine (Fig. 3.4.7c). In conclusion, extracellular application of αB-crystallin protected astrocytes from apoptosis through Akt signaling pathway.

MAPK were suggested to be related with the protective processes of αB-crystallin [140, 141]. In our current studies, it seems that the ERK signaling pathway played an unimportant role in cytoprotection, because we failed to observe the significantly increased level of phosphorylation of ERK after treatment of αB-crystallin (Fig. 3.4.7d).
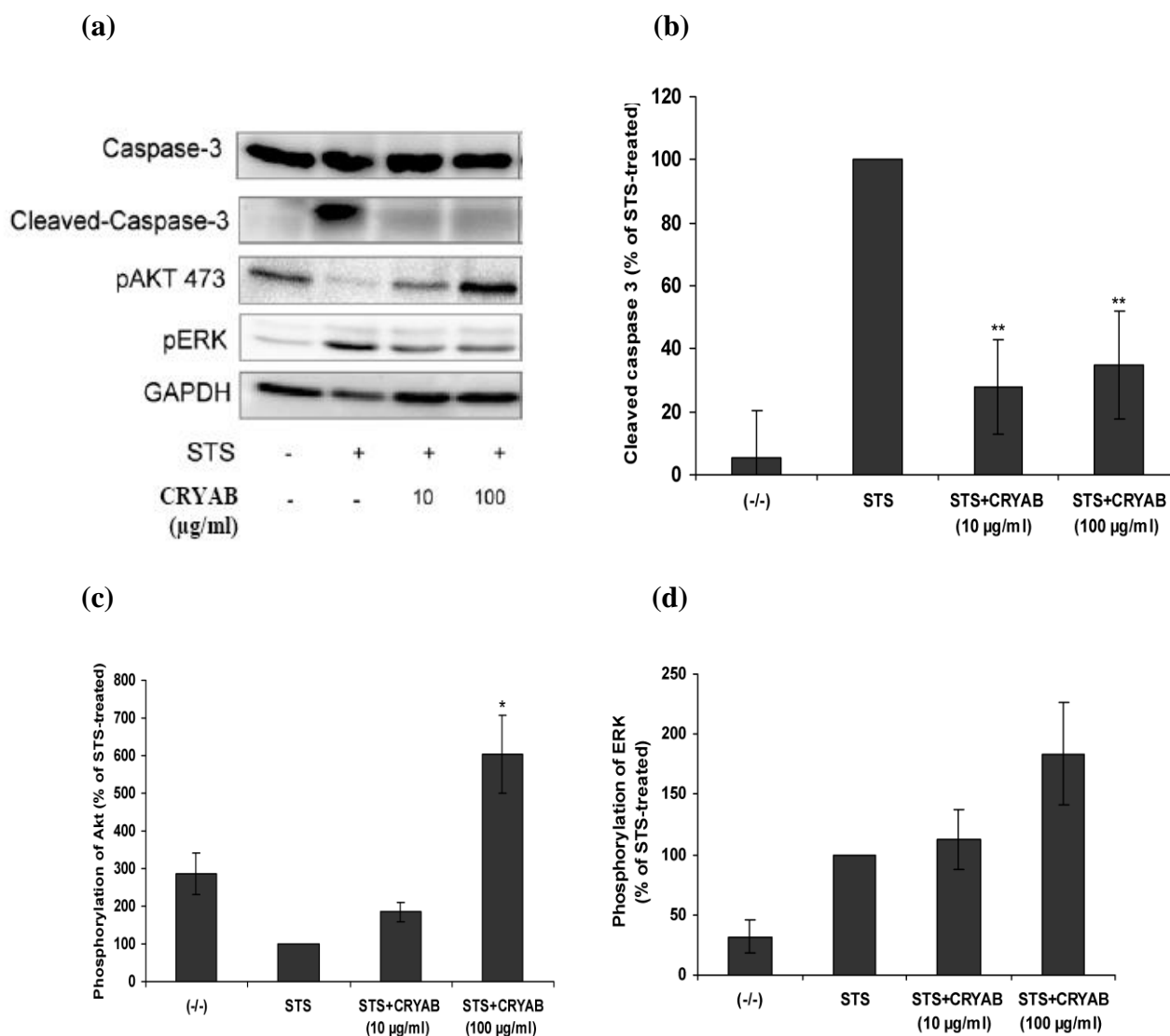
(a)

(b)

(c)

(d)

Fig. 3.4.7 αB-crystallin protects astrocytes from apoptosis through stimulating the Akt signaling pathway (a) Astrocytes were incubated with 0.2 µM of staurosporine (STS) in the absence or presence of different concentrations of αB-crystallin (CRYAB). The apoptosis determined by the cleaved caspase 3 as marker under different conditions in astrocytes was checked by Western blot. In parallel, the phosphorylation levels of Akt and ERK were also checked. Representative blots are shown (n=3). (b) The band density of cleaved caspase 3 under the indicated treatments was quantified and divided by the density value of GAPDH. The percentages of cleaved caspase 3 level are normalized to STS-treated cells. The value of cleaved caspase 3 under STS-treatment was taken as 100% (** $p<0.01$, n=3). (c) Akt phosphorylation was compared to that in the STS-treated cells, which was set as 100%. (d) The quantification of phosphorylation of ERK was compared to that in STS-treated cells which was taken as 100% (* $p<0.05$, n=3).

3.4.8   αB-crystallin blocks ROS generation in RBM

In order to investigate if αB-crystallin has any functions on ROS generation in RBM, the effects of treatment with αB-crystallin for 10 min on ROS production were tested. Glutamate and malate as the complex I-linked substrate are oxidized by dehydrogenases with reduction of nicotinamide adenine dinucleotide, then finally feeding electrons into Complex III which is

a key site for ROS production. Antimycin A inhibits complex III at the Qi centre and increases superoxide generation from the Q_0 centre. In the presence of SOD, superoxide was metabolized to H_2O_2, and therefore ROS were measured as generated H_2O_2 using the Amplex red assay described in methods. The wells which contained only Antimycin A and RBM were set as control value (Fig. 3.4.8, bar 1). Without respiratory substrates (-(G+M)), there are no obvious differences between the level of ROS generation induced by Antimycin A in RBM upon the treatment with different concentrations of αB-crystallin (Fig. 3.4.8, bar 3, 5, and 7) and control situation (Fig. 3.4.8, bar 1). Antimycin A caused 200% of ROS induction in the presence of glutamate, malate which were used as the respiratory substrate in RBM (Fig. 3.4.8, bar 2) as compared to the control (100%), confirming that the mixture containing Antimycin A, glutamate, malate, and RBM is an effective model to induce ROS. After application of 1 µg/ml of αB-crystallin in the presence of glutamate and malate, the level of Antimycin A-induced ROS production failed to show obvious changes (Fig. 3.4.8, bar 4 *vs* bar 2). When the concentration of αB-crystallin was elevated to 10 µg/ml and 50 µg/ml in the presence of the substrate and Antimycin A, a significant reduction of ROS production was observed (Fig. 3.4.8, bar 6 *vs* bar 2; bar 8 *vs* bar 2), with the percentages of ROS production declining from 200% to 130% and 126%, respectively. To sum up, αB-crystallin is capable to reduce the level of ROS generation in RBM.
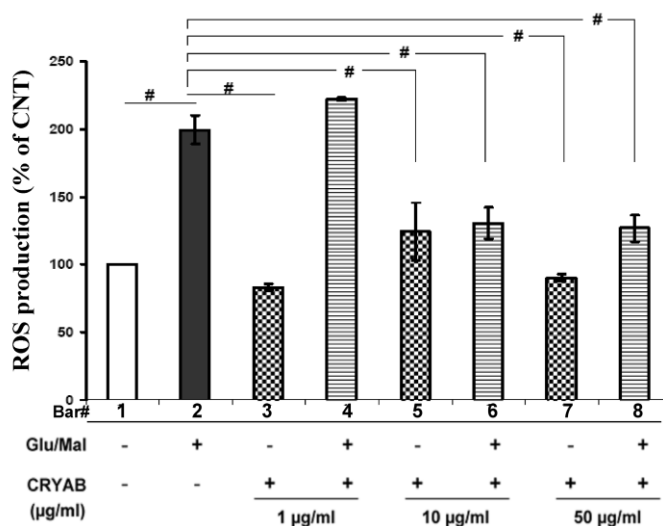
Fig. 3.4.8 The effect of αB-crystallin on ROS production in RBM treated with Antimycin A. Rat brain mitochondria were prepared as described in 2.2.3.4. ROS production was measured according to the protocol indicated in methods 2.2.3.4. Antimycin A was used as the inducer of mitochondrial ROS production in the presence of glutamate (Glu)/ malate (Mal) as substrates, which caused 200% of ROS generation (bar 2). The wells containing only the mixture of 50 µg of RBM and 1 µM of Antimycin A were set as control (CNT=100%). Treatment with 1 µg/ml of αB-crystallin (CRYAB) on RBM failed to reduce ROS generation induced by Antimycin A in the presence of Glu/Mal (bar 4 *vs* bar 2). With 10 µg/ml of αB-crystallin, ROS production is inhibited (130% *vs* 200%, bar 6 *vs* bar 2). With 50 µg/ml of αB-crystallin, the mitochondrial ROS production declined from 200% to 126% (bar 8 *vs* bar 2) (# $p<0.001$, n=3). The number under the X-axis indicates the bar's number as described in results.

4 Discussion

4.1 β-arrestin 1 as the signaling adaptor and interaction partner of PAR mediates cellular functions

A striking novel finding of our current study was that β-arrestin 1, an interaction partner of PAR-1, promotes anti-apoptotic effects in astrocytes and is involved in the PAR-1/PI3K/Akt survival signaling pathway activated by thrombin. Several partner-proteins of PAR were identified in our laboratory. For example, α-crystallin interacts with PAR-2 to rescue astrocytes from cell death [142], and the PAR-2-interacting protein Jab1 controls PAR-2-induced activation of the transcription factor activator protein-1 to regulate activity of c-Jun [92]. β-Arrestins were demonstrated to interact with PAR-1 and PAR-2. β-Arrestin 1 is essential for PAR-1 desensitization, but dispensable for receptor internalization [93]. The situation is different for PAR-2, because both β-arrestin 1 and β-arrestin 2 have been found to be crucial for receptor internalization as well as desensitization signaling.

Accumulating evidence emphasizes the functional role of β-arrestins as signaling adaptors. β-Arrestins were reported to mediate cytoprotection in different cell types by stimulation of various signaling pathways. For example, in β-arrestin $1/2^{-/-}$ mouse embryonic fibroblasts, cell death occurred upon stimulation of the N-formyl peptide receptor. The reintroduction of either β-arrestin 1 or β-arrestin 2 inhibited the apoptosis [101]. Moreover, in human endothelial cells, PAR-1 receptor stimulated by APC promoted cytoprotection through β-arrestin-mediated Ras-related signaling of C3 botulinum toxin substrate [100]. Activation of insulin-like growth factor 1 receptor initiated β-arrestin-dependent activation of Akt, and therefore protected the cells from apoptosis [143]. The overexpression of β-arrestin 2 significantly inhibited opioid-induced apoptosis and β-arrestins prevented cell apoptosis through ERK1/2 and p38 MAPKs and Akt pathways [102, 103, 144].

However, there is still limited information about the functional role of β-arrestins in regulating PAR signaling cascades which block cell death in CNS cells. Here, we for the first time explored the potential role of β-arrestin 1 in survival signaling pathways in astrocytes. We found that β-arrestin 1 played a pivotal role in inhibiting apoptosis, since the deficiency of β-arrestin 1 in astrocytes caused a much higher apoptosis (Fig. 3.1.1c and 3.1.5c). The molecular mechanisms accounting for the enhanced apoptosis in the absence of β-arrestin 1 in astrocytes is still not clear. It is possible that the over-stimulated G-protein signaling pathway without the inhibition from binding of β-arrestin 1 is responsible, or lacking of the β-arrestin 1 signal transduction contributes to apoptosis.

Activation of the PAR isoforms in the CNS has multiple biological effects including the stimulation of various signaling cascades, which has been detected in our laboratory. For instance, thrombin and other PAR-1-specific agonists stimulated proliferation of astrocytes through ERK1/2 activation [35]. In our current study, we also observed that different concentrations of thrombin promote the proliferation of astrocytes to different extents (Fig. 3.2.1). Moreover, the activation of PAR-1 by thrombin rescued astrocytes from C2-ceramide-induced cell death through stimulating JNK and ERK1/2 to increase the levels of GRO/CINC [36]. On the other side, PAR-2 activation in astrocytes remarkably protects the cells from C2-ceramide-induced cell death. PAR-2 activation elicited the upregulation of JNK, P38 and ERK1/2 [145]. Thrombin as PAR-1 agonist has either protective or toxic effects in the CNS. Low concentrations of thrombin (10 pM-10 nM) protect hippocampal neurons or astrocytes from cell death caused by oxygen-glucose deprivation, hypoglycemia, growth supplement deprivation, oxidative stress or C2-ceramide [24, 30, 146]. However, the high concentration of thrombin (500 nM) induces a more severe cellular damage than oxygen-glucose deprivation alone [30]. We found in the present study that the activation of PAR-1 by thrombin concentration-dependently exerted cytoprotection; the optimal concentration for protection is between 0.5 and 1 U/ml (Fig. 3.1.2).

In this study, we elucidated whether activation of PAR produces the protective effects, when β-arrestin 1 is silenced in astrocytes. The specific PAR-2 agonist was studied firstly in this situation. However, we did not observe that the activation of the PAR-2 receptor protected astrocytes from staurosporine-induced cell death in both non-silenced and β-arrestin 1-silenced astrocytes (Fig. 3.4.4). The situation was quite different when the PAR-1 receptor was activated by thrombin. In this case, the activation of PAR-1 significantly promoted the cell viability under the exposure to staurosporine (Fig. 3.1.2 and Fig. 3.1.3).

To make it clear whether the cell death caused by staurosporine was due to apoptosis or necrosis, we investigated the protein level of a typical apoptotic protein that is cleaved caspase 3. We studied cell death or cell protection. We detected that this apoptotic marker was increased after staurosporine treatment and decreased with the combined treatment of thrombin and staurosporine (Fig. 3.1.3a and b). However, we could rule out that thrombin decreased the population of early apoptotic cells (Fig. 3.1.3d), but thrombin significantly reduced the number of late apoptotic cells / dead cells (Fig. 3.1.3b and c). As a result, we speculated that thrombin could hamper the early apoptotic cells going to the stage of late apoptotic period or the stage of cell death. This could explain why we detect a decreased level

of cleaved caspase 3 after thrombin treatment, but not a significant reduction in the number of early apoptotic cells.

Another quite interesting finding was that β-arrestin 1 negatively regulated the protective signaling pathway stimulated by thrombin. In β-arrestin 1-deficient astrocytes, activation of PAR-1 initiated a significant increase of phosphorylation of Akt as compared to the control situation (Fig. 3.1.4). This result confirmed that thrombin-activated PAR-1 protected β-arrestin 1-deficient astrocytes from cell death through the PI3K/Akt signaling pathway.

Thus, we conclude that the thrombin-stimulated phosphorylation level of Akt plays a pivotal role in the cytoprotection effects. Thrombin may trigger growth factors to facilitate the Akt phosphorylation in astrocytes. This hypothesis was investigated by using specific inhibitors to block EGF and PDGF receptors in both non-silenced and β-arrestin 1-silenced astrocytes. In the absence of β-arrestin 1, the transactivation of EGF and PDGF receptors contribute to thrombin-induced Akt phosphorylation, which is necessary for the thrombin-induced cytoprotection (Fig. 3.1.6).

We summarize our data in Fig. 4.1.
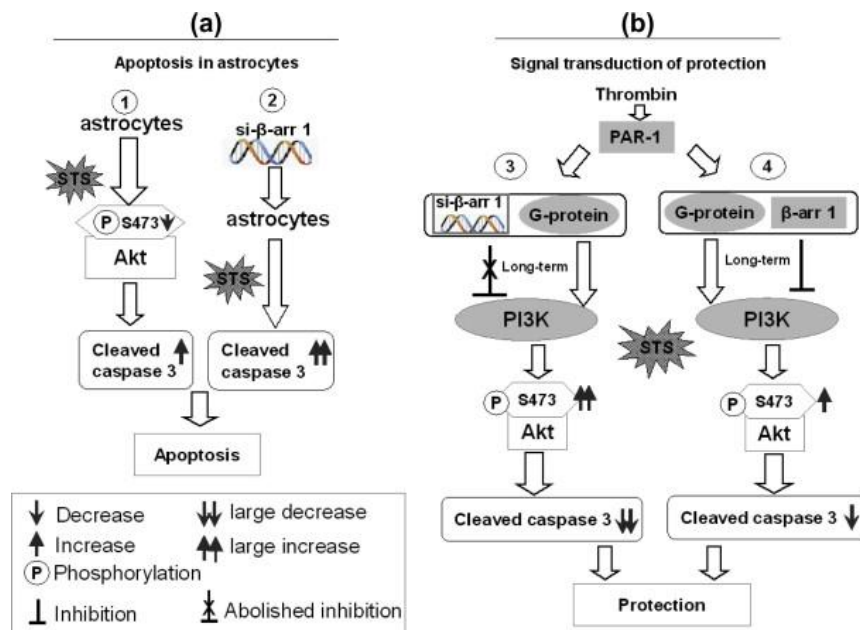
Fig. 4.1 Signaling pathways in staurosporine-caused apoptosis and signaling pathways in thrombin-induced protection in astrocytes under the influence of β-arrestin 1. Staurosporine is an effective inducer of apoptosis in both non-silenced astrocytes and β-arrestin 1-deficient astrocytes through increasing the cleavage of caspase 3 (Fig. 4.1a). The possible mechanism of the staurosporine-induced apoptosis in wild-type astrocytes implies inhibition of the phosphorylation of Akt (signal transduction ①). In contrast, this mechanism cannot explain the apoptosis induced by staurosporine in β-arrestin 1-deficient astrocytes (see Fig. 4.1b). In β-arrestin 1-lacking astrocytes, staurosporine-induced signal transduction results

in a considerably higher level of cleaved caspase-3 caused by staurosporine as compared to the control situation (Fig. 3.1.3a and b) (signal transduction ② in (a)).

The signal transductions initiated by thrombin-activated PAR-1 via both the β-arrestin 1 and G-protein signaling arms are displayed in Fig. 4.1b. On the one hand, thrombin initiates signal transduction after PAR-1 activation in the absence of β-arrestin 1 in gene-silenced astrocytes (signal transduction ③), in which the PI3K/Akt signaling pathway is triggered only by G-protein. There Akt is over-phosphorylated (Fig 3.1.4b, bar 10). On the contrary, in β-arrestin 1-containing astrocytes (signal transduction ④), thrombin induced an increased level of phosphorylation of Akt that is lower than that seen in the β-arrestin 1-deficent astrocytes (Fig. 3.1.4b, bar 5 *vs* bar 10). Therefore, we conclude that β-arrestin 1 inhibits the long-term (24 h) phosphorylation of Akt (Ser 473). Blockade of the sustained PI3K/Akt signaling pathway by the specific PI3K inhibitor LY294002 decreased thrombin-induced Akt (Ser 473) phosphorylation level (Fig. 3.1.5a) and abolished the protection exerted by thrombin treatment (Fig. 3.1.5b and c). Thus, the thrombin-induced activation of the PI3K/Akt signaling pathway accounts for the protection of astrocytes from cell death induced by staurosporine. In addition, the thrombin-induced transactivation of the EGF and PDGF receptor contributes to the phosphorylation of Akt (Ser 473) in β-arrestin 1-deficient astrocytes rather than in the non-silenced astrocytes (Fig. 3.1.6). The latter is not included in Fig. 4.1.

Astrocytes in the CNS are responsible for neuronal survival and functioning, neurogenesis and neuronal repair. As a result, the survival of astrocytes under different stimuli is important for neuroprotection. Thrombin has neuroprotective effects, which have been confirmed in several independent studies. Therefore, it is important to understand the signal transduction initiated by thrombin to protect astrocytes from cell death. Our present study points out that the thrombin-stimulated PAR-1 activation initiates the PI3K/Akt signaling pathway to rescue astrocytes from cell death. This signal transduction is negatively regulated by the PAR-1-interacting partner protein β-arrestin 1. Our work provides knowledge on the question how to save astrocytes from apoptosis through controlling the activation of the PI3K/Akt signaling pathway. This could help to improve potential therapeutic methods to reduce neurotoxicity.

4.2 Multiple mechanisms account for thrombin-accelerated astrocytes proliferation

4.2.1 The important role of Ca^{2+} / MAPK and PI3K/Akt signaling pathways in cell proliferation

Mitogen-activated protein kinase (MAPK) cascades have been shown to play a key role in transduction of extracellular signals to cellular responses to promote cell proliferation. The classical MAPK family includes ERK, C-Jun N-terminal kinase/ stress-activated protein kinase (JNK/SAPK) and p38 kinase. Stimulation of GPCRs or exposure to growth factors results in the activation of ERK, p38 and JNK, which were very well summarized by Zhang et al [147] more than 10 years ago. Based on the published information, the scheme in Fig. 4.2.1 explains the activator-triggered MAPK signal transduction and induced cell responses, such as proliferation and differentiation. In our current study, thrombin was found to stimulate the ERK and JNK signaling cascades to promote astrocytes proliferation; the interesting founding is that the p38 signaling cascade was not involved in the proliferative activities (Fig. 3.2.6)
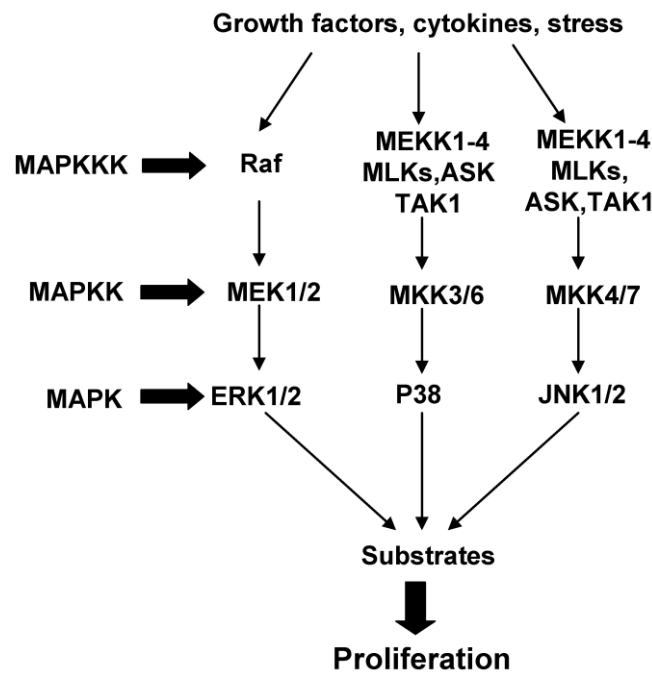
Fig. 4.2.1 Scheme of MAPK signalling transductions mediating cell proliferation. MAPK signaling cascades play a pivotal role in controlling cell cycle progression. ERK/JNK cross-activation was observed to be important for accelerating progression of cell cycle from phase G1 to S phase, in which DNA synthesis happens [148], which is the hallmark of cell proliferation. In our current study, the specific inhibitors of ERK and JNK abolished thrombin-induced astrocytes proliferation. It is reasonable to conclude that thrombin-induced activation of ERK and JNK is necessary for accelerating the cell cycle transition from G1 phase to S phase, as described before.

Although numerous signaling cascades may be involved in mediation of cell proliferation, one of the destinations of these signals is the well-known check point: the enhanced transition of cell cycle phase G1/S. Among the multiple signaling cascades, Ca^{2+} signaling has attracted much attention. The Ca^{2+} signaling pathway was implicated in mediating G1/S and G2/M transition. Ca^{2+} signaling triggered the genes responsible for stimulating resting cells (G_0) to re-enter the cell cycle, and subsequently initiates DNA synthesis at the G1/S transition [149]. According to our results, thrombin activates PAR-1-induced intracellular Ca^{2+} increase and also contributes to astrocytes proliferation, since the BAPTA-AM-intracellular chelator of Ca^{2+} eliminates thrombin-caused astrocytes proliferation (Fig. 3.2.4). This implies that thrombin-activated PAR-1 eliciting Ca^{2+} may also contribute to the G1/S transition and therefore result in cell proliferation.

The PI3K/Akt pathway has been well documented as an eminent signaling pathway, which is capable of proceeding cell cycle progression. The PI3K/Akt pathway is believed to induce cell cycle progression by stabilizing cyclin D and p21Cip1 to inhibit Cdks. The suggested mechanism is that Akt can directly phosphorylate p21Cip1 on S146 to increase its stability. Moreover, Akt may prolong the half-life of both p21Cip1 and cyclin D through inactivation of GSK-3, which phosphorylates p21Cip1 and cyclin D to induce their degradation [150]. Alternatively, the stimulation of PI3K/Akt, in a Ras-dependent or -independent manner, increases the translation of cyclin D [151]. Here we also found that thrombin induces increases of Akt Ser 473 phosphorylation, which needs the transactivation of EGF and PDGF receptors (Fig. 3.2.7). Furthermore, thrombin causes the accumulation of cyclin D1 in astrocytes in time-dependent way (Fig. 3.2.8a), which is also dependent on the phosphorylation status of Akt at Ser 473 (Fig. 3.2.8b). Another observation is that blocking PI3K signaling pathway by LY294002, both the phosphorylation of Akt Ser 473 and accumulation of cyclin D1 were largely decreased (Fig. 3.2.7 and Fig. 3.2.8b). Further, it was found that the level of accumulated cyclin D1 stimulated by thrombin declined by the treatment with EGF and PDGF inhibitor (Fig. 3.2.8b). In sum, the data strongly support that thrombin induced accumulation of cyclin D1 depends on the activation of Akt Ser 473 which leads to accelerated proliferation of astrocytes.

In the present study, we tried to explore the signaling cascades which are responsible for thrombin-induced astrocytes proliferation. It is observed that thrombin caused intracellular Ca^{2+} increase, activation of ERK and JNK, phosphorylation of Akt, and accumulation of cyclin D1, which contribute to astrocytes proliferation. If the check point of the cell proliferation is selected as the accumulation of cyclin D1 which is an important linkage

between cell cycle progression and PI3K/Akt signaling cascades, it is possible that accumulation of cyclin D1 is the destination of thrombin-activated phosphorylation of ERK, JNK and PI3K/Akt. This possibility has been confirmed by Lavoie *et al* [152]. In their study, activation of the Raf/MKK1/p42/p44MAPK cascade was sufficient to fully induce cyclin D1. However, the p38 cascade showed an opposite effect on the regulation of cyclin D1 [152]. Coincidentally, in our study, thrombin failed to activate the phosphorylation of p38 (Fig. 3.2.5c). Further, it was demonstrated that blockade of the p38 signaling pathway has no obvious inhibitory effects on astrocytes proliferation stimulated by thrombin (Fig. 3.2.6).

4.2.2 Thrombin-activated ROS stabilizes HIF-1, which might be involved in increased glucose uptake to promote astrocytes proliferation

Indeed, there has been a long-lasting debate about the role of ROS in oxygen sensing. The debate mainly focuses on three points: first, whether ROS work as signaling molecules; second, whether ROS derived from the mitochondrial respiratory chain could contribute to oxygen signaling; and third, whether ROS production is linked to the activity of signaling of HIF-1α such as hydroxylases or kinases [153]. Currently, ROS is appreciated as signaling molecule to regulate a variety of pathways in physiology, and many reports transduction provide evidence to highlight the important role of mitochondrial ROS in mediating signaling in a variety of systems [154].

It has been proposed that ROS generated from the mitochondrial complex I and complex III can stabilize HIF-1 under hypoxia [81]. HIF-1 increases the expression of glucose transporters, such as GLUT-1, GLUT-3 and GLUT-4 which are important for the entry of glucose into cells. In our present study, with the increase of glucose uptake in astrocytes (Fig. 3.2.10a), the protein level of HK2 in astrocytes was also upregulated by thrombin after 24 h (Fig. 3.2.11a and c), and blockade of HK2 accumulation by Apigenin eliminates astrocytes proliferation induced by thrombin (Fig. 3.2.10b). Moreover, it is observed that thrombin induced the accumulation of HIF-1α after 24 h (Fig. 3.2.12a). As a result, we speculate that HIF-1α may be involved in increasing HK2 to accelerate the utilization of increased glucose uptake and to stimulate astrocytes proliferation.

Since other studies already pointed out that activations of the Ras-MAPK and Akt pathways lead to the accumulation of HIF-1α [75, 155], we were wondering whether thrombin-triggered ERK, JNK and PI3K/Akt impinge also on the accumulation of HIF-1α. From our data, thrombin induced HIF-1α accumulation can be decreased by cotreatment with inhibitors of ERK, JNK and PI3K (Fig. 3.2.12a). These data imply that accumulation of HIF-1α induced by thrombin is dependent on the activation of the ERK, JNK, and PI3K/Akt

signaling cascades. Moreover, our data confirmed that inhibition of these pathways significantly decreased the proliferation of astrocytes stimulated by thrombin (Fig. 3.2.6 and Fig. 3.2.9), indicating that increases of HIF-1α in astrocytes is an important mechanism to account for thrombin-induced astrocytes proliferation.

As mentioned before, thrombin-stabilized HIF-1α may be involved in the increase of glucose metabolism through mediating protein level of HK2 in astrocytes. To demonstrate our hypothesis, we checked the protein level of HK2 under the inhibitors of ERK, JNK and PI3K (Fig. 3.2.12b). Interestingly, thrombin-induced increases of HK2 were attenuated by these three signal pathways' inhibitors, which highly correspond to the level of HIF-1α under these inhibitors (Fig. 3.2.12a). In addition, our preliminary data suggested that blockade of thrombin-initiated mitochondrial ROS also eliminated the stabilization of HIF-1α. Moreover, thrombin-caused mitochondrial ROS can be blocked by the inhibitors of ERK, JNK, and PI3K. In conclusion, our data help to depict the following three axes of thrombin-induced astrocytes proliferation: (1) ERK, JNK/ROS/HIF-1α/HK2, (2) PI3K/Akt/ROS/HIF-1α/HK2 and (3) PI3K/Akt/cyclin D1.

We summarized the signaling pathways triggered by thrombin which are responsible for astrocytes proliferation in Fig 4.2.2.
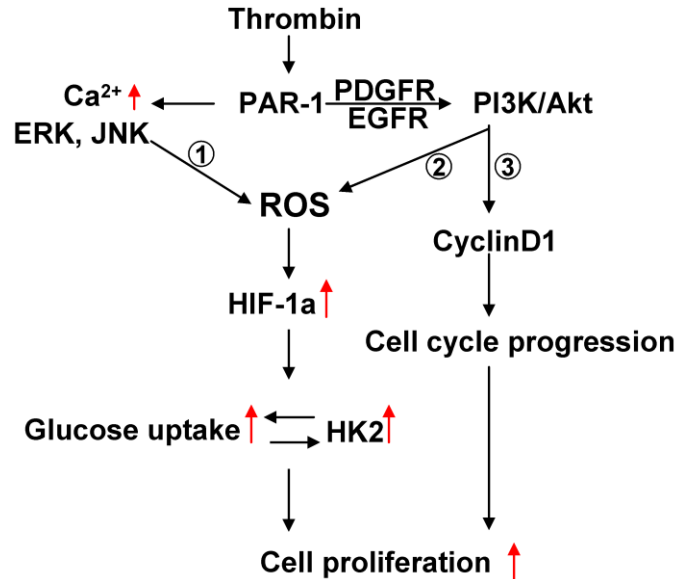
Fig. 4.2.2. Scheme of thrombin-triggered signaling cascades responsible for astrocytes proliferation.

According to Fig. 4.2.2., 1 U/ml of thrombin mainly activates the PAR-1 receptor to induce the intracellular Ca^{2+} increase and activation of ERK, JNK pathways, which subsequently stimulated ROS production (Signaling transduction ①). The generated ROS stabilized HIF-1α. In addition, thrombin stimulates PI3K/Akt, which contributed to

stabilization of HIF-1α (Signaling transduction ②). As a result, HIF-1α accelerated glucose uptake in astrocytes, with upregulating HK2. When DPI was used to block the mitochondrial ROS production induced by thrombin, there were no changes observed in the phosphorylation of ERK, JNK and Akt (Fig. 3.2.13). These results indicate that phosphorylation of ERK, JNK and Akt was not triggered by thrombin-induced mitochondrial ROS. To clarify whether thrombin-stimulated ERK, JNK and Akt signaling pathways regulate mitochondrial ROS production, we measured the ROS level under thrombin in the presence of inhibitors of ERK, JNK and Akt. Our preliminary study support that mitochondrial ROS are the downstream signaling cascade of ERK and JNK, since inhibitors of these two pathways eliminated the increase of ROS production induced by thrombin. However, we did not observe similar results when the inhibitor of PI3K was applied.

These data indicate that ROS was downstream signaling molecule of ERK, JNK, and PI3K. The stabilized HIF-1α upregulated HK2 is frequently taken as the hallmark to manifest the increased glucose uptake. Data from glucose uptake assay showed that thrombin was able to accelerate glucose uptake in astrocytes (Fig. 3.2.10a), demonstrating that the ROS/HIF-1α/HK2 pathway was responsible for glucose metabolism signaling to regulate astrocytes proliferation.

4.3 Functional roles of PAR-2 carboxyl tail in regulating receptor's trafficking and intracellular signaling to cell death

4.3.1 The carboxyl tail of the PAR-2 receptor controls the receptor internalization and desensitization

The role of phosphorylation in desensitization of activated PAR-2 has been documented. Activation of PAR-2 was observed to induce a transient and robust increase in phosphorylation of wild type PAR-2. However, the mutant receptor, in which all serines and threonines in the cytoplasmic tail were modified to alanines (PAR-2 0P) lost the capacity of desensitization [90]. The authors concluded that all the PAR-2 phosphorylation sites within the cytoplasmic tail are essential for receptor desensitization. However, a discrepancy existed, since Stalheim *et al.* found that a mutant of PAR-2 with the double mutation: S363A/T366A showed comparable internalization and desensitization like the wild-type PAR-2 in both COS-7 and HeLa cells, implying that these two residues were dispensable for desensitization and internalization [156]. This implication can be confirmed by our present study. Our study of internalization showed that all the different truncations of PAR-2 receptor except for the 348-Del were capable of internalization upon trypsin stimulation. Although it was not explored whether lack of the different phosphorylation sites has any influence on desensitization, our data strongly demonstrate that the short peptide containing 13 amino acids in 361-Del in the carboxyl tail of PAR-2 receptor are definitely sufficient for the receptor's internalization (Fig. 3.3.2). Interestingly, in the carboxyl tail of 361-Del, there is only one serine phosphorylation site, Ser 349. The expression and internalization assay of 361-Del highlighted the important role of Ser 349, which might play a key role in maintaining PAR-2 receptor localization on the cell membrane and the ability of the receptor to internalize upon trypsin stimulation.

In the current study, the expression of the mutated PAR-2 receptors in HEK-293 cells was investigated. On the one side, it is obvious that the mutant 348-Del which is the PAR-2 receptor truncation lacking the complete carboxyl tail, diffused in the whole cytosol with a quite low expression level at the cell membrane (Fig. 3.3.2). This observation was partially in accordance with the suggestions of Stalheim's study, in which the authors found a rather low expression level of this mutant in HeLa cells [156], but did not mention whether they failed to localize it on the cell membrane or not. Moreover, according to their study, mutant 361-GFP also shows relatively low expression on the cell membrane. On the other side, it was shown that PAR-2 0P mutant, in which all serines and threonines in the cytoplasmic tail were modified to alanines, diffused in the cytosol of the transfected cells [90], which might be

attributed to the deficiency of phosphorylation site Ser 349, since mutant 348-Del in our study showed the same expression pattern as observed for the PAR-2 0P mutant. However, the mutant 361-Del, in which the phosphorylation site Ser 349 was included, was capable to internalize and to localize on the cell membrane. As a result, our data highlight that the phosphorylation site Ser 349 plays an important role in receptor expression and internalization.

4.3.2 The carboxyl tail of PAR-2 is responsible for the interaction with multiple adaptor proteins to signal transduction

The most prominent adaptor proteins of activated PAR-2 are β-arrestins. The binding of β-arrestin to the activated receptor facilitates signal transduction, which is independent of heterotrimeric G protein coupling [157]. Interesting findings show that β-arrestins transiently interact with activated PAR-2 independent of the carboxyl tail, which is sufficient to promote desensitization and internalization. However, the carboxyl tail is essential for stable PAR2-β-arrestins interaction and prolonged ERK1/2 activation, but is not essential for rapid β-arrestin recruitment nor β-arrestins-dependent receptor desensitization or internalization [156]. Although it is still unclear which cluster of the serine/threonines in the carboxyl tail is important for the interaction with β-arrestin, our present study confirms that the carboxyl tail of PAR-2 is responsible for the transient peak of ERK1/2 activation, since after 30 min of stimulation by trypsin, different abilities of PAR-2 truncations coupling to the ERK signal were found (Fig. 3.3.4a). As shown in HEK-GFP cells, we can see that 348-Del completely lost the capacity to cause the fast phosphorylation of ERK. The ERK phosphorylation signal appears in 361-Del, which emphasizes that Ser 349 is also important for initiating ERK signaling. Moreover, in the truncation mutants 361-Del, 368-Del, 379-Del, and 386-Del show almost the similar level of ERK phosphorylation, which is lower than that in wild type receptor. These data point out that the clusters of phosphorylation sites between 387 to 397 are important to obtain maximum responses of ERK phosphorylation. As to the Akt signaling, there were no significant differences as shown in Akt phosphorylation for the different mutants. It is obvious to find that the mutants 348-Del, 361-Del, 368-Del, 379-Del have the similar level of Akt phosphorylation as compared to that in HEK-GFP cells. However, 386-Del shows the comparable Akt phosphorylation level as compared to the wild type receptor (Fig. 3.3.4b).

In addition to β-arrestins, it has been investigated in our laboratory that Jun activating binding protein-1 (Jab1) binds to PAR-2 to stabilize the complexes of c-Jun or Jun D with the transcription factor AP-1 DNA binding sites. The overexpression of Jab1 facilitates the fast phosphorylation of c-Jun [92]. These data also delineate that the carboxyl tail of PAR-2 and

the intracellular loop 3 are mainly responsible for the interaction with Jab1. The examples mentioned above highlight that the carboxyl tail is important for multiple adaptors binding and signaling.

4.3.3 The carboxyl tail of PAR-2 is important for the ERK signal transduction which might be responsible for cell survival

The activation of PAR-2 was demonstrated to couple to multiple heterotrimeric G protein subtypes, such as Gαq, Gαi, and Gα12/13. In addition, PAR-2 can mediate the signal transduction pathways independent from G proteins through interacting with β-arrestins, which was well documented by Soh *et al.* [158].

The hypothesis of the present study is that the mutant 348-Del will lose the capacity to react with PAR-2 agonist. The results shown here support this hypothesis, since the phosphorylation of ERK was undetectable in this mutant under trypsin stimulation for 30 min. Moreover, in the HEK 293 cells transfected with 348-Del, the long term incubation with the specific agonist of PAR-2 did not change the cell's survival curve (Fig. 3.3.5), which in parallel confirmed that this mutant totally lost the typical characterisation of PAR-2 receptor, with rather low expression on the cell membrane and distribution among the whole cytosol without the obvious biological effects after treatment with PAR-2 agonist such as Ca^{2+} responses (Fig 3.3.3). In conclusion, the carboxyl tail of PAR-2 maintains the localization of the receptor and initiation of intracellular signaling under the challenge with the agonist.

The long-lasting activation of the PAR-2 receptor promotes proliferation of endometriotic stromal cells [159]. However, it is unknown what will happen if the overexpressed PAR-2 receptor in cells is activated. Here, we for the first time investigated activation of PAR-2 receptor in the mutant-transfected HEK 293 cells. The data manifested that without the treatment with PAR-2 agonist, HEK-293 cells transfected with the PAR-2 truncation mutants showed no differences in cell survival for 24 h culture (Fig. 3.3.5). However, when the truncations-transfected HEK-293 cells were treated with PAR-2 agonist for 48 h, the proportions of live cells were changed as compared to the unchallenged situation (Fig. 3.3.5). The cell survival assay implied that mutants which have the higher responses of intracellular signaling have the higher ratio of dead cells when exposed to PAR-2 agonist for long time.

We summarize the possible functions of different clusters of serines and threonines at the PAR-2 receptor carboxyl tail in Fig. 4.3.3.

Fig. 4.3.3. Functional roles of different serine/threonine clusters at PAR-2 carboxyl tail
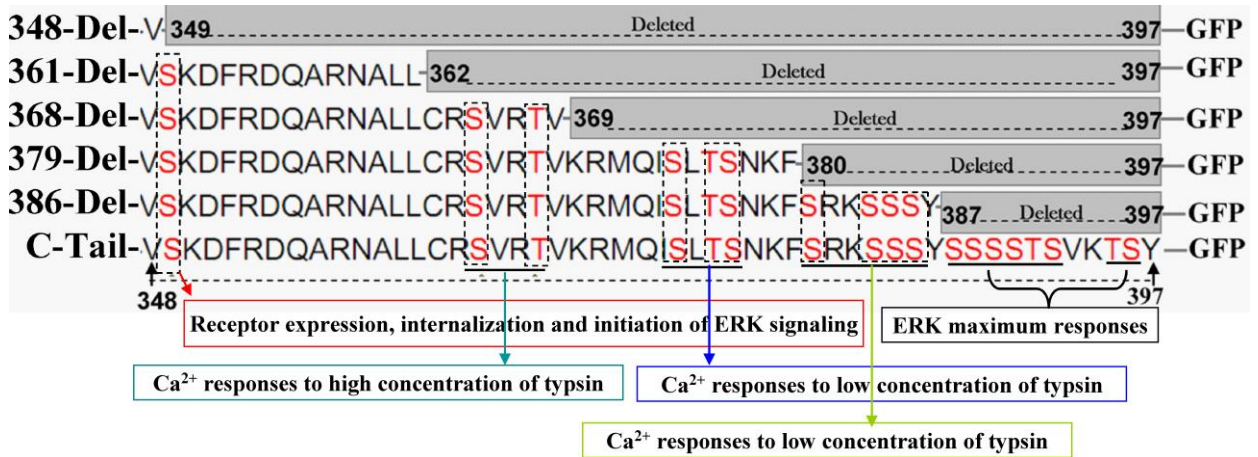
The serine 349 is supposed to be important for localizing receptor on cell membrane, internalization and signaling to ERK pathway. The clusters of serine/threonine underlined by light blue are suggested to be responsible for Ca^{2+} signaling under the high concentration of trypsin. The clusters of serine/threonine underlined by blue are important for giving Ca^{2+} responses under the low concentration of trypsin. Moreover, the serines and threonines underlined by green are suggested to account for the Ca^{2+} responses under the very low concentration of trypsin. The black underlined phosphorylation sites control the maximum ERK phosphorylation upon trypsin challenge. The summarized functions of different serine/threonine clusters are also given in Table. 4.3.3.

Table. 4.3.3. Functional roles of different serine/threonine clusters at PAR-2 carboxyl tail

Clusters of Ser/Thr	Functional role in intracellular signaling
Ser 349	Receptor localization, internalization Initiation of ERK signaling
Ser364/Thr367	Ca^{2+} responses to high concentration of trypsin
Ser373/Thr375/Ser376	Ca^{2+} responses to low concentration of trypsin
Ser380/Ser383/Ser384/Ser385	Ca^{2+} responses to very low concentration of trypsin
Ser387-390/Thr391/Ser392 /Thr395/Ser396	ERK maximum responses

4.4 The interaction between αB-crystallin and β-arrestins and the functional roles of extracellular and intracellular αB-crystallin on astrocytes

Previously it was found in our laboratory that overexpressed αA-crystallin in the intracellular environment is involved in protection of astrocytes from C2-ceramide- and staurosporine-induced cell death [122]. Specific phosphorylation of αA-crystallin at Ser122 and Ser148, or αB-crystallin at Ser45 and Ser59 are required for the α-crystallin-induced protection of astrocytes against chemical induced-toxicity [139, 160]. We here investigated whether the interaction between αB-crystallin and β-arrestins happened by the activation of PAR-2. Our results demonstrated that as the binding proteins of PAR-2 receptor, αB-crystallin and β-arrestins were capable to interact with each other under the stimulation of PAR-2 by trypsin. Previous study confirmed that activation of PAR-2 induced increase of phosphorylation of αB-crystallin at Ser 59, which is important for cytoprotective effects [123]. In the current study, we found that β-arrestin 1 modulated the phosphorylation of αB-crystallin at Ser 59 under activation of PAR-2. Specifically, the transient phosphorylation of αB-crystallin at Ser 59 was largely decreased upon the stimulation of PAR-2 in β-arrestin 1-deficient astrocytes (Fig. 3.4.3b). This might explain why we failed to detect the cytoprotective effects upon the activation of PAR-2 in β-arrestin 1-deficient astrocytes (Fig. 3.4.4).

We further studied whether extracellular application of αB-crystallin protein has protective effects on astrocytes. Astrocytes were exposed to serum-free medium in the absence or presence of αB-crystallin. As a result, the cells with exogenous αB-crystallin treatment showed higher survival (Fig. 3.4.5a).

α-Crystallin was demonstrated as anti-apoptotic protein that provides protection against a wide range of cellular stress in several kinds of cells by binding to the proapoptotic molecules p53, Bax and Bcl-X$_{(S)}$, and therefore to block their translocation to mitochondria during apoptosis [120, 121]. However, it was not fully understood how the anti-apoptotic functions are produced by α-crystallin in the CNS. With the increasing amount of data implicating that the apoptosis of astrocytes is also involved in brain injury, the regulation of astrocytes apoptosis became an important target in understanding the physiological and pathological processes in the CNS.

To examine if exogenous αB-crystallin has anti-apoptotic effects in astrocytes, different concentrations of αB-crystallin were applied in the absence or presence of staurosporine. Staurosporine is used to induce apoptosis by activating caspase 3 [161], or inhibiting ERK, and Akt kinase activities [162]. In our previous study, we found staurosporine-induced

elevation of cleaved caspase 3 through inhibiting Akt phosphorylation in astrocytes [163]. In the current study, astrocytes exposed to staurosporine in the absence of αB-crystallin suffered from a higher apoptosis with a higher level of cleavage of caspase 3. However, astrocytes co-treated with 10 μg/ml or 100 μg/ml of the exogenous αB-crystallin and staurosporine were observed to have a lower level of cleaved caspase 3 (Fig. 3.4.7a and b). These data demonstrate that αB-crystallin potently blocks the apoptosis of astrocytes.

MAPK were suggested to be involved in the protective processes of αB-crystallin [140, 141]. In the present study, our data support that αB-crystallin works as signaling ligand to trigger the ERK1/2, p38, JNK and Akt signaling cascades to promote the viability of astrocytes under the serum-deprived situation (Fig. 3.4.5b). When specific inhibitors were used to block these pathways, the protective effects on the survival of astrocytes stimulated by αB-crystallin were largely reduced and even abolished (Fig. 3.4.6). In addition to the MAPK signaling pathways, the PI3K/Akt/ mTOR might play a pivotal role in astrocytes viability activated by αB-crystallin (Fig. 3.4.6). Although MAPK signaling pathways and the PI3K/Akt signaling pathway are demonstrated to be important for astrocytes viability under the serum-free conditions, αB-crystallin rescues astrocytes from staurosporine-induced late apoptosis only through the intracellular PI3K/Akt signalling pathway, since αB-crystallin inhibits the cleavage of caspase 3, and at the same time induced the enhanced phosphorylation of Akt without any effects on ERK phosphorylation (Fig. 3.4.7). Therefore, we summarize the signal transduction pathways initiated by αB-crystallin which contribute to the cytoprotection and the increased cell viability in Fig. 4.4.

Fig. 4.4 The cytoprotective and cell survival signaling pathways initiated by αB-crystallin.
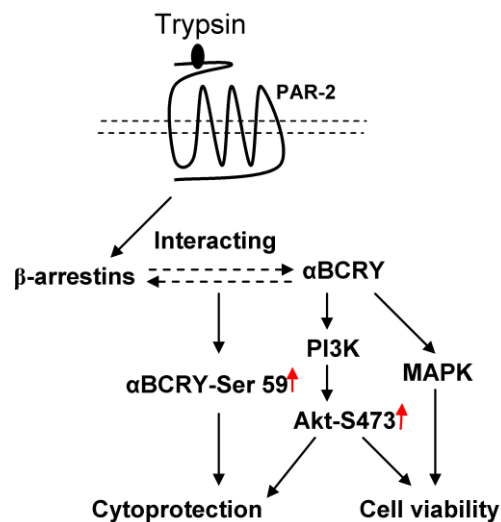
αB-Crystallin has been recently reported to prevent the arrhythmogenic effects of particulate matter isolated from ambient air by attenuating ROS generation [164]. The

production of ROS by mitochondria is believed to account for the oxidative damage in pathology, contributing to retrograde redox signaling from the organelle to the cytosol and nucleus. Pre-treatment with α-crystallin has been demonstrated to decrease the level of ROS production in astrocytes, hepatocytes and lymphocytes from mice that suffered from the silver nitrate-induced inflammation Moreover, αB-Crystallin was reported to prevent the arrhythmogenic effect by attenuating ROS generation and CaMKII phosphorylation [165]. However, less is known about drugs which can be used to protect brain mitochondria from oxidative stimuli. In this study, we found that αB-crystallin inhibits the production of ROS in RBM under complex III inhibition by Antimycin A (Fig. 3.4.8), which emphasized the important role of αB-crystallin in dealing with oxidative damage in brain.

The mechanisms of α-crystallin carrying out the antioxidative effects in mitochondria can be suggested as follows: α-crystallin as molecular chaperon binds to the outer membrane of mitochondria to prevent the damage by oxidative stimuli, and finally reduces the production of mitochondrial ROS. Alternatively, the oxidative damage happened prior to the α-crystallin binding, and then α-crystallin works as the scavenger to clear the excessive ROS released by the damaged mitochondria. It is also reasonable to speculate that both of them work synergistically to reduce the level of mitochondrial ROS. Further studies should be done to investigate the molecular mechanisms of αB-crystallin in inhibiting mitochondrial ROS production in RBM to pave the way for pharmaceutical development.

How does αB-crystallin work like an extracellular signaling ligand? A previous study provides a clue to the answer. It was reported that exogenous of αB-crystallin is internalized and then protected retinal pigment epithelial cells under oxidative stress [166]. The authors observed that the uptake of exogenous αB-crystallin happened in adjacent retinal cells providing protection from oxidant stress. To this point, we tried to find out whether αB-crystallin could translocate from extracellular to intracellular environments. Astrocytes were incubated with 100 μg/ml of αB-crystallin for 48 h, and then the cells were harvested for Western blot. The interesting finding was that a higher level of αB-crystallin could be observed than that seen in non-αB-crystallin treated astrocytes (data are not shown). It is quite possible that the uptake of exogenous αB-crystallin happened in astrocytes. Thus, αB-crystallin could work like a chaperon molecule or as a signaling ligand to exert the protective properties. However, it is quite possible that exogenous αB-crystallin stimulates the expression of endogenous αB-crystallin through still unknown mechanisms. As a consequence, a tag attached to αB-crystallin protein will be a useful method to monitor

whether the trafficking of αB-crystallin from extracellular to intracellular environment really happened through tracking the tag.

In sum, our current study illustrates that exogenous αB-crystallin inhibits the ROS production from RBM, suggesting an important role of αB-crystallin in the anti-oxidative effect by blocking ROS production in RBM. Moreover, exogenous αB-crystallin protects astrocytes from cell death under serum deprivation and different toxic stimuli. The mechanisms of the protective process include the stimulation of MAPK signaling pathways and PI3K/Akt/mTOR. In addition, the PI3K/Akt signaling pathway was also important for the anti-apoptotic effects from exogenous αB-crystallin treatment in astrocytes. Finally, this study highlights that the striking functional properties of exogenous αB-crystallin in promoting the viability of astrocytes and anti-oxidative effects make it a good candidate to deal with degenerative CNS diseases.

5   Abstract

Protease-activated receptors are seven transmembrane-domains G-protein-coupled receptors (GPCRs) with four members PAR-1, PAR-2, PAR-3, and PAR-4. Thrombin is the serine protease generated from the proenzyme prothrombin, which has been confirmed to cleave PAR-1, PAR-3 or PAR-4 in many kinds of cells, while PAR-2 is activated by trypsin. The scaffold proteins β-arrestin 1 and β-arrestin 2 have been shown to mediate responses of various agonists of GPCRs, including PAR-1 and PAR-2. αB-crystallin, a member of the superfamily of small heat shock proteins was demonstrated to interact with only PAR-2 among PARs. The aim of this study was to investigate whether activation of PAR will initiate the intracellular signaling transductions to regulate astrocytes proliferation and cytoprotection. Moreover, we were interested in how the interaction partners, β-arrestins and αB-crystallin, are involved in the cytoprotective and/or proliferative signaling pathways initiated by PAR-1 and PAR-2 stimulation.

We found that β-arrestin 1 is necessary for astrocytes to resist to staurosporine-induced apoptosis. Moreover, β-arrestin 1 is also involved in the thrombin-activated PI3K/Akt signaling pathway, which is important for antiapoptotic effects exerted by thrombin. In detail, thrombin rescues β-arrestin 1-lacking astrocytes from apoptosis through enhanced increase in Akt (Ser473) phosphorylation. β-arrestin 1 inhibits long-term phosphorylation of Akt (Ser 473) that is stimulated by thrombin. In addition, we also found that thrombin-induced phosphorylation of Akt (Ser473) is increased by transactivation of PDGF receptor and EGF receptor in β-arrestin 1-deficient astrocytes.

In this study, we clarified whether thrombin-activated PAR-1 will affect the glucose metabolism signaling pathways to accelerate the proliferation of astrocytes. In addition, we investigated if thrombin has any effects on cell cycle transition to promote astrocytes proliferation. It was firstly observed that thrombin activated PAR-1 to induce the increases of intracellular Ca^{2+} and ROS production which contribute to the proliferation of astrocytes. We further confirmed that ROS stabilized HIF-1α. The latter subsequently accelerated glucose uptake in astrocytes. On the other hand, we observed that thrombin triggered PI3K/Akt/cyclin D1 signal transduction, which promoted the cell cycle transition, contributing to astrocytes proliferation. As a result, three main signaling pathways were discovered accounting for cell proliferation induced by thrombin: (1) thrombin-stimulated ERK, JNK/ROS/HIF-1α, (2) PI3K/Akt/ROS/HIF-1α pathways increase expression of hexokinase 2 (HK2) which mediates glucose metabolism in astrocytes, and (3) thrombin stimulates PAR-1/PI3K/Akt/cyclin D1 to promote the cell cycle transition and finally to increase cell proliferation.

We next investigated the functional roles of the phosphorylation sites located in the PAR-2 carboxyl tail in cellular signaling and cell death. PAR-2 carboxyl tail was suggested to be important for the binding of β-arrestin 1 or other adaptor proteins. We generated a series of truncated mutants containing different clusters of serine/threonine. Firstly, it was observed that lack of the whole C-terminus of PAR-2 in the mutated receptor gave a relatively low expression on the cell membrane. Secondly, the HEK293 cells expressing these truncation mutants showed deficient capacity in coupling to intracellular Ca^{2+} and signaling to ERK but not Akt upon trypsin challenge. Moreover, HEK293 cells carrying different PAR-2 truncation mutants displayed the decreased levels of cell viability after long-lasting stimulation by trypsin.

αB-crystallin was found to interact with PAR-2, and activation of PAR-2 resulted in the increase in phosphorylation of αB-crystallin at Ser45 and Ser59, which played a pivotal role in cytoprotection. β-arrestin1/2 were also demonstrated to interact with PAR-2 to regulate the intracellular signaling, such as ERK. We studied whether there exits an interaction between αB-crystallin and β-arrestin1/2. β-arrestin1/2 colocalized with αB-crystallin detected by microscopy. Further data from co-immuno-precipitaton supported the hypothesis that these two proteins interact with each other. In addition, downregulation of β-arrestin 1 in astrocytes inhibited the transient phosphorylation of αB-crystallin at Ser59 stimulated by the PAR-2 agonist. We conclude that the binding of β-arrestin 1 to αB-crystallin is important for the phosphorylation of αB-crystallin at Ser59. We further demonstrate that extra-cellular application of αB-crystallin has protective effects preventing cell apoptosis. Exogenous αB-crystallin improves the viability of astrocytes through MAPK and PI3K/Akt/mTOR signaling pathways. In contrast, extracellular application of αB-crystallin exerts antiapoptotic effects through the PI3K/Akt signaling pathway. αB-crystallin is also confirmed to block ROS production in isolated RBM, emphasizing the potential antioxidative activity exerted, which may also contribute to the cytoprotective effects.

6   Zusammenfassung

Die Familie der Protease-aktivierten Rezeptoren zählt zu den heptahelikalen G-Protein-gekoppelten Rezeptoren (GPCR), welche die vier Mitglieder PAR-1, PAR-2, PAR-3 und PAR-4 umfasst. PAR's werden durch proteolytische Spaltung im N-terminalen Bereich aktiviert, wodurch ein den Rezeptor aktivierender neuer N-Terminus entsteht. An zahlreichen Zelltypen wurde gezeigt, dass die Serinprotease Thrombin, welche aus dem Proenzym Prothrombin generiert wird, PAR-1, PAR-3 und PAR-4 spaltet, wohingegen PAR-2 von Trypsin aktiviert wird. Die Adapterproteine β-Arrestin 1 und β-Arrestin 2 vermitteln Zellantworten auf verschiedenste Agonisten von GPCR's, einschließlich PAR-1 und PAR-2. Weiterhin wurde beschrieben, daß αB-Crystallin, ein Mitglied der Familie der kleinen Hitzeschock Proteine, spezifisch mit PAR-2, aber nicht mit anderen PAR's, interagiert. Das Ziel der vorliegenden Arbeit war es, PAR-abhängige intrazelluläre Signaltransduktionswege hinsichtlich der Regulation von Proliferation und Zytoprotektion von Astrozyten zu untersuchen. Ferner waren wir an der Rolle der PAR-Interaktionspartner β-Arrestin und αB-Crystallin in den protektiven und/oder proliferativen Signalwegen interessiert, welche durch PAR-1 und PAR-2 Stimulation initiiert werden.

Wir konnten zeigen, dass β-Arrestin 1 eine protektive Wirkung hinsichtlich Staurosporin-induzierter Apoptose in Astrozyten hat. Außerdem ist β-Arrestin 1 im Thrombin-aktivierten PI3K/Akt Signalweg involviert, welcher für die von Thrombin ausgelösten anti-apoptotischen Funktionen wichtig ist. Im Detail konnten wir zeigen, dass Thrombin Astrozyten, welche nicht über β-Arrestin 1 verfügen, vor Apoptose schützt, indem es zu einer verstärkten Phosphorylierung von Akt an Serin 473 führt. β-Arrestin 1 inhibiert die durch Thrombin stimulierte Langzeit-Phosphorylierung von Akt an Serin 473. Zusätzlich konnten wir zeigen, dass die Thrombin-induzierte Phosphorylierung von Akt an Serin 473 durch die Transaktivierung von PDGF- und EGF-Rezeptoren in β-Arrestin 1-defizienten Astrozyten verstärkt wird.

Thrombin ist bekannt dafür, die Proliferation von Astrozyten zu stimulieren. Wir sind hier der Frage nachgegangen, inwieweit die Aktivierung von PAR-1 durch Thrombin mit dem Glucose-Metabolismus verknüpfte Signalwege beeinflusst, um damit die Proliferation von Astrozyten zu beschleunigen. Zusätzlich haben wir mögliche Einflüsse von Thrombin auf den Zellzyklus untersucht, welche die Proliferation von Astrozyten vermitteln könnten. Wir konnten zum einen beobachten, dass Thrombin PAR-1 aktiviert und damit einen Anstieg des intrazellulären Ca^{2+} sowie die verstärkte ROS-Produktion auslöst, was zur Proliferation der Astrozyten beiträgt. Ferner konnten wir bestätigen, dass ROS HIF-1α stabilisierten. Letzteres

führte zu einer beschleunigten Glucoseaufnahme in den Astrozyten. Zum anderen konnten wir eine Thrombin-induzierte Aktivierung der PI3K/Akt/cyclin D1-Signaltransduktion beobachten, was den Zellzyklus-Übergang und damit die Proliferation der Astrozyten vermittelte. Es konnten im Rahmen dieser Studie drei hauptsächliche Signaltransduktionswege identifiziert werden, die für die Thrombin-induzierte Proliferation der Zellen maßgeblich waren: (1) der durch Thrombin stimulierte ERK, JNK/ROS/HIF-1α Signalweg, (2) die durch den PI3K/Akt/ROS/HIF-1α Signalweg ausgelöste Verstärkung der Expression der Hexokinase 2 (HK2), welche den Glucose-Metabolismus in den Astrozyten reguliert, und (3) der durch Thrombin-induzierte PAR-1/PI3K/Akt/cyclin D1 Signalweg, welcher einen Zellzyklus-Übergang auslöst und in der Folge zu einer erhöhten Zellproliferation führt.

Des Weiteren haben wir die Funktion der Phosphorylierungsstellen im C-terminalen Bereich von PAR-2 hinsichtlich ihrer Rolle in zellulären Signalwegen und Zelltod untersucht. Der C-Terminus von PAR-2 wurde mit der Interaktion mit β-Arrestin 1 und anderen Adapterproteinen in Verbindung gebracht. Wir haben dazu eine Reihe verkürzter Mutanten von PAR-2 erzeugt, welche verschiedene Serin/Threonin-Regionen enthielten. Erstens wurde eine relativ schwache Expression des PAR-2 an der Zellmembran beobachtet, wenn der gesamte C-Terminus deletiert wurde. Zweitens zeigten Trypsin-behandelte HEK 293-Zellen eine defiziente Kopplung an den intrazellulären Ca^{2+}- und ERK-Signalweg, aber keine Beeinträchtigung des Akt-Signalweges, wenn sie die verkürzten Mutanten exprimierten. Außerdem wiesen HEK 293-Zellen mit verschiedenen PAR-2 Mutanten eine verminderte Zellviabilität bei Langzeitstimulation mit Trypsin auf.

αB-Crystallin interagiert mit PAR-2 und die Aktivierung von PAR-2 resultiert in der Phosphorylierung von αB-Crystallin an Serin 45 und 59, was eine ausschlaggebende Rolle für die Zellprotektion spielt. Für die Interaktion von β-arrestin1/2 mit dem PAR-2 wurde zudem eine Regulation intrazellulärer Signalwege, wie ERK, demonstriert. Wir untersuchten, ob eine Interaktion zwischen αB-Crystallin und β-Arrestin1/2 stattfindet. Mittels mikroskopischer Untersuchungen konnte eine Co-Lokalisation von β-Arrestin1/2 und αB-Crystallin nachgewiesen werden. Co-Immunoprezipitations-Experimente bestätigten die Hypothese daß diese beiden Proteine miteinander interagieren. Außerdem hemmte die Herunterregulierung von β-Arrestin 1 in Astrozyten die PAR-2-Agonist-stimulierte transiente Phosphorylierung von αB-Crystallin an Serin 59. Wir schlussfolgern, dass die Bindung von β-Arrestin 1 an αB-Crystallin wichtig für die Phosphorylierung von αB-Crystallin an Serin 59 ist. Des Weiteren konnten wir zeigen, dass die extrazelluläre Gabe von αB-Crystallin eine protektive,

anti-apoptotische Wirkung hat. Exogenes αB-Crystallin verbessert die Viabilität von Astrozyten über MAPK und PI3K/Akt/mTOR Signalwege. Im Gegensatz dazu werden die anti-apoptotischen Wirkungen von der extrazellulären Applikation von αB-Crystallin über den PI3K/Akt Signaltransduktionsweg vermittelt. αB-Crystallin blockiert außerdem die Produktion von ROS in isolierten Hirnmitochondrien aus Ratte, was eine potentielle anti-oxidative Wirkung hervorhebt, die zu den zytoprotektiven Effekten beitragen kann.

Zusammenfassend zeigt die vorliegende Arbeit, daß β-arrestin 1 anti-apoptotische Effekte vermittelt und an der Regulation der PAR-1/PI3K/Akt Signal-Kaskade beteiligt ist, welche eine zentrale Role bei der Zellprotektion spielt. Darüberhinaus, konnte gezeigt werden daß verschiedene Serin/Threonin-reiche Regionen im carboxyterminalen Teil von PAR-2 die intrazelluläre Ca^{2+} und ERK Signaltransduktion, sowie das Überleben der Zellen kontrollieren. αB-Crystallin ist in der Lage die PI3K/Akt und/oder MAPK Signalwege zu aktivieren und Astrozyten vor Apoptose zu schützen.

7   Reference

1.   Wang H, Ubl JJ, Reiser G. (2002) Four subtypes of protease-activated receptors, co-expressed in rat astrocytes, evoke different physiological signaling. Glia, 37, 53-63.
2.   Adams MN, Ramachandran R, Yau MK, Suen JY, Fairlie DP, Hollenberg MD, Hooper JD. (2011) Structure, function and pathophysiology of protease activated receptors. Pharmacol Ther, 130, 248-82.
3.   Hamm HE. (2001) How activated receptors couple to G proteins. Proc Natl Acad Sci U S A, 98, 4819-21.
4.   Vu TK, Hung DT, Wheaton VI, Coughlin SR. (1991) Molecular cloning of a functional thrombin receptor reveals a novel proteolytic mechanism of receptor activation. Cell, 64, 1057-68.
5.   Jacques SL, Kuliopulos A. (2003) Protease-activated receptor-4 uses dual prolines and an anionic retention motif for thrombin recognition and cleavage. Biochem J, 376, 733-40.
6.   Nieman MT. (2008) Protease-activated receptor 4 uses anionic residues to interact with alpha-thrombin in the absence or presence of protease-activated receptor 1. Biochemistry, 47, 13279-86.
7.   Luo W, Wang Y, Reiser G. (2007) Protease-activated receptors in the brain: receptor expression, activation, and functions in neurodegeneration and neuroprotection. Brain Res Rev, 56, 331-45.
8.   Grand RJ, Turnell AS, Grabham PW. (1996) Cellular consequences of thrombin-receptor activation. Biochem J, 313 (Pt 2), 353-68.
9.   Fenton JW, 2nd. (1986) Thrombin. Ann N Y Acad Sci, 485, 5-15.
10.   Davie EW, Fujikawa K, Kisiel W. (1991) The coagulation cascade: initiation, maintenance, and regulation. Biochemistry, 30, 10363-70.
11.   Narayanan S. (1999) Multifunctional roles of thrombin. Ann Clin Lab Sci, 29, 275-80.
12.   Rydel TJ, Ravichandran KG, Tulinsky A, Bode W, Huber R, Roitsch C, Fenton JW, 2nd. (1990) The structure of a complex of recombinant hirudin and human α-thrombin. Science, 249, 277-80.
13.   Ishihara H, Connolly AJ, Zeng D, Kahn ML, Zheng YW, Timmons C, Tram T, Coughlin SR. (1997) Protease-activated receptor 3 is a second thrombin receptor in humans. Nature, 386, 502-6.
14.   Xu WF, Andersen H, Whitmore TE, Presnell SR, Yee DP, Ching A, Gilbert T, Davie EW, Foster DC. (1998) Cloning and characterization of human protease-activated receptor 4. Proc Natl Acad Sci U S A, 95, 6642-6.
15.   Schuepbach RA, Madon J, Ender M, Galli P, Riewald M. (2012) Protease-activated receptor-1 cleaved at R46 mediates cytoprotective effects. J Thromb Haemost, 10, 1675-84.
16.   Shi X, Gangadharan B, Brass LF, Ruf W, Mueller BM. (2004) Protease-activated receptors (PAR1 and PAR2) contribute to tumor cell motility and metastasis. Mol Cancer Res, 2, 395-402.
17.   Kalashnyk O, Petrova Y, Lykhmus O, Mikhalovska L, Mikhalovsky S, Zhukova A, Gnatenko D, Bahou W, Komisarenko S, Skok M. (2013) Expression, function and cooperating partners of protease-activated receptor type 3 in vascular endothelial cells and B lymphocytes studied with specific monoclonal antibody. Mol Immunol, 54, 319-26.
18.   Kahn ML, Nakanishi-Matsui M, Shapiro MJ, Ishihara H, Coughlin SR. (1999) Protease-activated receptors 1 and 4 mediate activation of human platelets by thrombin. J Clin Invest, 103, 879-87.

19. Arai T, Miklossy J, Klegeris A, Guo JP, McGeer PL. (2006) Thrombin and prothrombin are expressed by neurons and glial cells and accumulate in neurofibrillary tangles in Alzheimer disease brain. J Neuropathol Exp Neurol, 65, 19-25.

20. Mhatre M, Nguyen A, Kashani S, Pham T, Adesina A, Grammas P. (2004) Thrombin, a mediator of neurotoxicity and memory impairment. Neurobiol Aging, 25, 783-93.

21. Choi SH, Lee DY, Kim SU, Jin BK. (2005) Thrombin-induced oxidative stress contributes to the death of hippocampal neurons in vivo: role of microglial NADPH oxidase. J Neurosci, 25, 4082-90.

22. Park KW, Jin BK. (2008) Thrombin-induced oxidative stress contributes to the death of hippocampal neurons: role of neuronal NADPH oxidase. J Neurosci Res, 86, 1053-63.

23. Suo Z, Wu M, Citron BA, Palazzo RE, Festoff BW. (2003) Rapid tau aggregation and delayed hippocampal neuronal death induced by persistent thrombin signaling. J Biol Chem, 278, 37681-9.

24. Vaughan PJ, Pike CJ, Cotman CW, Cunningham DD. (1995) Thrombin receptor activation protects neurons and astrocytes from cell death produced by environmental insults. Journal of Neuroscience, 15, 5389-401.

25. Festoff BW, Smirnova IV, Ma J, Citron BA. (1996) Thrombin, its receptor and protease nexin I, its potent serpin, in the nervous system. Semin Thromb Hemost, 22, 267-71.

26. Turgeon VL, Houenou LJ. (1997) The role of thrombin-like (serine) proteases in the development, plasticity and pathology of the nervous system. Brain Res Brain Res Rev, 25, 85-95.

27. Déry O, Corvera CU, Steinhoff M, Bunnett NW. (1998) Proteinase-activated receptors: novel mechanisms of signaling by serine proteases. Am J Physiol, 274, C1429-52.

28. Acharjee S, Zhu Y, Maingat F, Pardo C, Ballanyi K, Hollenberg MD, Power C. (2011) Proteinase-activated receptor-1 mediates dorsal root ganglion neuronal degeneration in HIV/AIDS. Brain, 134, 3209-21.

29. Donovan FM, Pike CJ, Cotman CW, Cunningham DD. (1997) Thrombin induces apoptosis in cultured neurons and astrocytes via a pathway requiring tyrosine kinase and RhoA activities. Journal of Neuroscience, 17, 5316-26.

30. Striggow F, Riek M, Breder J, Henrich-Noack P, Reymann KG, Reiser G. (2000) The protease thrombin is an endogenous mediator of hippocampal neuroprotection against ischemia at low concentrations but causes degeneration at high concentrations. Proc Natl Acad Sci U S A, 97, 2264-9.

31. Wang Y, Luo W, Reiser G. (2007) Activation of protease-activated receptors in astrocytes evokes a novel neuroprotective pathway through release of chemokines of the growth-regulated oncogene/cytokine-induced neutrophil chemoattractant family. Eur J Neurosci, 26, 3159-68.

32. Cannon JR, Keep RF, Hua Y, Richardson RJ, Schallert T, Xi G. (2005) Thrombin preconditioning provides protection in a 6-hydroxydopamine Parkinson's disease model. Neurosci Lett, 373, 189-94.

33. Cannon JR, Keep RF, Schallert T, Hua Y, Richardson RJ, Xi G. (2006) Protease-activated receptor-1 mediates protection elicited by thrombin preconditioning in a rat 6-hydroxydopamine model of Parkinson's disease. Brain Res, 1116, 177-86.

34. Liu F, Liu F, Wang L, Hu H. (2013) [Roles of protease-activated receptor-1 in thrombin-induced brain injury and neurogenesis in rats]. Zhejiang Da Xue Xue Bao Yi Xue Ban, 42, 283-90.

35. Wang H, Ubl JJ, Stricker R, Reiser G. (2002) Thrombin (PAR-1)-induced proliferation in astrocytes via MAPK involves multiple signaling pathways. Am J Physiol Cell Physiol, 283, C1351-64.

36. Wang Y, Luo W, Stricker R, Reiser G. (2006) Protease-activated receptor-1 protects rat astrocytes from apoptotic cell death via JNK-mediated release of the chemokine GRO/CINC-1. J Neurochem, 98, 1046-60.

37. Vaughan PJ, Pike CJ, Cotman CW, Cunningham DD. (1995) Thrombin receptor activation protects neurons and astrocytes from cell death produced by environmental insults. J Neurosci, 15, 5389-401.

38. Chance B, Sies H, Boveris A. (1979) Hydroperoxide metabolism in mammalian organs. Physiol Rev, 59, 527-605.

39. Schonfeld P, Schluter T, Fischer KD, Reiser G. (2011) Non-esterified polyunsaturated fatty acids distinctly modulate the mitochondrial and cellular ROS production in normoxia and hypoxia. J Neurochem, 118, 69-78.

40. Sullivan PG, Brown MR. (2005) Mitochondrial aging and dysfunction in Alzheimer's disease. Prog Neuropsychopharmacol Biol Psychiatry, 29, 407-10.

41. Greenamyre JT, Hastings TG. (2004) Biomedicine. Parkinson's--divergent causes, convergent mechanisms. Science, 304, 1120-2.

42. Warner DS, Sheng H, Batinic-Haberle I. (2004) Oxidants, antioxidants and the ischemic brain. J Exp Biol, 207, 3221-31.

43. Kirkinezos IG, Moraes CT. (2001) Reactive oxygen species and mitochondrial diseases. Semin Cell Dev Biol, 12, 449-57.

44. Lo YY, Cruz TF. (1995) Involvement of reactive oxygen species in cytokine and growth factor induction of c-fos expression in chondrocytes. J Biol Chem, 270, 11727-30.

45. Maki J, Hirano M, Hoka S, Kanaide H, Hirano K. (2010) Involvement of reactive oxygen species in thrombin-induced pulmonary vasoconstriction. Am J Respir Crit Care Med, 182, 1435-44.

46. Zundorf G, Reiser G. (2011) The phosphorylation status of extracellular-regulated kinase 1/2 in astrocytes and neurons from rat hippocampus determines the thrombin-induced calcium release and ROS generation. J Neurochem, 119, 1194-204.

47. Abramov AY, Scorziello A, Duchen MR. (2007) Three distinct mechanisms generate oxygen free radicals in neurons and contribute to cell death during anoxia and reoxygenation. J Neurosci, 27, 1129-38.

48. Noh KM, Koh JY. (2000) Induction and activation by zinc of NADPH oxidase in cultured cortical neurons and astrocytes. J Neurosci, 20, RC111.

49. Kim SH, Won SJ, Sohn S, Kwon HJ, Lee JY, Park JH, Gwag BJ. (2002) Brain-derived neurotrophic factor can act as a pronecrotic factor through transcriptional and translational activation of NADPH oxidase. J Cell Biol, 159, 821-31.

50. Choi SH, Lee DY, Chung ES, Hong YB, Kim SU, Jin BK. (2005) Inhibition of thrombin-induced microglial activation and NADPH oxidase by minocycline protects dopaminergic neurons in the substantia nigra in vivo. J Neurochem, 95, 1755-65.

51. Patterson C, Ruef J, Madamanchi NR, Barry-Lane P, Hu Z, Horaist C, Ballinger CA, Brasier AR, Bode C, Runge MS. (1999) Stimulation of a vascular smooth muscle cell NAD(P)H oxidase by thrombin. Evidence that p47(phox) may participate in forming this oxidase in vitro and in vivo. J Biol Chem, 274, 19814-22.

52. Wang Z, Castresana MR, Newman WH. (2004) Reactive oxygen species-sensitive p38 MAPK controls thrombin-induced migration of vascular smooth muscle cells. J Mol Cell Cardiol, 36, 49-56.

53. Lopez JJ, Salido GM, Gomez-Arteta E, Rosado JA, Pariente JA. (2007) Thrombin induces apoptotic events through the generation of reactive oxygen species in human platelets. J Thromb Haemost, 5, 1283-91.

54. Lopez JJ, Salido GM, Pariente JA, Rosado JA. (2008) Thrombin induces activation and translocation of Bid, Bax and Bak to the mitochondria in human platelets. J Thromb Haemost, 6, 1780-8.

55. Hawkins BJ, Solt LA, Chowdhury I, Kazi AS, Abid MR, Aird WC, May MJ, Foskett JK, Madesh M. (2007) G protein-coupled receptor Ca2+-linked mitochondrial reactive oxygen species are essential for endothelial/leukocyte adherence. Mol Cell Biol, 27, 7582-93.

56. Tsukagoshi H, Busch W, Benfey PN. (2010) Transcriptional regulation of ROS controls transition from proliferation to differentiation in the root. Cell, 143, 606-16.

57. Greene EL, Velarde V, Jaffa AA. (2000) Role of reactive oxygen species in bradykinin-induced mitogen-activated protein kinase and c-fos induction in vascular cells. Hypertension, 35, 942-7.

58. Parrales A, Lopez E, Lopez-Colome AM. (2011) Thrombin activation of PI3K/PDK1/Akt signaling promotes cyclin D1 upregulation and RPE cell proliferation. Biochim Biophys Acta, 1813, 1758-66.

59. Liu JJ, Chao JR, Jiang MC, Ng SY, Yen JJ, Yang-Yen HF. (1995) Ras transformation results in an elevated level of cyclin D1 and acceleration of G1 progression in NIH 3T3 cells. Mol Cell Biol, 15, 3654-63.

60. Filmus J, Robles AI, Shi W, Wong MJ, Colombo LL, Conti CJ. (1994) Induction of cyclin D1 overexpression by activated ras. Oncogene, 9, 3627-33.

61. Arisato T, Sarker KP, Kawahara K, Nakata M, Hashiguchi T, Osame M, Kitajima I, Maruyama I. (2003) The agonist of the protease-activated receptor-1 (PAR) but not PAR3 mimics thrombin-induced vascular endothelial growth factor release in human smooth muscle cells. Cell Mol Life Sci, 60, 1716-24.

62. Duarte M, Kolev V, Soldi R, Kirov A, Graziani I, Oliveira SM, Kacer D, Friesel R, Maciag T, Prudovsky I. (2006) Thrombin induces rapid PAR1-mediated non-classical FGF1 release. Biochem Biophys Res Commun, 350, 604-9.

63. Shimizu S, Gabazza EC, Hayashi T, Ido M, Adachi Y, Suzuki K. (2000) Thrombin stimulates the expression of PDGF in lung epithelial cells. Am J Physiol Lung Cell Mol Physiol, 279, L503-10.

64. Bian ZM, Elner SG, Elner VM. (2007) Thrombin-induced VEGF expression in human retinal pigment epithelial cells. Invest Ophthalmol Vis Sci, 48, 2738-46.

65. Hayakawa Y, Kurimoto M, Nagai S, Kurosaki K, Tsuboi Y, Hamada H, Hayashi N, Endo S. (2007) Thrombin-induced cell proliferation and platelet-derived growth factor-AB release from A172 human glioblastoma cells. J Thromb Haemost, 5, 2219-26.

66. Gadea A, Schinelli S, Gallo V. (2008) Endothelin-1 regulates astrocyte proliferation and reactive gliosis via a JNK/c-Jun signaling pathway. J Neurosci, 28, 2394-408.

67. Narayan S, Prasanna G, Tchedre K, Krishnamoorthy R, Yorio T. (2010) Thrombin-induced endothelin-1 synthesis and secretion in retinal pigment epithelial cells is rho kinase dependent. J Ocul Pharmacol Ther, 26, 389-97.

68. Ohuchi N, Hayashi K, Iwamoto K, Koike K, Kizawa Y, Nukaga M, Kakegawa T, Murakami H. (2009) Thrombin-stimulated proliferation is mediated by endothelin-1 in cultured rat gingival fibroblasts. Fundam Clin Pharmacol, 24, 501-8.

69. Tabernero A, Giaume C, Medina JM. (1996) Endothelin-1 regulates glucose utilization in cultured astrocytes by controlling intercellular communication through gap junctions. Glia, 16, 187-95.

70. Tabernero A, Jimenez C, Velasco A, Giaume C, Medina JM. (2001) The enhancement of glucose uptake caused by the collapse of gap junction communication is due to an increase in astrocyte proliferation. J Neurochem, 78, 890-8.

71. Sanchez-Alvarez R, Tabernero A, Medina JM. (2004) Endothelin-1 stimulates the translocation and upregulation of both glucose transporter and hexokinase in astrocytes: relationship with gap junctional communication. J Neurochem, 89, 703-14.

72. Ehrenreich H, Costa T, Clouse KA, Pluta RM, Ogino Y, Coligan JE, Burd PR. (1993) Thrombin is a regulator of astrocytic endothelin-1. Brain Res, 600, 201-7.

73. Kanda Y, Watanabe Y. (2005) Thrombin-induced glucose transport via Src-p38 MAPK pathway in vascular smooth muscle cells. Br J Pharmacol, 146, 60-7.

74. Denko NC. (2008) Hypoxia, HIF1 and glucose metabolism in the solid tumour. Nat Rev Cancer, 8, 705-13.

75. Zundel W, Schindler C, Haas-Kogan D, Koong A, Kaper F, Chen E, Gottschalk AR, Ryan HE, Johnson RS, Jefferson AB, Stokoe D, Giaccia AJ. (2000) Loss of PTEN facilitates HIF-1-mediated gene expression. Genes Dev, 14, 391-6.

76. Bardos JI, Ashcroft M. (2004) Hypoxia-inducible factor-1 and oncogenic signalling. Bioessays, 26, 262-9.

77. Kietzmann T, Samoylenko A, Roth U, Jungermann K. (2003) Hypoxia-inducible factor-1 and hypoxia response elements mediate the induction of plasminogen activator inhibitor-1 gene expression by insulin in primary rat hepatocytes. Blood, 101, 907-14.

78. Fukuda R, Hirota K, Fan F, Jung YD, Ellis LM, Semenza GL. (2002) Insulin-like growth factor 1 induces hypoxia-inducible factor 1-mediated vascular endothelial growth factor expression, which is dependent on MAP kinase and phosphatidylinositol 3-kinase signaling in colon cancer cells. J Biol Chem, 277, 38205-11.

79. Gorlach A, Diebold I, Schini-Kerth VB, Berchner-Pfannschmidt U, Roth U, Brandes RP, Kietzmann T, Busse R. (2001) Thrombin activates the hypoxia-inducible factor-1 signaling pathway in vascular smooth muscle cells: Role of the p22(phox)-containing NADPH oxidase. Circ Res, 89, 47-54.

80. Richard DE, Berra E, Pouyssegur J. (2000) Nonhypoxic pathway mediates the induction of hypoxia-inducible factor 1α in vascular smooth muscle cells. J Biol Chem, 275, 26765-71.

81. Chandel NS, McClintock DS, Feliciano CE, Wood TM, Melendez JA, Rodriguez AM, Schumacker PT. (2000) Reactive oxygen species generated at mitochondrial complex III stabilize hypoxia-inducible factor-1α during hypoxia: a mechanism of O2 sensing. J Biol Chem, 275, 25130-8.

82. Brunelle JK, Bell EL, Quesada NM, Vercauteren K, Tiranti V, Zeviani M, Scarpulla RC, Chandel NS. (2005) Oxygen sensing requires mitochondrial ROS but not oxidative phosphorylation. Cell Metab, 1, 409-14.

83. Guzy RD, Hoyos B, Robin E, Chen H, Liu L, Mansfield KD, Simon MC, Hammerling U, Schumacker PT. (2005) Mitochondrial complex III is required for hypoxia-induced ROS production and cellular oxygen sensing. Cell Metab, 1, 401-8.

84. Gerald D, Berra E, Frapart YM, Chan DA, Giaccia AJ, Mansuy D, Pouyssegur J, Yaniv M, Mechta-Grigoriou F. (2004) JunD reduces tumor angiogenesis by protecting cells from oxidative stress. Cell, 118, 781-94.

85. Vaidyula VR, Rao AK. (2003) Role of Gaq and phospholipase C-β2 in human platelets activation by thrombin receptors PAR1 and PAR4: studies in human platelets deficient in Gaq and phospholipase C-β2. Br J Haematol, 121, 491-6.

86. Smith-Swintosky VL, Cheo-Isaacs CT, D'Andrea MR, Santulli RJ, Darrow AL, Andrade-Gordon P. (1997) Protease-activated receptor-2 (PAR-2) is present in the rat hippocampus and is associated with neurodegeneration. J Neurochem, 69, 1890-6.

87. Wang P, Jiang Y, Wang Y, Shyy JY, DeFea KA. (2010) β-arrestin inhibits CAMKKβ-dependent AMPK activation downstream of protease-activated-receptor-2. BMC Biochem, 11, 36.

88. Jin K, Sun Y, Xie L, Mao XO, Childs J, Peel A, Logvinova A, Banwait S, Greenberg DA. (2005) Comparison of ischemia-directed migration of neural precursor cells after intrastriatal, intraventricular, or intravenous transplantation in the rat. Neurobiol Dis, 18, 366-74.

89. DeWire SM, Ahn S, Lefkowitz RJ, Shenoy SK. (2007) β-arrestins and cell signaling. Annu Rev Physiol, 69, 483-510.

90. Ricks TK, Trejo J. (2009) Phosphorylation of protease-activated receptor-2 differentially regulates desensitization and internalization. J Biol Chem, 284, 34444-57.

91. Böhm SK, Khitin LM, Grady EF, Aponte G, Payan DG, Bunnett NW. (1996) Mechanisms of desensitization and resensitization of proteinase-activated receptor-2. J Biol Chem, 271, 22003-16.

92. Luo W, Wang Y, Hanck T, Stricker R, Reiser G. (2006) Jab1, a novel protease-activated receptor-2 (PAR-2)-interacting protein, is involved in PAR-2-induced activation of activator protein-1. J Biol Chem, 281, 7927-36.

93. Paing MM, Stutts AB, Kohout TA, Lefkowitz RJ, Trejo J. (2002) beta -Arrestins regulate protease-activated receptor-1 desensitization but not internalization or Down-regulation. J Biol Chem, 277, 1292-300. Epub 2001 Nov 2.

94. Kumar P, Lau CS, Mathur M, Wang P, DeFea KA. (2007) Differential effects of β-arrestins on the internalization, desensitization and ERK1/2 activation downstream of protease activated receptor-2. Am J Physiol Cell Physiol, 293, C346-57.

95. Dery O, Thoma MS, Wong H, Grady EF, Bunnett NW. (1999) Trafficking of proteinase-activated receptor-2 and β-arrestin-1 tagged with green fluorescent protein. β-Arrestin-dependent endocytosis of a proteinase receptor. J Biol Chem, 274, 18524-35.

96. Ayoub MA, Trinquet E, Pfleger KD, Pin JP. (2010) Differential association modes of the thrombin receptor PAR_1 with $G\alpha i_1$, $G\alpha_{12}$, and β-arrestin 1. FASEB J, 24, 3522-35.

97. Luan B, Zhao J, Wu H, Duan B, Shu G, Wang X, Li D, Jia W, Kang J, Pei G. (2009) Deficiency of a β-arrestin-2 signal complex contributes to insulin resistance. Nature, 457, 1146-9.

98. Beaulieu JM, Sotnikova TD, Marion S, Lefkowitz RJ, Gainetdinov RR, Caron MG. (2005) An Akt/β-arrestin 2/PP2A signaling complex mediates dopaminergic neurotransmission and behavior. Cell, 122, 261-73.

99. Ahn S, Kim J, Hara MR, Ren XR, Lefkowitz RJ. (2009) β-Arrestin-2 Mediates Anti-apoptotic Signaling through Regulation of BAD Phosphorylation. J Biol Chem, 284, 8855-65.

100. Soh UJ, Trejo J. (2011) Activated protein C promotes protease-activated receptor-1 cytoprotective signaling through β-arrestin and dishevelled-2 scaffolds. Proc Natl Acad Sci U S A, 108, E1372-80.

101. Revankar CM, Vines CM, Cimino DF, Prossnitz ER. (2004) Arrestins block G protein-coupled receptor-mediated apoptosis. J Biol Chem, 279, 24578-84.

102. Yang X, Zhou G, Ren T, Li H, Zhang Y, Yin D, Qian H, Li Q. (2012) β-Arrestin prevents cell apoptosis through pro-apoptotic ERK1/2 and p38 MAPKs and anti-apoptotic Akt pathways. Apoptosis, 17, 1019-26.

103. Sun X, Zhang Y, Wang J, Wei L, Li H, Hanley G, Zhao M, Li Y, Yin D. (2010) β-arrestin 2 modulates resveratrol-induced apoptosis and regulation of Akt/GSK3β pathways. Biochim Biophys Acta, 1800, 912-8.

104. Fort PE, Lampi KJ. (2011) New focus on α-crystallins in retinal neurodegenerative diseases. Exp Eye Res, 92, 98-103.

105. Li R, Rohatgi T, Hanck T, Reiser G. (2009) αA-crystallin and αB-crystallin, newly identified interaction proteins of protease-activated receptor-2, rescue astrocytes from C2-ceramide- and staurosporine-induced cell death. J Neurochem, 110, 1433-44.

106. Sharma KK, Olesen PR, Ortwerth BJ. (1987) The binding and inhibition of trypsin by alpha-crystallin. Biochim Biophys Acta, 915, 284-91.

107. Wang YH, Li YC, Huo SJ, Yin ZQ. (2012) α-crystallin promotes rat olfactory ensheathing cells survival and proliferation through regulation of PI3K/Akt/mTOR signaling pathways. Neurosci Lett, 531, 170-5.

108. Cobb BA, Petrash JM. (2000) Characterization of alpha-crystallin-plasma membrane binding. J Biol Chem, 275, 6664-72.

109. Nicholl ID, Quinlan RA. (1994) Chaperone activity of alpha-crystallins modulates intermediate filament assembly. Embo J, 13, 945-53.

110. Andley UP, Song Z, Wawrousek EF, Fleming TP, Bassnett S. (2000) Differential protective activity of alpha A- and alphaB-crystallin in lens epithelial cells. J Biol Chem, 275, 36823-31.

111. den Engelsman J, Bennink EJ, Doerwald L, Onnekink C, Wunderink L, Andley UP, Kato K, de Jong WW, Boelens WC. (2004) Mimicking phosphorylation of the small heat-shock protein alphaB-crystallin recruits the F-box protein FBX4 to nuclear SC35 speckles. Eur J Biochem, 271, 4195-203.

112. den Engelsman J, Gerrits D, de Jong WW, Robbins J, Kato K, Boelens WC. (2005) Nuclear import of {alpha}B-crystallin is phosphorylation-dependent and hampered by hyperphosphorylation of the myopathy-related mutant R120G. J Biol Chem, 280, 37139-48.

113. Yaung J, Jin M, Barron E, Spee C, Wawrousek EF, Kannan R, Hinton DR. (2007) alpha-Crystallin distribution in retinal pigment epithelium and effect of gene knockouts on sensitivity to oxidative stress. Mol Vis, 13, 566-77.

114. Dou G, Sreekumar PG, Spee C, He S, Ryan SJ, Kannan R, Hinton DR. (2012) Deficiency of alphaB crystallin augments ER stress-induced apoptosis by enhancing mitochondrial dysfunction. Free Radic Biol Med, 53, 1111-22.

115. Masilamoni JG, Jesudason EP, Bharathi SN, Jayakumar R. (2005) The protective effect of alpha-crystallin against acute inflammation in mice. Biochim Biophys Acta, 1740, 411-20.

116. Rao NA, Saraswathy S, Wu GS, Katselis GS, Wawrousek EF, Bhat S. (2008) Elevated retina-specific expression of the small heat shock protein, alphaA-crystallin, is associated with photoreceptor protection in experimental uveitis. Invest Ophthalmol Vis Sci, 49, 1161-71.

117. Li DW, Liu JP, Mao YW, Xiang H, Wang J, Ma WY, Dong Z, Pike HM, Brown RE, Reed JC. (2005) Calcium-activated RAF/MEK/ERK signaling pathway mediates p53-dependent apoptosis and is abrogated by alpha B-crystallin through inhibition of RAS activation. Mol Biol Cell, 16, 4437-53.

118. Wang YH, Wang DW, Wu N, Wang Y, Yin ZQ. (2012) alpha-Crystallin promotes rat axonal regeneration through regulation of RhoA/rock/cofilin/MLC signaling pathways. J Mol Neurosci, 46, 138-44.

119. Kamradt MC, Chen F, Cryns VL. (2001) The small heat shock protein alpha B-crystallin negatively regulates cytochrome c- and caspase-8-dependent activation of caspase-3 by inhibiting its autoproteolytic maturation. J Biol Chem, 276, 16059-63.

120. Mao YW, Liu JP, Xiang H, Li DW. (2004) Human alphaA- and alphaB-crystallins bind to Bax and Bcl-X(S) to sequester their translocation during staurosporine-induced apoptosis. Cell Death Differ, 11, 512-26.

121. Liu S, Li J, Tao Y, Xiao X. (2007) Small heat shock protein alphaB-crystallin binds to p53 to sequester its translocation to mitochondria during hydrogen peroxide-induced apoptosis. Biochem Biophys Res Commun, 354, 109-14.

122. Li R, Rohatgi T, Hanck T, Reiser G. (2009) Alpha A-crystallin and alpha B-crystallin, newly identified interaction proteins of protease-activated receptor-2, rescue astrocytes from C2-ceramide- and staurosporine-induced cell death. J Neurochem, 110, 1433-44.

123. Li R, Reiser G. (2011) Phosphorylation of Ser45 and Ser59 of αB-crystallin and p38/extracellular regulated kinase activity determine αB-crystallin-mediated protection of rat brain astrocytes from C2-ceramide- and staurosporine-induced cell death. J Neurochem, 118, 354-64.

124. Rojanathammanee L, Harmon EB, Grisanti LA, Govitrapong P, Ebadi M, Grove BD, Miyagi M, Porter JE. (2009) The 27-kDa heat shock protein confers cytoprotective effects through a beta 2-adrenergic receptor agonist-initiated complex with beta-arrestin. Mol Pharmacol, 75, 855-65.

125. Qi S, Xin Y, Qi Z, Xu Y, Diao Y, Lan L, Luo L, Yin Z. (2014) HSP27 phosphorylation modulates TRAIL-induced activation of Src-Akt/ERK signaling through interaction with β-arrestin2. Cell Signal, 26, 594-602.

126. Hamprecht B, Löffler F. (1985) Primary glial cultures as a model for studying hormone action. Methods Enzymol, 109, 341-5.

127. Schonfeld P, Kruska N, Reiser G. (2009) Antioxidative activity of the olive oil constituent hydroxy-1-aryl-isochromans in cells and cell-free systems. Biochim Biophys Acta, 1790, 1698-704.

128. Grabham P, Cunningham DD. (1995) Thrombin receptor activation stimulates astrocyte proliferation and reversal of stellation by distinct pathways: involvement of tyrosine phosphorylation. J Neurochem, 64, 583-91.

129. Vuong PT, Malik AB, Nagpala PG, Lum H. (1998) Protein kinase C β modulates thrombin-induced Ca2+ signaling and endothelial permeability increase. J Cell Physiol, 175, 379-87.

130. Lambert AJ, Buckingham JA, Boysen HM, Brand MD. (2008) Diphenyleneiodonium acutely inhibits reactive oxygen species production by mitochondrial complex I during reverse, but not forward electron transport. Biochim Biophys Acta, 1777, 397-403.

131. Fatrai S, Elghazi L, Balcazar N, Cras-Meneur C, Krits I, Kiyokawa H, Bernal-Mizrachi E. (2006) Akt induces βcell proliferation by regulating cyclin D1, cyclin D2, and p21 levels and cyclin-dependent kinase-4 activity. Diabetes, 55, 318-25.

132. Melstrom LG, Salabat MR, Ding XZ, Milam BM, Strouch M, Pelling JC, Bentrem DJ. (2008) Apigenin inhibits the GLUT-1 glucose transporter and the phosphoinositide 3-kinase/Akt pathway in human pancreatic cancer cells. Pancreas, 37, 426-31.

133. Valle-Casuso JC, Gonzalez-Sanchez A, Medina JM, Tabernero A. (2012) HIF-1 and c-Src mediate increased glucose uptake induced by endothelin-1 and connexin43 in astrocytes. PLoS One, 7, e32448.

134. Wang X, Liu JZ, Hu JX, Wu H, Li YL, Chen HL, Bai H, Hai CX. (2011) ROS-activated p38 MAPK/ERK-Akt cascade plays a central role in palmitic acid-stimulated hepatocyte proliferation. Free Radic Biol Med, 51, 539-51.

135. Sato A, Okada M, Shibuya K, Watanabe E, Seino S, Narita Y, Shibui S, Kayama T, Kitanaka C. (2014) Pivotal role for ROS activation of p38 MAPK in the control of differentiation and tumor-initiating capacity of glioma-initiating cells. Stem Cell Res, 12, 119-31.

136. Hirota Y, Osuga Y, Hirata T, Harada M, Morimoto C, Yoshino O, Koga K, Yano T, Tsutsumi O, Taketani Y. (2005) Activation of protease-activated receptor 2 stimulates proliferation and interleukin (IL)-6 and IL-8 secretion of endometriotic stromal cells. Hum Reprod, 20, 3547-53.

137. Masamune A, Kikuta K, Satoh M, Suzuki N, Shimosegawa T. (2005) Protease-activated receptor-2-mediated proliferation and collagen production of rat pancreatic stellate cells. J Pharmacol Exp Ther, 312, 651-8.

138. Sreekumar PG, Chothe P, Sharma KK, Baid R, Kompella U, Spee C, Kannan N, Manh C, Ryan SJ, Ganapathy V, Kannan R, Hinton DR. (2013) Antiapoptotic properties of alpha-crystallin-derived peptide chaperones and characterization of their uptake transporters in human RPE cells. Invest Ophthalmol Vis Sci, 54, 2787-98.

139. Li R, Reiser G. (2011) Phosphorylation of Ser45 and Ser59 of alphaB-crystallin and p38/extracellular regulated kinase activity determine alphaB-crystallin-mediated protection of rat brain astrocytes from C2-ceramide- and staurosporine-induced cell death. J Neurochem, 118, 354-64.

140. Hoover HE, Thuerauf DJ, Martindale JJ, Glembotski CC. (2000) alpha B-crystallin gene induction and phosphorylation by MKK6-activated p38. A potential role for alpha B-crystallin as a target of the p38 branch of the cardiac stress response. J Biol Chem, 275, 23825-33.

141. Piao CS, Kim SW, Kim JB, Lee JK. (2005) Co-induction of alphaB-crystallin and MAPKAPK-2 in astrocytes in the penumbra after transient focal cerebral ischemia. Exp Brain Res, 163, 421-9.

142. Li R, Rohatgi T, Hanck T, Reiser G. (2009) αA-crystallin and αB-crystallin, newly identified interaction proteins of protease-activated receptor-2, rescue astrocytes from C2-ceramide- and staurosporine-induced cell death. J Neurochem, 110, 1433-44.

143. Povsic TJ, Kohout TA, Lefkowitz RJ. (2003) Beta-arrestin1 mediates insulin-like growth factor 1 (IGF-1) activation of phosphatidylinositol 3-kinase (PI3K) and anti-apoptosis. J Biol Chem, 278, 51334-9.

144. Sun X, Zhang Y, Wang J, Wei L, Li H, Hanley G, Zhao M, Li Y, Yin D. (2010) Beta-arrestin 2 modulates resveratrol-induced apoptosis and regulation of Akt/GSK3β pathways. Biochim Biophys Acta, 1800, 912-8.

145. Li R, Reiser G. (2011) Phosphorylation of Ser45 and Ser59 of αB-crystallin and p38/extracellular regulated kinase activity determine αB-crystallin-mediated protection of rat brain astrocytes from C2-ceramide- and staurosporine-induced cell death. J Neurochem, 118, 354-64.

146. Wang Y, Luo W, Reiser G. (2007) The role of calcium in protease-activated receptor-induced secretion of chemokine GRO/CINC-1 in rat brain astrocytes. J Neurochem, 103, 814-9.

147. Zhang W, Liu HT. (2002) MAPK signal pathways in the regulation of cell proliferation in mammalian cells. Cell Res, 12, 9-18.

148. Ip YT, Davis RJ. (1998) Signal transduction by the c-Jun N-terminal kinase (JNK)--from inflammation to development. Curr Opin Cell Biol, 10, 205-19.

149. Berridge MJ. (1995) Calcium signalling and cell proliferation. Bioessays, 17, 491-500.

150. Chang F, Lee JT, Navolanic PM, Steelman LS, Shelton JG, Blalock WL, Franklin RA, McCubrey JA. (2003) Involvement of PI3K/Akt pathway in cell cycle progression, apoptosis, and neoplastic transformation: a target for cancer chemotherapy. Leukemia, 17, 590-603.

151. Muise-Helmericks RC, Grimes HL, Bellacosa A, Malstrom SE, Tsichlis PN, Rosen N. (1998) Cyclin D expression is controlled post-transcriptionally via a phosphatidylinositol 3-kinase/Akt-dependent pathway. J Biol Chem, 273, 29864-72.

152. Lavoie JN, L'Allemain G, Brunet A, Muller R, Pouyssegur J. (1996) Cyclin D1 expression is regulated positively by the p42/p44MAPK and negatively by the p38/HOGMAPK pathway. J Biol Chem, 271, 20608-16.

153. Martinez-Sanchez G, Giuliani A. (2007) Cellular redox status regulates hypoxia inducible factor-1 activity. Role in tumour development. J Exp Clin Cancer Res, 26, 39-50.

154. Collins Y, Chouchani ET, James AM, Menger KE, Cocheme HM, Murphy MP. (2012) Mitochondrial redox signalling at a glance. J Cell Sci, 125, 801-6.

155. Sheta EA, Trout H, Gildea JJ, Harding MA, Theodorescu D. (2001) Cell density mediated pericellular hypoxia leads to induction of HIF-1α via nitric oxide and Ras/MAP kinase mediated signaling pathways. Oncogene, 20, 7624-34.

156. Stalheim L, Ding Y, Gullapalli A, Paing MM, Wolfe BL, Morris DR, Trejo J. (2005) Multiple independent functions of arrestins in the regulation of protease-activated receptor-2 signaling and trafficking. Mol Pharmacol, 67, 78-87.

157. Shenoy SK, Lefkowitz RJ. (2005) Receptor-specific ubiquitination of beta-arrestin directs assembly and targeting of seven-transmembrane receptor signalosomes. J Biol Chem, 280, 15315-24.

158. Soh UJ, Dores MR, Chen B, Trejo J. (2010) Signal transduction by protease-activated receptors. Br J Pharmacol, 160, 191-203.

159. Saito A, Osuga Y, Yoshino O, Takamura M, Hirata T, Hirota Y, Koga K, Harada M, Takemura Y, Yano T, Taketani Y. (2011) TGF-β1 induces proteinase-activated receptor 2 (PAR2) expression in endometriotic stromal cells and stimulates PAR2 activation-induced secretion of IL-6. Hum Reprod, 26, 1892-8.

160. Li R, Zhu Z, Reiser G. (2012) Specific phosphorylation of αA-crystallin is required for the αA-crystallin-induced protection of astrocytes against staurosporine and C2-ceramide toxicity. Neurochem Int, 60, 652-8.

161. Chae HJ, Kang JS, Byun JO, Han KS, Kim DU, Oh SM, Kim HM, Chae SW, Kim HR. (2000) Molecular mechanism of staurosporine-induced apoptosis in osteoblasts. Pharmacol Res, 42, 373-81.

162. Antonsson A, Persson JL. (2009) Induction of apoptosis by staurosporine involves the inhibition of expression of the major cell cycle proteins at the G(2)/m checkpoint accompanied by alterations in Erk and Akt kinase activities. Anticancer Res, 29, 2893-8.

163. Zhu Z, Reiser G. (2013) PAR-1 activation rescues astrocytes through the PI3K/Akt signaling pathway from chemically induced apoptosis that is exacerbated by gene silencing of beta-arrestin 1. Neurochem Int.

164. Park H, Park S, Jeon H, Song BW, Kim JB, Kim CS, Pak HN, Hwang KC, Lee MH, Chung JH, Joung B. (2013) Alpha B-crystallin prevents the arrhythmogenic effects of particulate matter isolated from ambient air by attenuating oxidative stress. Toxicol Appl Pharmacol, 266, 267-75.

165. Wang K, Spector A. (1995) Alpha-crystallin can act as a chaperone under conditions of oxidative stress. Invest Ophthalmol Vis Sci, 36, 311-21.

166. Sreekumar PG, Kannan R, Kitamura M, Spee C, Barron E, Ryan SJ, Hinton DR. (2010) alphaB crystallin is apically secreted within exosomes by polarized human retinal pigment epithelium and provides neuroprotection to adjacent cells. PLoS One, 5, e12578.

8 Abbreviation list

AP	activating peptide
AD	Alzheimer's disease
AMPK	Adenosine monophosphate-activated protein kinase
Akt	Protein Kinase B
APC	Activated protein C
CAMKKb	Ca^{2+}-dependent kinase kinase b
Cdks	Cyclin D associated kinase
CINC	Cytokine-induced neutrophil chemoattractant
CNS	Central nervous system
CRYAA	αA-crystallin
CRYAB	αB-crystallin
COX4i2	Cytochrome c oxidase subunit 4 isform 2
ECL	Extracellular loops
EGF	Epidermal growth factor
ERK	Extracellular signal-regulated kinase
ET	Endothelins
FCS	fetal calf serum
FGF	Fibroblast growth factor
FITC	Fluorescein
GPCRs	G-protein-coupled-receptors
GRO	Growth Related Oncogene
GLUT-1	Glucose transporter-1
HA	Haemagglutinin epitope
HIF-1α	Hypoxia-inducible factor-1 α
HK1(2)	Hexokinases type 1(2)
ICL	Intracellular loop
IL	interleukin
Jab1	Jun activation domain-binding protein 1
JNK	c-Jun N-terminal kinase
LDHA	Lactate dehydrogenase A
MAPK	mitogen-activated protein kinases
MCT4	Monocarboxylate transporter 4
MEK	mitogen-activated and extracellular signal-regulated kinase
mTOR	mammalian target of rapamycin
MXI	Max interactor
NF-κB	nuclear factor κ B

OD	Optical Density
PAR	protease-activated receptors
P38	p38 mitogen-activated protein kinases
PI3K	Phosphatidylinositol 3 kinase
PD	Parkinson's disease
PDGF	platelet-derived growth factor
PDK	Pyruvate dehydrogenase kinase
PFK	Phosphofructokinase
PGK	Phosphoglycerate kinase
PGI	Phosphoglucose isomerase
PGM,	Phosphoglycerate mutase
PHD	Prolyl 4-hydroxylase
PI	Propidium iodide
PKC	Protein kinase C
PTK	Protein tyrosine kinases
PK	Pyruvate kinase
PFKFB	Phosphofructokinase-2/Fructose-2,6-bisphosphatase
Ras	Rat sarcoma member A
RBM	rat brain mitochondria
RPE	Retinal pigment epithelial cells
ROS	reactive oxygen species
RhoA	Ras homolog gene family
Src	steroid receptor coactivator
siRNA	small interfering RNA
SDS-PAGE	sodium dodecyl sulfate-polyacrylamide gel electrophoresis
STS	staurosporine
sHSPs	small heat shock proteins
THR	Thrombin
TM	Transmembrane
TPI	Triosephosphate
UVA	Ultraviolet A
VSMC	Vascular smooth muscle cells

9   Appendix

List of Publications

Zhu Z, Reiser G. (2014) PAR-1 activation rescues astrocytes through the PI3K/Akt signaling pathway from chemically induced apoptosis that is exacerbated by gene silencing of β-arrestin 1. Neurochem Int, 67, 46-56.

Li R, **Zhu Z**, Reiser G. (2012) Specific phosphorylation of αA-crystallin is required for the αA-crystallin-induced protection of astrocytes against staurosporine and C2-ceramide toxicity. Neurochem Int, 60, 652-8.

Curriculum Vitae

Name: Zhihui, Zhu

Birthday: 7th Oct. 1982

Place of Birth: Inner Mongolia, China

Nationality: China

Education

10/2010 - present

Otto-von- Guericke University of Magdeburg Deutschland

(Magdeburg University, Germany)

Doctoral study of Neurobiochemistry

Subject of thesis: Functional studies of β-arrestins and αB-crystallin as interaction partners of PAR-1 and PAR-2 and their involvement in protective and proliferative signaling pathways in astrocytes.

09/ 2007 - 06/2010

Central University of Nationalities, China (MinZu University of China)

Master degree of Medicine

Subject of thesis: The polymorphisms of *CYP2D6* gene distributed in Uighur ethnic group in China.

09/2002 – 06/2006

Inner Mongolia Medical University

Bachelor degree of Science

Subject of thesis: Depiction of the fingerprint of traditional Chinese medicine-Cortex phellodenri.

Selbstständigkeitserklärung

Zhihui Zhu
Fermersleber Weg 45f
39112 Magdeburg

Erklärung

Hiermit erkläre ich, dass die von mir eingereichte Dissertation zu dem Thema

Functional studies of β-arrestins and αB-crystallin as interaction partners of PAR-1 and PAR-2 and their involvement in protective and proliferative signaling pathways in astrocytes

selbständig verfasst, nicht schon als Dissertation verwendet habe und die benutzten Hilfsmittel und Quellen vollständig angegeben wurden.

Weiterhin erkläre ich, dass ich weder diese noch eine andere Arbeit zur Erlangung des akademischen Grades doctor rerum naturalium (Dr. rer. nat.) an anderen Einrichtungen eingereicht habe.

Magdeburg, den 28.04.2014

Zhihui Zhu